POLITECNICO
MILANO 1863

SCUOLA DI INGEGNERIA INDUSTRIALE
E DELL'INFORMAZIONE

EFFECT OF THE SODIUM ALGINATE CONCENTRATION AND THE IONIC STRENGTH ON THE RHEOLOGICAL PROPERTIES OF SODIUM ALGINATE-BASED HYDROGELS

Master Thesis in Materials Engineering & Nanotechnology

Author: **Fatma Nalan Cetin**

Student ID: 940389
Advisor: Prof. Francesco Briatico Vangosa
Co-advisor: Prof. Paola Petrini
Academic Year: 2020-2021

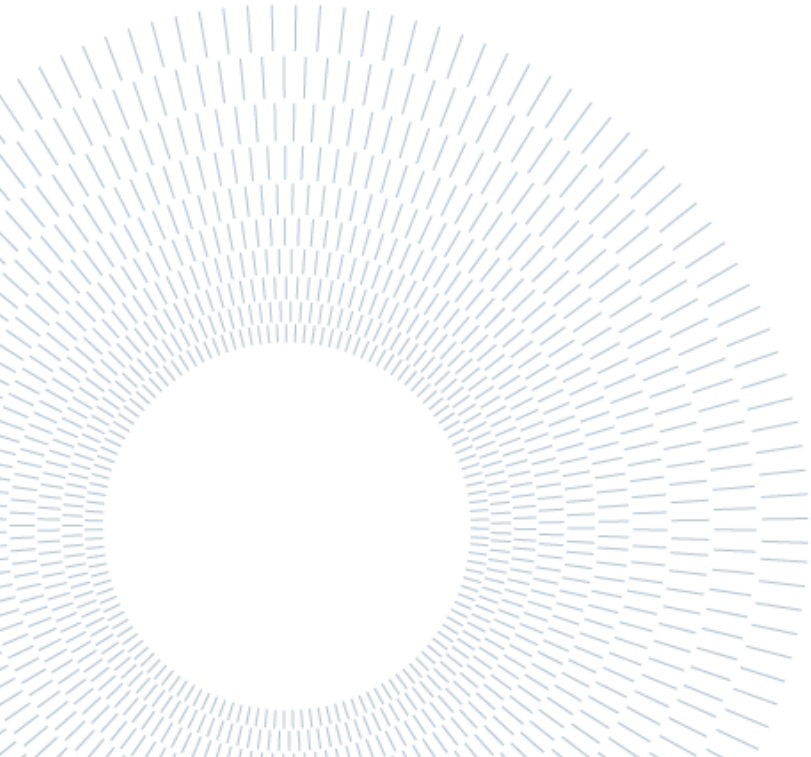

Abstract

The scope of this thesis work is the rheological characterization of sodium alginate solutions (SA) and SA-based hydrogels to investigate the effect of SA concentration and solution ionic strength, controlled through the addition of known amounts of NaCl. The interest in the SA-based hydrogels comes from their potential use for in vitro mucus models. These hydrogels have proved to be successful at mimicking the complex structure and the mechanical properties of physiological and pathological mucus. Considering that the mucus viscoelasticity depends on physicochemical factors such as salt concentration, an investigation on the ionic strength effect on the proposed in vitro models was required. Viscosity of the solutions and the dynamic modulus of the hydrogels showed an increasing trend with SA concentration. However, the effect of ionic strength seemed to be more complex. The viscosity of the solutions at low SA concentration decreased by NaCl addition while it increased with NaCl concentration when the SA concentration was high. A similar effect was reported for the dynamic moduli of the hydrogels: G' and G'' decreased by NaCl addition at low SA concentrations, however after a certain SA concentration was reached, they started to show an increasing trend. Moreover, we looked for a correlation between viscosity of the solutions and dynamic modulus of the hydrogels. A map which connects these properties was found, with a trend which could be correlated to the SA solution concentration regime only in the case of the neutral solution. Further investigation is required to establish a correlation within the experimental map and some structural features in the case of solutions containing NaCl.

Key-words: sodium alginate, in vitro mucus models, rheological characterization

Abstract in italiano

Lo scopo di questo lavoro di tesi è la caratterizzazione reologica di soluzioni di alginato di sodio(SA), di idrogeli a base di SA per studiare l'effetto della concentrazione dell'alginato e della forza ionica della soluzione, controllata attaverso l'aggiunta di quantità note di NaCl. L'interesse per gli idrogel a base di SA deriva dal loro potenziale utilizzo per modelli di muço in vitro. Questi idrogel si sono rivelati efficaci nell'imitare la struttura complessa e le proprietà meccaniche del muco fisiologico e patologico. Considerando che la viscoelasticità del muço dipende da fattori fisico-chimici come la concentrazione di sale, è stata necessaria un'indagine sull'effetto della forza ionica sui modelli in vitro proposti. La viscosità delle soluzioni e il valore del modulo dinamico degli idrogeli hanno mostrato un andamento crescente con la concentrazione di SA. Tuttavia, l'effetto della forza ionica sembrava essere più complesso. La viscosità delle soluzioni a bassa concentrazione di SA diminuisce con l'aggiunta di NaCl,

mentre aumenta quando la concentrazione di SA è più elevata. Un effetto simile è stato riportato per il modulo dinamico degli idrogel: G' e G" diminuiscono per concentrazioni crescenti di NaCl a basse concentrazioni di SA,mentre oltre una certa concentrazione di SA, mostrano invece un aumento al crescere della concentrazione di NaCl. Inoltre, abbiamo cercato una correlazione tra viscosità delle soluzioni e il modulo dinamico degli idrogel. È stata definita una mappa che correla queste proprietà. In assenza di NaCl l'andamento osservato può essere messo in relazione con i regimi di concentrazione della soluzione di SA. Nel caso delle soluzioni contenenti NaCl è invece necessario uno studio più approfondito per dare una interpretazione della correlazione individuata empiricamente.

Parole chiave: alginato di sodio, modelli di muco in vitro, caratterizzazione reologica

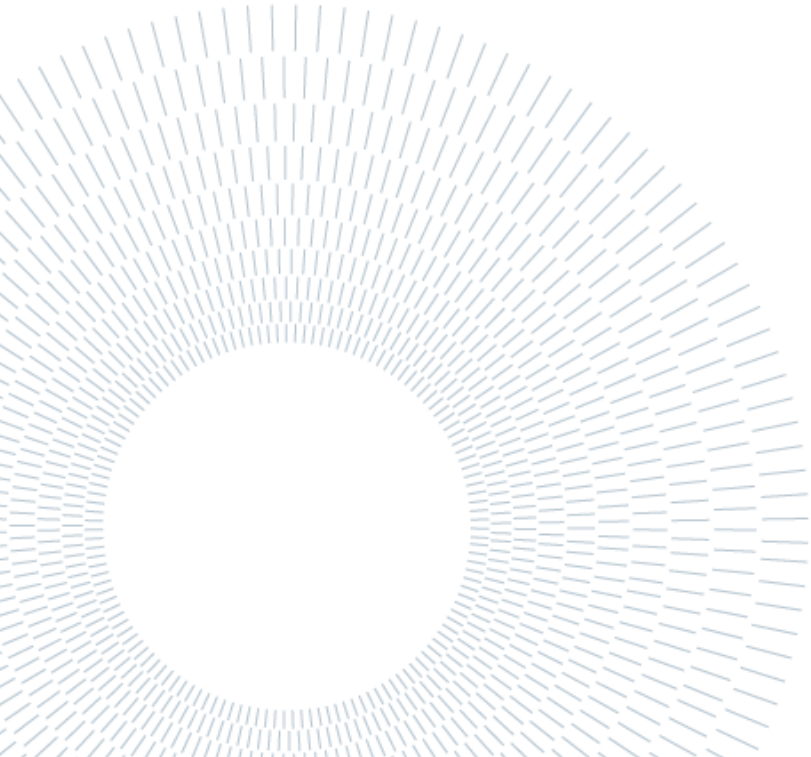

Contents

Aim of the Thesis

Insights gained from the recent advances in research revealed a complex bidirectional communication between the central and the enteric nervous system which is termed as the gut-brain axis (GBA). This communication links the emotional and cognitive centers of the brain with peripheral intestinal functions. It has been proved that the gut microbiota that is hosted by mucus influences these interactions. [1] Therefore, many research councils have expanded this research topic to study this intercorrelation. To limit the animal studies, reliable in vitro models are required as they offer the advantage to simplify a complex phenomenon and facilitate its comprehension when supported with in vivo and ex vivo examinations. Besides the GBA studies, the importance of developing in vitro models which can replicate both the biological structure and the function of intestinal mucus is also evident for the drug delivery/screening and for the regenerative medicine research. [41] Moreover, in vivo and ex vivo models show other drawbacks such as low repeatability, high costs and the difficulty of obtaining large sample volumes which can be eliminated by in vitro models. [26] [41]

Mucus is a biological hydrogel with important selective barrier properties for the human body. Its 3D structure, viscoelastic properties and compositional complexity define the relation between the human tissue and the external environment. To mimic some of mucus' properties such as drug diffusion, permeability, viscosity and other rheological properties, alginate-based hydrogels are proposed as the initial polymer structure. What makes it more promising than the other in vitro models proposed before is that alginate-based hydrogels are proved to be efficient in vitro models that include the double layer structure with resulting mesh, protein concentration and oxygen gradients which are the influencing factors for mucus role as a selective barrier and environment for bacterial culture. That's why the sodium alginate hydrogels are the focus of our study. Our examination is by the means of rheology as the ability of reproducing mechanical properties of mucus is a fundamental requirement in a mucus model. Indeed, mucus has a viscoelastic behavior which is affected

also by alterations in its composition. One of the most influencing factors is the ionic strength as it directly leads to the shrinkage or swelling of the mucus. Also, we know that the salt concentration in mucus varies in different body districts, and it also changes in pathological conditions. Given the importance of this parameter, in this study we are investigating the effect of ionic strength and sodium alginate concentration on rheological properties of sodium alginate hydrogels. This study is the continuation of a previous one by our research group aimed at investigating the same effects on sodium alginate solutions. We will try to see if we can reveal a correlation between the rheological properties of SA hydrogels and of solutions since such a relation would give the advantage of predicting the properties of SA hydrogels beforehand.

1 Introduction

1.1. Mucus Modelling

1.1.1. Mucus

Mucus is a hydrogel that forms the first line of defense of the immune system in mammals. It is a highly complex mixture of mucins, DNA, lipids, ions, proteins, cells and cellular debris, and water. It lubricates and protects the human lungs, gastrointestinal (GI) tract, vagina, eyes, and other moist mucosal surfaces. It functions as a selective barrier in the biochemical level to allow the passage of selected gases, ions, nutrients, and many proteins while stopping the foreign particles such as toxins and pathogens. At the macroscopic level, it is a non-Newtonian, thixotropic hydrogel which shows shear thinning at high shear rates. [26]

Mucus constitutes a complex system which underlies the challenge of mimicking its structure and reproducing its properties by in vitro models. In some cases, such as that of intestinal mucus, it has *structural anisotropy* that comes from its double-layer structure. The first layer is firmly attached to the epithelium, whereas the other layer is superimposed to the first one loosely. Although the attached and the loose layers have the same composition, their network mesh architecture is different. It is known that structural properties such as the mesh size highly influences the screening models for oral drugs and the development of drug carriers. [41]

Another challenge arises from the *chemical complexity* of the mucus which makes it harder to achieve compositional similarity with in vitro or even in vivo models. The primary constituents of the mucus hydrogel are the proteins that are called mucins (Figure 1-1) which are secreted from the goblet cells in the epithelium. Core structure of the gel forming mucin (GFM) network is formed by the disulfide bonds. GFMs vary in different parts of the human body; the only GFM of intestinal mucus is polymerized mucin-2 (MUC2). Although the

mechanism of their polymerization is not well understood, these branched structures should be a priority to mimic in an in vitro model as they play an important role in bacterial adhesion and hostile activities as well as providing the required environment for microbiota growth.

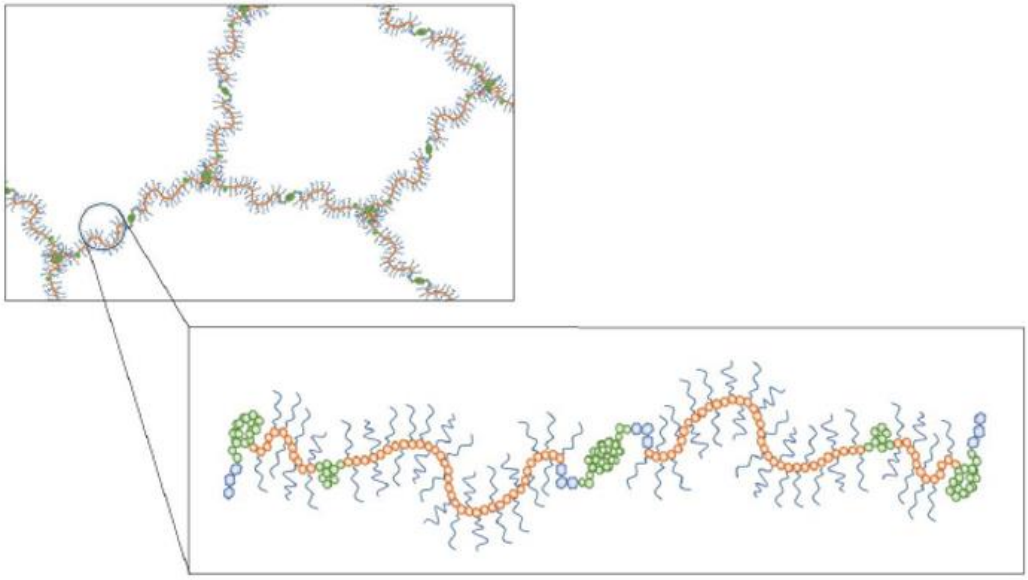

Figure 1-1 : Mucin structure and GFM. [52]

Other chemical components that mucus has such as lipids, DNA and many other proteins highly affect the mesh size, viscoelastic properties and drug diffusivity and response to microbial activity. Although structural anisotropy and chemical complexity play a major role in intestinal mucus functions, they haven't been completely realized in *in vitro* mucus models, especially in the field of drug delivery.

1.1.1.1. Mucus Viscoelasticity

Mucus is a viscoelastic material, and its rheological properties mostly depend on the gel network constituted by GFM, hence GFM concentration and the entanglements are crucial factors in mucus viscoelasticity. However, physicochemical parameters such as ionic strength and pH of the environment alter the gel network and change the rheological properties of mucus. Ionic strength changes the swelling degree of mucus and affects the osmotic properties [27] whereas a decrease in pH can lead to sol-gel transition in gastric mucus, preventing the auto-digestion. Although studies have displayed different outcomes

for the effect of ionic strength in mucus viscoelasticity, some has shown that increases in ion concentration correlate to a decrease in the viscosity of mucus at the macroscale. [26] On the other hand, elastic properties of mucus increase with greater ion valency. [4]

1.1.1.2. In vitro Mucus Models

We can classify in vitro mucus models as cellular, physiological, and artificial models. Cellular models are based on the use of cells that have a certain degree of similarity to enterocytes. However, they mostly fail in replicating the hierarchical structure of mucosa. Human physiological mucus is obviously the best representative sample, but it is hard to isolate/extract in addition to the lack of volunteers and the difficulty in obtaining large volume samples except for the cervicovaginal mucus. [4] [26] Artificial mucus models with multi components, although successful at some extent, fail in reproducing the physical and biochemical anisotropy of mucus. They are well known in literature and reported in [4] [54].

1.1.2. Sodium Alginate (SA) for in vitro Mucus Modeling

Evolution towards a more realistic in vitro mucus model seems to be possible with the use of alginate-based hydrogels as the initial polymer structure. [36] [42] Alginate is a natural polysaccharide that is mostly found in brown seaweeds and its chemical nature shows certain resemblances to the glycosylated ramifications present in the natural mucins. It is naturally found as a mixed calcium/sodium/ potassium salt of alginic acid. The sodium salt of alginic acid (Figure 1-2), which is referred as the sodium alginate ($NaC_6H_7O_6$) is commonly used in food, pharmaceutical, textile and paper industries as a jellifying agent. Recently, SA has gained a lot of interest for tissue engineering and drug delivery studies due to its non-toxicity, non-immunogenicity, biocompatibility, and biodegradability. [9] [12] [33]

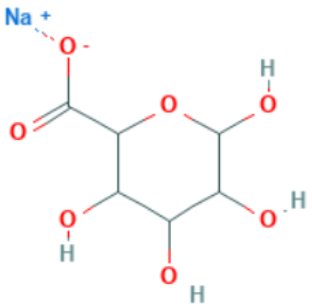

Figure 1-2: Sodium salt of alginic acid

SA is a linear block copolymer which is comprised of 1,4-β-D-mannuronic (M) and α-L-guluronic (G) acid monomers linked by a β-(1,4) glycosidic bond (Figure 1-3). Let us refer them as M and G blocks. G block has a higher degree of hindered rotation around the glycosidic bonds which leads to a chain configuration that is more extended than that of M block. [31]

The chain can have 3 different arrangements: M blocks (M-), G blocks(G-), and alternate sequences of two monomers (MG) blocks. Distribution pattern these blocks vary, and M/G ratio highly influences the solution and gel properties. Increase of G blocks leads to stiffer, more brittle, and mechanically more stable gels while it decreases the deformability of the network.

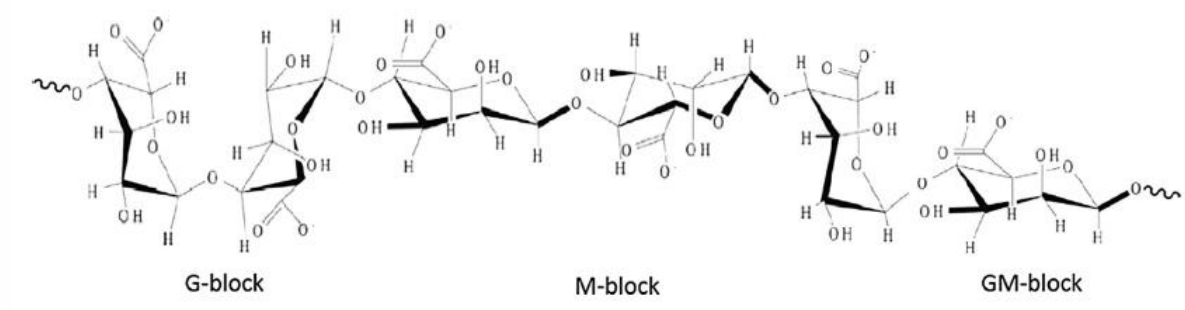

Figure 1-3: Chemical structure of sodium alginate [9]

1.1.2.1. Gelation Mechanism of Sodium Alginate

Many studies have shown that SA undergoes a sol-gel transition which refers to a change from liquid to gel accompanying a physical cross-linking in the presence of divalent cations

such as Ca^{2+}, Ba^{2+}, Sr^{2+}, Mg^{2+}. Carboxyl groups on G blocks allow the intermolecular cross-linking with divalent cations since the G blocks contribute to a high degree of coordination of these cations. By this coordination, G blocks on a SA chain connect to the G blocks on another alginate chain, and this leads to the formation of a three-dimensional gel network of alginate strands as it can be seen from the Figure 1-4 below. As the G-block density increases, number of possible crosslinks increase, and this leads to stiffer networks as aforementioned. This is how the composition and sequential characteristics of alginate change the mechanical properties of the resulting hydrogel. The connection which is formed by a divalent cation and G blocks of 2 adjacent polymer chain is termed as the egg-box model [29]. This ionotropic gelation with divalent cations even under mild conditions leads to the common use of SA as a gelling agent in many applications.

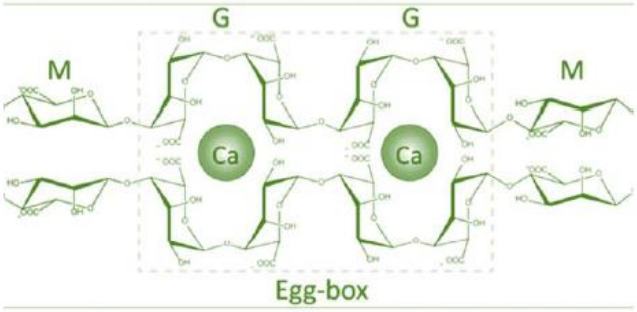

Figure 1-4: Representation for egg box model.

SA based hydrogels proved to be efficient in mimicking the double layer structure of mucus through different gelation mechanisms. The loose layer of the intestinal mucus with uniform properties can be modeled by a slow and homogeneous crosslinking of SA which is called the internal gelation process. In this case, the source of Ca^{2+} ions should be insoluble in the medium until a homogeneous dispersion is achieved. Afterwards, an acidifier is introduced to the system to decrease the pH. Hence, it facilitates the dissolution of Ca^{2+} ions in a controlled way and allows for the initiation of crosslinking. On the other hand, the attached intestinal mucus layer with some crosslinking gradient can be modeled via a rapid and hardly controllable external gelation wherein the source of Ca^{2+} ions is already soluble in the solvent. Upon meeting the solution of SA, free Ca^{2+} ions lead to the crosslinking of SA

chains before a homogeneous dispersion is achieved, therefore creating a crosslinking gradient. [52]

1.1.2.2. Importance of Rheology for Mucus Modelling

Rheology is a branch of physics which helps us to understand the deformation behavior of solids and flow behavior of liquids. The rheological experiments reveal information about the deformation produced by shear forces that cause many materials to flow. Hence, the rheology has proved to be a useful tool to assess the dynamic mechanical properties of biological materials such as viscous liquids, soft solids, pastes, gels, and polymer melts since their behavior is based on the combination of both the viscous and the elastic portion and therefore, it is called viscoelastic.

In rheology, complex modulus G* can be used as a measure of viscoelasticity and it has 2 components: storage (G') and loss (G'') shear modulus. While G' corresponds to the elasticity or the ability of the material to store the applied mechanical energy, G'' corresponds to the viscous component which correlate to the dissipation of the mechanical energy. Furthermore, the flow resistance which can be determined in terms of viscosity by rheological experiments, is another important property to characterize all flowing fluids since their molecules show a relative motion between each other combined with internal frictional forces.

Both macro- and microrheology methods (which are distinguished by the scale of observations) have been used to investigate mucus [26] since changes in elastic and viscous responses in altering physiological conditions are of great importance for biological and bioengineering studies. Since one of the requirements for an efficient in vitro mucus model is the reproducing the rheological characteristics such as dynamic moduli, our interest lies in macrorheology i.e. the study on bulk fluid flow.

1.2. Polymers Theory

The theoretical comprehension of the origin of viscoelastic properties of polymer solutions and those of gels is essential to understand the experimental findings obtained from the rheology tests. Many theories have been developed to explain the polymer conformation and

the linear viscoelasticity, and these theories guide us in explaining the salient features of polymeric systems in liquid and gel states. This chapter will briefly recall the basic concepts in polymer physics of neutral polymers and the polyelectrolytes solutions, followed by the theory of gelation and gel networks. The aim is to give the main concepts on scaling properties which will come in handy in the bibliographical and the experimental sections to investigate the rheological properties of SA solutions and hydrogels. Since the polymers can have a great number of conformations, only statistical approaches are successful at describing the shape and behavior of polymer chains. [10] In this sense, polymer physics which refer to the branch of statistical mechanics applied to the polymeric materials, is our guide to understand the theory and the origin of viscoelastic properties that we will investigate in the scope of this work.

Although the polymers are very complex molecules and their interaction with their surroundings and within themselves, their behavior can be explained by deducing the mean properties such as the average size of the polymer coil. As we will see in the next paragraphs, the different systems can obey the same rules, and their properties can be described by some universal formulas.

1.2.1. Preliminary Concepts

1.2.1.1. Ideal Chains

In the concept of the ideal chains, we assume that there are no interactions between the monomers which are far from each other along the polymer chain, and this assumption remains valid even when the monomers approach each other in space. Clearly, this assumption is not realized in the case of real chains since the real chains interact with both their solvent and each other, however the ideal chain conformation with no interactions between monomers is an essential starting point for most of the modelling in polymer physics.

To understand the polymer chain conformations, we need to look at the flexibility mechanisms. Polymer flexibility comes mostly from the variation in torsion angles along the chain.

When all the torsion angles are in the trans state on a polymer chain as in a rod-like zig-zag conformation, we achieve the largest possible end-to-end distance, R_{max}, which is also called the contour length. R_{max} can be written as the product of number of bonds (n), and the projected length of these bonds (lcos(θ/2)): $R_{max} = nlcos\left(\frac{\theta}{2}\right)$

Considering a flexible polymer chain of n+1 backbone atoms, the sum of all n bond vectors is called end-to-end vector, $\vec{R}_n$. Since different chains have different $\vec{R}_n$, a distribution of end-to-end vectors is formed and it is important to note that average end-to-end vector of an isotropic collection of polymer chains of n bonds, is zero. Therefore, it is more useful to come up with a non-zero term to characterize the ideal chain conformations. The simplest non-zero average is the mean-square end-to-end distance: $\langle \vec{R}_n^{\,2} \rangle = \langle \vec{R}_n \rangle . \langle \vec{R}_n \rangle$

Assuming that the bond length, l is constant and there are no correlations between the directions of different bond vectors as it is the case in the *freely jointed chain model*; $\langle \vec{R}_n^{\,2} \rangle$ can be written in the following form: $\langle \vec{R}_n^{\,2} \rangle = nl^2$

However, a better approximation would be: $\langle \vec{R}_n^{\,2} \rangle = C_n nl^2$ wherein C_n is the *Flory's characteristic ratio* which describes the fact that correlations between bond vectors for all the bond vectors along a long and flexible chain converge to a finite value and this parameter is related to local stiffness of the polymer chain. In fact, C_n saturates at C_∞ for longer chains and therefore, $\langle \vec{R}_n^{\,2} \rangle = C_\infty nl^2$ can be written.

To be able to neglect the chemical structure to describe the universal properties of the flexible polymers, a simple concept of *equivalent freely jointed chain* is provided. The equivalent chain is composed of N freely-jointed effective bonds which can be called as Kuhn monomers that have the effective bond length b, the Kuhn length. Inside the Kuhn monomers, the polymer behaves like an ideal chain. Then the contour length can be written as $R_{max} = Nb$ since the equivalent chain has the same maximum end-to-end distance R_{max} and same mean-square end-to-end distance $\langle \vec{R}_n^{\,2} \rangle$.

Therefore; $\langle \vec{R}_n^{\,2} \rangle = Nb^2 = bR_{max} = C_\infty nl^2$ and from this relation, number of Kuhn monomers N and the Kuhn length b can be found. In freely jointed chains, each bond of

Kuhn length b is assumed to be completely rigid, so Kuhn length b indicates the flexibility of the chain in this sense.

While the size of linear chains can be characterized by their mean-square end-to-end distance, characterization of the branched or ring polymers require another quantity because they might have a different architecture with too many ends or no end at all. For this reason, it is better to define a quantity called the *radius of gyration* which is the average square distance between the monomers and the centre of mass of the polymer chain.

1.2.1.2. Real Chains

As aforementioned, the ideal chain models neglect the interaction between monomers to provide a simple approach to modelling, however we sometimes need more realistic approaches to be able to investigate more complex phenomena such as the effect of ionic strength on the polymer chains. To take the monomer-monomer interactions into consideration, one needs to estimate the number of contacts along a single coil and the probability of the monomers that are separated by many bonds encountering each other. If we think of the ideal chain as an ideal gas of monomers N in its pervaded volume in d-dimensional space (~R^d), this probability is basically the overlap volume fraction ϕ^* which is the product of monomer volume b^d and the number density of the monomers in this pervaded volume $\frac{N}{R^d}$. Since the ideal chains obey the Gaussian statistics in any dimension, we can replace R as $bN^{0.5}$ and then we can write the number of monomer-monomer contacts for a long ideal chain in three-dimensional space as: $N\phi^* \approx N^{0.5} \gg 1$ as $N \gg 1$. Hence, it is important to understand how these contacts affect the conformations of a polymer chain. The effective interaction between monomers can be thought of as a competition between two opposing interactions: when the monomers like to stick together rather than being surrounded by solvent molecules, it means that the monomer-monomer interaction energy is low and there is an attractive effective interaction. Whereas when they prefer being in contact with the surrounding molecules rather than interacting with other monomers, there is a repulsive effective interaction. However, there is a third intermediate case wherein attractive and repulsive interactions cancel each other out and the polymer behaves almost ideally. [38] When distant polymer segments approach each other in space, they interact but they cannot occupy each other's region since the polymer segments have finite volume, this steric effect

contributes to the repulsive forces and leads to the swelling of the polymer chain. This long-range repulsive interaction between segments which are far apart is called the excluded volume (v) effect and it can be said that a net attraction has a negative excluded volume whereas a net repulsion has a positive excluded volume. Excluded volume effect has a big impact on the statistical property of the polymer chain. Due to this effect, $\langle \vec{R}_n^{\,2} \rangle$ becomes proportional to a higher power of N which can be written as $\langle \vec{R}_n^{\,2} \rangle \propto N^{2v}$.

Excluded volume(v) has different values depending on the solvent in which the polymer is present. [10] When the attractive and repulsive interactions counterbalance each other, this environment is called *θ-solvent* in which the excluded volume is zero and the ideal chain conformation holds: $R_0 = bN^{0.5}$. This θ-condition corresponds to a particular *θ-temperature* for a given solvent. When the repulsive interactions dominate over the attractive ones, the excluded volume is positive which means that the polymer chain swells. Such an environment is called the *good solvent* at a temperature higher than *θ-temperature*. Due to the swelling, the coil size gets larger than that of the ideal one and the optimum size of the real chain in the Flory theory (R_F) can be written as: $R_F \approx b\left(\frac{v}{b^3}\right)^{0.18} N^{0.588}$

The opposite case takes place when the attractive interactions dominate over the repulsive ones meaning that excluded volume is negative and the polymer chain assumes the form of a collapsed globular conformation to avoid interacting with the solvent. Such an environment is called the *poor solvent* and this phenomenon occurs at temperatures below *θ-temperature*. As expected, the size of this globule (R_{gl}) is smaller than the size of the ideal chain: $R_{gl} \approx |v|^{-1\backslash 3} b^2 N^{1\backslash 3}$. However, not all the solvent is avoided by this collapsed globular conformation unless we go far below the *θ-temperature*. At the limit wherein attractive interactions dominate completely, a polymer chain would have a complete collapsed conformation, and this is called the *non-solvent* case. As the excluded volume becomes $v \approx -b^3$, the size of the chain: $R \approx bN^{1\backslash 3}$. What we observe would be the precipitation of chains where they take a polymer melt form excluding all the solvent.

Contrarily at the high temperature limit, excluded volume becomes independent of temperature ($v \approx b^3$). Monomer-monomer & monomer-solvent interactions counterbalance, hence the net interaction becomes zero. Then the only interaction left is the hard-core barrier

which corresponds to the energy penalty of the steric repulsion between two overlapping monomers. This is called the *athermal solvent* case at which: $R \approx bN^{0.588}$.

1.2.2. Concentration Regimes

Liquid polymer systems can be examined in 2 categories: polymer melts and polymer solutions. Polymer solutions are obtained by dissolving the polymer with a mass concentration of c in a solvent wherein the c is the ratio between the mass of polymer dissolved and the volume of the solution. Depending on the c, polymer solutions have different concentration regimes such as dilute, semi-dilute and concentrated. In each concentration regime, the polymer-solvent interaction is different as a consequence of a specific way in which the polymer chain perceives its surrounding solvent molecules. Figure 1-5 below represents the concentration regimes of polyelectrolyte solutions in neutral conditions.

We will cover these concentration regimes briefly in the following section, however an introduction to polyelectrolytes theory is fundamental to understand the scales that form the boundaries of these regimes.

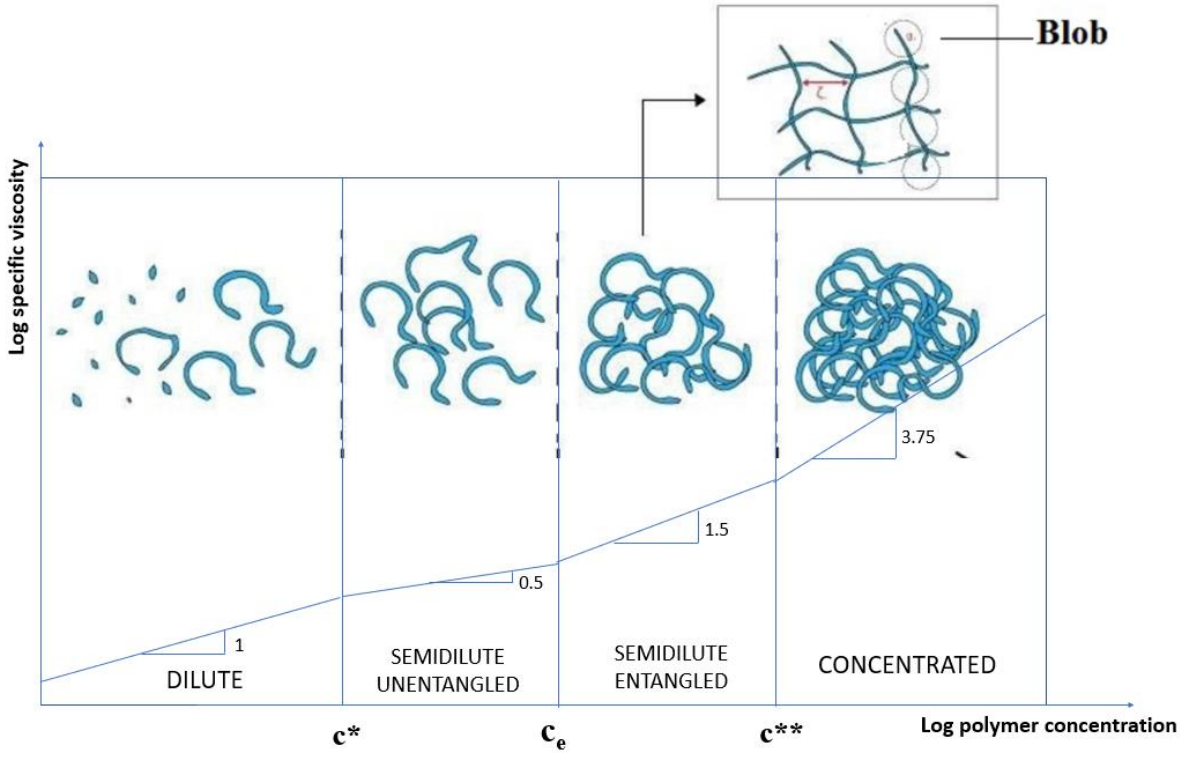

Figure 1-5: Scaling behavior and the concentration regimes for polyelectrolyte solutions in neutral conditions [15]

Theories for Polyelectrolytes

The scaling theory which explains the differences between neutral polymers and the polyelectrolytes is available thanks to the works of de Gennes [3], Colby, Dobrynin and Rubinstein [39] [8]. The main element that distinguishes the polyelectrolytes from neutral polymers is the charges along the polyelectrolyte chain which raise new contributions to their physical properties. Charges contribute to the electrostatic persistence length which is the length of a segment that is persistent (or stiff) (l_p). Odijk, Skolnick and Fixman(OSF) put forward the electrostatic persistence length idea and they predicted that l_p is proportional to the square of the Debye screening length. Debye screening length was defined by Debye-Hückel theory, and it expresses the scale over which the electrostatic effects of a charge carrier in a solution are screened. [8] OSF theory is in accordance with de Gennes' idea of electrostatic blobs inside which the Coulomb repulsion is not sufficient to deform the chain. Hence, the theories suggest that if the Debye screening length is much larger than the

electrostatic blobs, Coulomb repulsion stretches the chain into a stiff straight conformation. However, the computer simulations showed that the distribution of ions along the polyelectrolyte chain is perturbed much more than predicted by theories which result as stronger screening of the electrostatic repulsion and much shorter l_p than the theory predicts. Also, the dependence of the l_p on salt concentration was found to be weaker than expected by these simulations. In disagreement with OSF theory, l_p is proportional to the Debye screening length over a wide range of concentrations. [8]

1.2.2.1. Dilute Regime

In the case of dilute solutions, where the mass concentration of polymer c is smaller than the overlap concentration c*, polymers can be thought of as individual chains. The overlap concentration c* is defined as the point at which the conformations of individual chains start to overlap each other, or the concentration within a given dilute conformation's pervaded volume is equal to the solution concentration: $c^* = \frac{\rho N v_{mon}}{R^3_{dilute}}$ where N is the number of Kuhn monomers in the chain, R_{dilute} is the coil size in dilute solution, ρ is the polymer density, v_{mon} is the occupied volume of a single monomer.

Knowing that $R_{dilute} \sim N^v$, $c^* \approx \frac{N}{R^3_{dilute}} \sim N^{1-3v}$ with v=0.5 for θ-solvent, v=0.588 for good solvent and v=1 for polyelectrolytes in salt-free solutions.

The conformation of individual chains in dilute solutions and their coil size depend on the type of the solvent and whether the polymer is a neutral one or a polyelectrolyte. Neutral polymers' conformation in poor solvent, θ-solvent, good solvent and athermal solvent environments are described in the previous section. Conformation of polyelectrolytes in salt-free dilute solutions, however, is quite different than these as it can be seen from the relation $R_{dilute} \sim N^v \sim N$ as v=1 in this case. Each macromolecule in this regime can be represented as a chain of electrostatic blobs of size D as Figure 1-6 represents below.

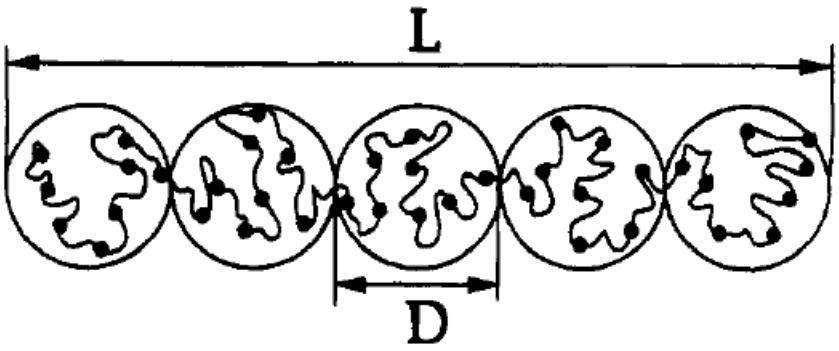

Figure 1-6: Polyelectrolyte chain in dilute salt-free solution. Filled circles represent the charged groups on the polyelectrolyte chain and the chain takes an extended (rod-like) configuration of electrostatic blobs of size D. [8]

On a polyelectrolyte chain, we can imagine that there are charges that repel each other such that the charge repulsion dominates the other interactions and stretches the chain into a directed random walk of electrostatic blobs.

Hence, for polyelectrolytes in salt-free solutions $c^* \approx \frac{N}{L^3} \sim N^{-2}$; for neutral polymers in good solvent $c^* \sim N^{-0.76}$; and for neutral polymers in θ-solvent $c^* \sim N^{-0.5}$.

1.2.2.2. Semi-dilute Regime

i.Semi-dilute Unentangled

By a concept first introduced by Edwards [14], that is called the correlation length ξ, we can define the boundaries of the semi-dilute regime that covers the solutions with a concentration above c^*. We can think of the correlation length ξ, as a measure of distance between two chains in the given solvent and it also gives an estimation of the mesh size. On scales shorter than the ξ, we can imagine that there are mostly only monomers and solvent molecules such that the dilute solutions' rules apply to both structure and dynamics. However, as we go up to the scales larger than the ξ, there are many other chains, and the chain assumes a conformation of random walk of correlation blobs of size ξ. At this point, melt-like rules apply and ξ starts to be termed as the screening length because excluded volume interactions, hydrodynamic interactions, and for polyelectrolytes, charge repulsion interactions get screened.

De Gennes showed that ξ does not depend on the chain length no matter what the solution is, and the concentration dependence of ξ can be written as: $\xi \approx c^{-v/(3v-1)}$.

For θ-solvent, $\xi \sim c^{-1}$ as v=0.5 and, for good solvent, $\xi \sim c^{-0.76}$ as v=0.588 and, for polyelectrolytes in salt-free solution $\xi \sim c^{-0.5}$ as v=1. As the end-to-end distance of the chain in semi-dilute solution is $R \approx \xi(\frac{N}{g})^{0.5} \sim N^{0.5} c^{-(v-0.5)/(3v-1)}$ where g is the number of monomers per correlation blobs; for neutral polymers in θ-solvent $R \sim N^{0.5} c^{0}$, for neutral polymers in good solvent $R \sim N^{0.5} c^{-0.12}$.

From the scaling assumption by De Gennes[6] we also know that the correlation length ξ has a power law concentration dependence for c>c*: $\xi \approx L(c/c^*)^m$ where m can be determined as -0.5 from the molecular weight dependence of the overlap concentration $c \sim N^{-2}$ and the dilute chain size L~N for polyelectrolytes with a fully extended chain of electrostatic blobs. Then we can find the concentration dependence of the size of a polyelectrolyte chain in the semi-dilute regime to be $R \sim c^{-0.25}$ as it was described in [8]. Therefore, we can note that size of the chain has a stronger concentration dependence for the polyelectrolyte chain than it has for a neutral polymer in the semi-dilute region. [3]

ii. Semi-dilute Entangled

Topological constraints such as the fact that chains cannot cross each other leads to the formation of chain entanglements. [38] The most successful model for chain entanglements is called the Edwards tube model which confines the motion of any long chain to a tube-like region. The chain entanglement starts to take place at a specific concentration called the entanglement concentration, c_e which shows itself at the point where there is an abrupt change in the power-law exponent for the concentration dependence of viscosity. Scaling factor increases roughly with a factor of three as the concentration regime changes from unentangled to entangled in the semi-dilute range. It has been reported that $c_e \sim 10c^*$ for neutral polymers in good solvent, whereas for high molar mass polyelectrolytes in salt-free solutions $c_e >> c^*$ by almost a factor of 1000 which results as a wider semi-dilute unentangled concentration regime for polyelectrolytes when compared to neutral polymers. [3]

1.2.2.3. Concentrated Regime

It is possible to define the concentration regimes as dilute, semi-dilute unentangled and semi-dilute entangled for neutral polymers, however, for polyelectrolytes, there is a fourth regime that is called the concentrated regime at $c > c_D$, wherein the screening radius becomes of the order of the electrostatic blob size D. In this regime electrostatic blobs begin to overlap and the solution dynamics of polyelectrolytes crossover that of neutral polymers since the screening of Coulomb interactions is caused by the contribution of polyions along the polyelectrolyte chains in the system. Therefore, c_D can be expressed as the concentration at which this crossover takes place. [8][21][39]

1.2.3. Linear Viscoleasticity (LV) and Polymer Dynamics

To describe the viscoelastic properties of the solutions, there are different models to consider in different concentration regimes.

Linear viscoelasticity of dilute solutions and of semi-dilute solutions inside their correlation volumes is described by 1956 Zimm Model. LV of semi-dilute unentangled solutions and for entangled solutions on the scale of the entanglement strand is described by 1953 Rouse Model whereas LV of entangled solutions is described by 1971 De Gennes reptation model. Let us cover the polymer dynamics in two groups to display their viscoelastic response: entangled and unentangled polymer dynamics. [38]

1.2.3.1. Unentangled Polymer Dynamics ($c < c_e$)

There are two limits for unentangled polymer dynamics one of which is the Zimm limit that applies to dilute solutions whereas the other one is the Rouse limit, and it applies to the unentangled polymer melts. These two limits are separated from each other by a length scale that is called the hydrodynamic screening length ξ_h. On length scales shorter than ξ_h, the hydrodynamic interactions dominate and Zimm model can be used to describe the polymer dynamics. However, on length scales larger than ξ_h, the hydrodynamic interactions are screened by the presence of surrounding chains, therefore the dynamics are described by the Rouse model.

i. Zimm Model

The reason why the Zimm Model is best to describe the dynamics in dilute solutions is that it does not ignore the hydrodynamic interaction forces as Rouse model does and hydrodynamic interactions between the monomers in the polymer chain are too strong to ignore in dilute solutions. These interactions are also strong between monomers and the solvent within the pervaded volume of the chain such that the polymer chain drags the solvent in its pervaded volume with itself, as it moves. Therefore, we treat the pervaded volume of the chain as a solid object moving through the surrounding solvent and that is why the Zimm model is a good approach for dilute solutions.

The chain diffuses a distance of order of its own size during the Zimm time τ_z: $\tau_Z \approx \frac{R^2}{D_Z} \approx \tau_0 N^{3v}$ where D_z is the diffusion coefficient of a chain in the Zimm model and $\tau_0 \approx \frac{n_s b^3}{kT}$ is the monomer relaxation time.

ii. Rouse Model

In this model the chain is thought of as N monomers mapped onto a bead-spring chain of N beads connected by springs wherein the beads only interact with each other. The solvent is assumed to be freely moving independently from the chain. The polymer diffuses a distance of order of its size during the Rouse time, τ_R: $\tau_R \approx \frac{R^2}{D_R} \approx \tau_0 N^{1+2v}$ where D_R is the diffusion coefficient of a chain in the Rouse model.

Comparison of these shows that Zimm time has a weaker dependence on the chain length than the Rouse time when v<1. [38]

After determining the appropriate relaxation times in different models, we can find the value of the stress relaxation modulus $G(\tau)$ in either Rouse or Zimm models. Knowing that the polymer contribution to the viscosity in either of these models is

proportional to G(τ) τ, we obtain the scaling predictions that were reported by de Gennes. (Table 1-1)

	General equation	Neutral in θ-solvent	Neutral in good solvent	Polyelectrolyte with no salt
Scaling exponent	$\upsilon \equiv \partial(\log R_{\text{dilute}})/\partial(\log N)$	$\upsilon = 1/2$	$\upsilon = 0.588$	$\upsilon = 1$
Correlation blob size	$\xi \sim N^0 c^{-\upsilon/(3\upsilon-1)}$	$\xi \sim N^0 c^{-1}$	$\xi \sim N^0 c^{-0.76}$	$\xi \sim N^0 c^{-1/2}$
Polymer size	$R \sim N^{1/2} c^{-(\upsilon-1/2)/(3\upsilon-1)}$	$R \sim N^{1/2} c^0$	$R \sim N^{1/2} c^{-0.12}$	$R \sim N^{1/2} c^{-1/4}$
Chain relaxation time	$\tau_{\text{chain}} \sim N^2 c^{(2-3\upsilon)/(3\upsilon-1)}$	$\tau_{\text{chain}} \sim N^2 c$	$\tau_{\text{chain}} \sim N^2 c^{0.31}$	$\tau_{\text{chain}} \sim N^2 c^{-1/2}$
Terminal modulus	$G = N^{-1} c_n kT$	$G = N^{-1} c_n kT$	$G = N^{-1} c_n kT$	$G = N^{-1} c_n kT$
Polymer contribution to viscosity	$\eta - \eta_s \approx G\tau_{\text{chain}} \sim Nc^{1/(3\upsilon-1)}$	$\eta - \eta_s \sim Nc^2$	$\eta - \eta_s \sim Nc^{1.3}$	$\eta - \eta_s \sim Nc^{1/2}$
Diffusion coefficient	$D \approx R^2/\tau_{\text{chain}} \sim N^{-1} c^{-(1-\upsilon)/(3\upsilon-1)}$	$D \sim N^{-1} c^{-1}$	$D \sim N^{-1} c^{-0.54}$	$D \sim N^{-1} c^0$

Table 1-1: De Gennes scaling predictions for semi-dilute unentangled [3]

These predictions show a unique rheological behavior of polyelectrolytes; for polyelectrolytes in salt-free solution $\tau_{chain} \sim N^2 c^{-0.5}$ revealing a negative exponent for concentration dependence which means that their relaxation time increases as the concentration lowers. This explains why the shear thinning starts at much lower rates as the solution is diluted. The unusual concentration dependence of relaxation time leads to an unusually weak concentration dependence of specific viscosity as $\eta - \eta_s \sim Nc^{0.5}$. [3]

1.2.3.2. Entangled Polymer Dynamics

As aforementioned, the most successful model to describe the topological constraints when we go beyond the entanglement concentration was Edwards tube model. De Gennes reduced this many-body problem to the motion of a single chain confined to a tube of surrounding chains. The simplest tube models proposed by de Gennes for the motion of linear entangled polymers is called the reptation model.

Gennes Reptation Model

The name comes from the diffusion of an entangled chain along its confining tube in a way that is analogous to the motion of a snake. The chain diffuses out of its initial tube of average length $\langle L \rangle$ during the reptation time, τ_{rep}: $\tau_{rep} \approx \frac{\langle L \rangle^2}{D_c}$

where D_c is the curvilinear diffusion coefficient of a chain in the reptation model.

Using this model concentration dependence of relaxation time is found in the general form: $\tau_{rep} \sim N^3 c^{3(1-v)/(3v-1)}$. Similarly, polymer contribution to the viscosity can be found as: $\eta - \eta_s \sim N^3 c^{3/(3v-1)}$. It is important to note that scaling factor for the concentration dependence of viscosity increases by roughly a factor of 3 as we go from unentangled ($c < c_e$) to entangled ($c > c_e$) regimes. These scaling predictions for 3 universal classes of polymers are reported by De Gennes. (Table 1-2)

	General equation	Neutral in θ-solvent	Neutral in good solvent	Polyelectrolyte with no salt
Scaling exponent	$v \equiv \partial(\log R_{\text{dilute}})/\partial(\log N)$	$v = 1/2$	$v = 0.588$	$v = 1$
Correlation blob size	$\xi \sim N^0 c^{-v/(3v-1)}$	$\xi \sim N^0 c^{-1}$	$\xi \sim N^0 c^{-0.76}$	$\xi \sim N^0 c^{-1/2}$
Polymer size	$R \sim N^{1/2} c^{-(v-1/2)/(3v-1)}$	$R \sim N^{1/2} c^0$	$R \sim N^{1/2} c^{-0.12}$	$R \sim N^{1/2} c^{-1/4}$
Tube diameter	$a \sim \xi$ *	$a \sim N^0 c^{-2/3}$	$a \sim N^0 c^{-0.76}$	$a \sim N^0 c^{-1/2}$
Reptation time	$\tau_{\text{rep}} \sim N^3 c^{3(1-v)/(3v-1)}$ *	$\tau_{\text{rep}} \sim N^3 c^{7/3}$	$\tau_{\text{rep}} \sim N^3 c^{1.6}$	$\tau_{\text{rep}} \sim N^3 c^0$
Terminal modulus	$G_e = \frac{kT}{a^2 \xi}$	$G_e \sim N^0 c^{7/3}$	$G_e \sim N^0 c^{2.3}$	$G_e \sim N^0 c^{3/2}$
Polymer contribution to viscosity	$\eta - \eta_s \approx G\tau \sim N^3 c^{3/(3v-1)}$ *	$\eta - \eta_s \sim N^3 c^{14/3}$	$\eta - \eta_s \sim N^3 c^{3.9}$	$\eta - \eta_s \sim N^3 c^{3/2}$
Diffusion coefficient	$D \approx R^2/\tau \sim N^{-2} c^{-(2-v)/(3v-1)}$ *	$D \sim N^{-2} c^{-7/3}$	$D \sim N^{-2} c^{-1.85}$	$D \sim N^{-2} c^{-1/2}$

Table 1-2: De Gennes scaling predictions for semi-dilute entangled [3]

Scaling behavior of viscosity as a function of concentration predicted by theories is depicted for the 3 universal polymer classes: neutral polymer in θ solvent, neutral polymer in athermal/good solvent and polyelectrolytes in salt-free case in the Figure 1-7: Scaling behavior of viscosity as a function of concentration predicted by theories is depicted for the 3 universal polymer classes. below as a summary.

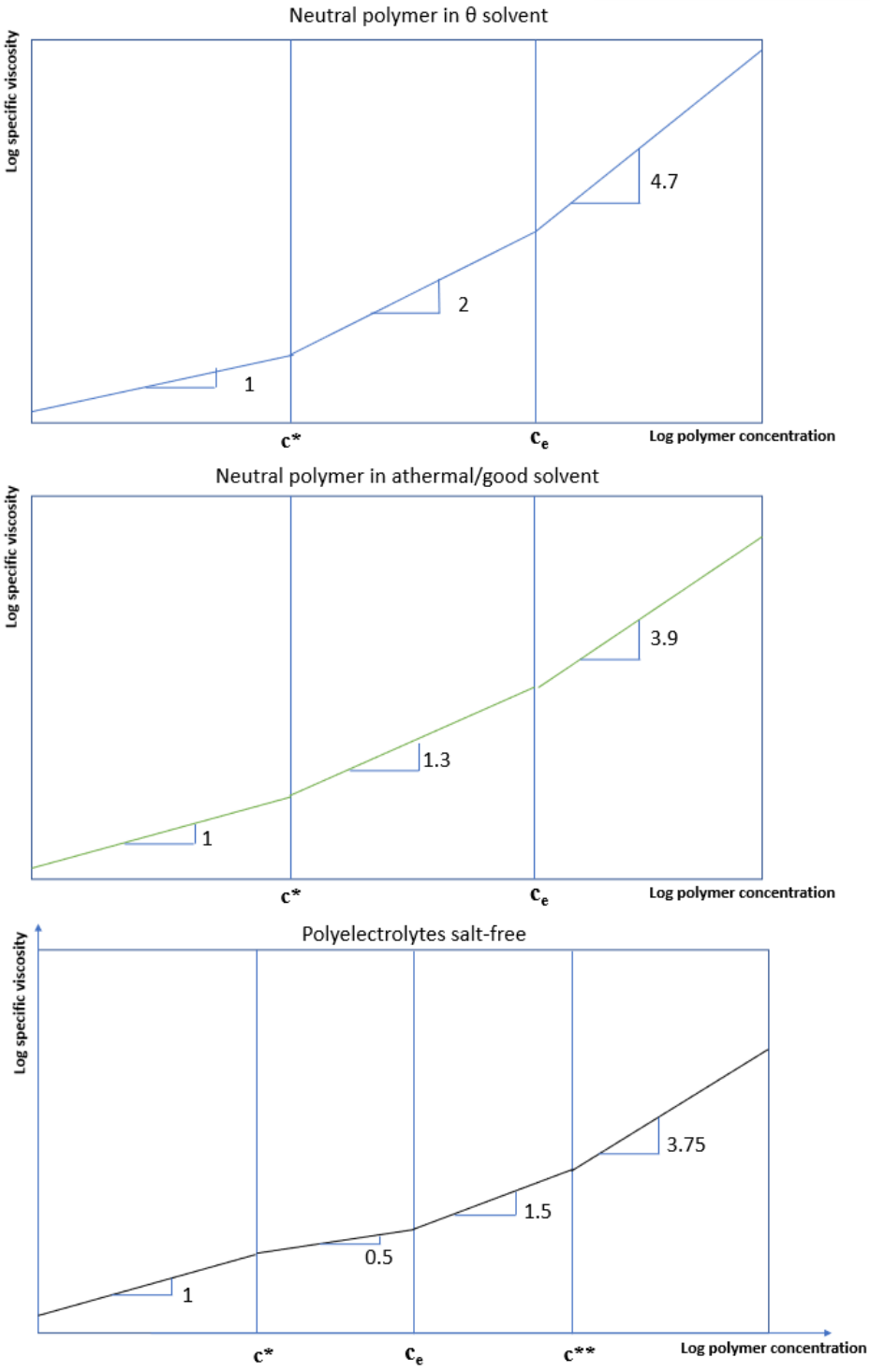

Figure 1-7: Scaling behavior of viscosity as a function of concentration predicted by theories is depicted for the 3 universal polymer classes.

1.2.4. Polyelectrolytes

As aforementioned, polyelectrolytes take a rigid rod like conformation in salt free solutions differently than the flexible polymers with a random coil structure. Some of the main distinctions between these two can be described as following:

i. If we imagine two polymers with the same molecular weight, rod-like polymers are much larger than the flexible polymers. Radius of gyration, R_g is proportional to the contour length or the molecular weight M of the polymer by the relation: $R_g \propto M^v$ wherein v=1 for rod-like polymers and v=0.6 for flexible polymers. In dilute solutions, this elongated form of rod-like polymers results as *larger intrinsic viscosity* and relaxation time, or smaller diffusion constant when compared to those of flexible polymers.

ii. Due to their larger size, interaction of the rod-like polymers becomes important at much lower concentrations when compared to the flexible polymers. Also, the effect of entanglement becomes much more remarkable in the case of rod-like polymers and the distinction between flexible and rod-like polymers gets more pronounced at higher concentrations. [10]

1.2.4.1. Effect of Salt on the Rheological Properties of the Polyelectrolyte Solutions

Polyelectrolyte conformation in salt-free solutions was described in the previous sections. However, this rod-like conformation of polyelectrolytes in salt-free solutions changes drastically with the addition of salt into the system. The electrostatic repulsion caused by the presence of polyions along the polyelectrolyte chain can be screened by salt ions added in the system. The salt ions screen the Coulomb interaction when the polymer concentration c is much lower than the crossover concentration $2Ac_s$ where c_s is the electrolyte concentration and A is a parameter describing the average number of monomers between the charges on the chain. [8] If $c >> 2Ac_s$, screening effect of salt ions is small enough to neglect and polyelectrolyte rod-like conformation in salt-free solutions is recovered. However, at the

high-salt limit when c << $2Ac_s$, rod-like conformation turns into a collapsed globular conformation of polymer coil as it is represented in the Figure 1-8 below.

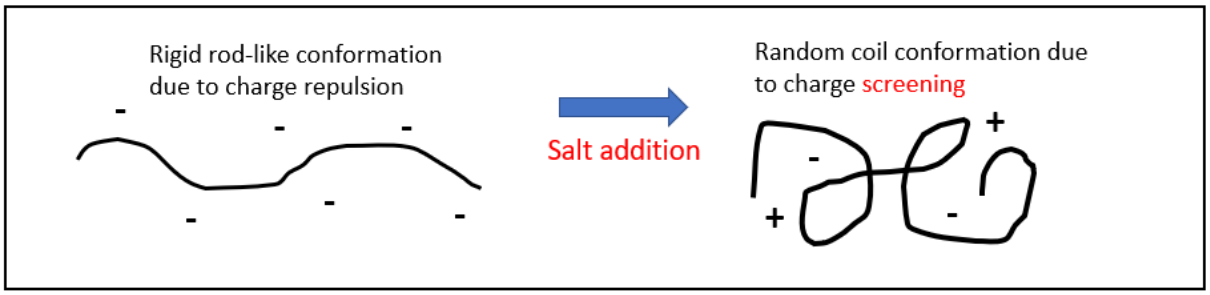

Figure 1-8: Screening effect of salt addition

In the high-salt limit, overlap concentration c^* and the correlation length ξ changes too while the degree of polymerization N dependence of c^* becomes the same as the one for neutral chains in good solvent. [8][48] Similarly concentration dependence of viscosity in high-salt limit takes the same form of the neutral polymers in good solvent.

	Semi-dilute unentangled	Semi-dilute entangled
Low-salt limit (c >> $2Ac_s$)	$\eta \sim c^{0.5}$	$\eta \sim c^{3/2}$
High-salt limit (c << $2Ac_s$)	$\eta \sim c^{5/4}$	$\eta \sim c^{15/4}$

Table 1-3: Concentration dependence of viscosity in semi-dilute unentangled and entangled region in low and high salt limits

Effect of monovalent salt addition to rheological properties was expressed by the form [39]: $\chi \approx \chi_0(1 + 2Ac_s/c)^{\alpha}$ where χ is some rheological property of the polyelectrolyte solution in the presence of salt whereas χ_0 is that in salt-free case. $2Ac_s/c$ is the ratio of salt ion to counterion. The values of α are reported in theTable 1-4 below taken from [39] for various properties.

	Statics			Unentangled				Entangled			
X	ξ	g	R	τ	G	D	η	τ	G	D	η
α	$\frac{1}{4}$	$\frac{3}{4}$	$-\frac{1}{8}$	$-\frac{3}{4}$	0	$\frac{1}{2}$	$-\frac{3}{4}$	$-\frac{3}{2}$	$-\frac{3}{4}$	$\frac{5}{4}$	$-\frac{9}{4}$

Table 1-4: predicted exponents alpha for varius properties χ [39]

1.2.4.2. Effect of Salt in Rheological Properties of Polyelectrolyte Hydrogels

The theoretical works of Rubinstein, Colby and Dobrynin[56] and the experimental findings [57][58] are in agreement on the effect of ionic strength on the shear modulus of polyelectrolyte gels. There are opposing effects of salt addition to the polyelectrolyte gel networks on their mechanical properties: modulus of polyelectrolyte gels can increase and decrease with salt addition. To understand the mechanisms behind these effects, let us introduce theory of gelation and swelling briefly.

The swollen gel is in fact a solution, an elastic one rather than a viscous one. As the network is swollen by the absorption of solvent, the chain segments in between network junctions assume some elongated configurations. In opposition to this swelling process, a force akin to the elastic retractive force starts to develop. This force increases as the swelling goes on, while the diluting force decreases until a state of equilibrium is reached at which these two forces are balanced. If the network is formed by polymer chains that contain ionizable groups, the swelling forces are increased due to the localization of the charges on the polymer chains. This large electrostatic repulsion that tends to expand the gel network. The equilibrium between the swollen ionic gel and its electrolyte surrounding resembles Donnan membrane equilibria wherein the polymer acts as its own membrane, preventing the charges distributed within itself from diffusing into the outer solution, creating an osmotic pressure. Hence, the polyelectrolyte gels are capable of swelling to much greater extents than their uncharged counterparts. The electrostatic repulsion might be screened by the addition of a salt that can equalize the concentrations of ions inside and outside, and thus to decrease the osmotic expansive force. [18][56]

If we consider polyelectrolyte gels, prepared by a randomly cross-linking semi-dilute solution of linear polyelectrolyte chains, the shear modulus of the network in its preparation state (G_0) is simply kT per strand wherein k is the Boltzmann constant and T is the temperature. Then, G_0 can be written in the form: $G_0 \cong \frac{c_0}{N} kT$ where c_0 is the monomer number density and N is the average number of monomers per strand. This relation holds for strongly crosslinked gels, independent of the charge on the chain and salt concentration.

When polyelectrolyte gels are swollen, the strands of the gel are stretched. We therefore need to consider stretching of polyelectrolyte chains by pulling their ends with force. There are 3 possibilities for the configuration of a stretched polyelectrolyte chain: weak, intermediate and strong stretching distinguished by the length scales on which the stretching occurs. In all cases, the modulus of a polyelectrolyte gel is the product of the energy for stretching a strand (E) and the number density of strands (c/N), where c is the number density of monomers: $G \cong \frac{c}{N} E$. This relation has been used to derive predictions for the modulus of polyelectrolyte gels as functions of polymer concentration, salt concentration and effective charge.

Here we will only mention the modulus in the weak stretching regime[56] since it fits nicely to the experimental studies [58][57] to comprehend the effect of ionic strength. The modulus in the weak stretching regime can be written as: $G \cong \frac{ckT}{N} \left(\frac{\lambda R_0}{R}\right)^2$ where R_0 is the strand size in the preparation state, λ is the expansion factor, R is the size of the strand would have, if it were a free chain of N monomers in the new state. This equation helps us to understand the increase of modulus with ionic strength: Since increasing the salt concentration decreases the free chain size (R) due to the screening of electrostatic repulsions along the polyelectrolyte chain, the modulus G increases.

On the other hand, when modulus dependence on the salt concentration and counterion condensation is compared in low-salt limit and high-salt limit [56], the predictions indicate a decrease in modulus with charge addition to the system.

1.3. Bibliographic Review on SA Solutions and SA-Based Hydrogels

This chapter provides a brief review of the approaches and findings in which previous studies have reported on SA solutions and SA-based hydrogels. The path to investigate the rheological properties of solutions and hydrogels is described along with the gelation phenomenon. There are also some studies on other polysaccharides reported that points out to the effect of ionic strength on rheological properties of those solutions and gels, which will be relevant for the discussion of our findings in the next chapters.

Sodium alginate-based materials are of great importance in the pharmaceutical and biomedical fields, and also in the food industry thanks to their biocompatibility, immunogenicity, non-toxicity, bioadhesion and gelling ability. Many studies have been carried out to study their properties, gelation mechanisms, responsive behaviors for their application in transplantation of cells, drug-delivery systems, scaffold for cell cultivation, bio-ink in the 3D bioprinting, microsensors and artificial muscles. [37][43][19][32][5][40]. There are both ionic and chemical[22] gelation methods developed, however one of the main advantages of SA for some of these applications is the ionotropic gelation which is facilitated by an instantaneous physical crosslinking phenomenon in the presence of multivalent cations. Although many cations have been used for the physical crosslinking such as Cu^{2+}, Co^{2+}, Mn^{2+}, Sr^{2+}, Ba^{2+}, Fe^{2+}/ Fe^{3+} and Al^{3+}, the studies on calcium alginate hydrogels are numerous because the first and most widespread model for alginate gelation was called the egg-box model which involved Ca^{2+} ions. [35] [9]

The egg-box model and the underlying gelation mechanism were introduced in the previous chapter about SA. This model proposed by Morris [35] has been improved by recent studies and, three distinctive steps in the binding of calcium to alginate with increasing Ca^{2+} concentration, were revealed: i) interaction of Ca^{2+} with a single guluronate unit forming monocomplexes; ii) pairing of these monocomplexes which leads to the formation and propagation of egg-box dimers; and iii) lateral association of the egg-box dimers to generate multimers. [17]

Adjusting the properties of SA solutions and gels for their specific use in the biotechnological applications requires a good comprehension of the materials' behavior

when a mechanical or chemical stimulus is applied. Hence, the investigation of the relationships between chemical, rheological properties along with the cross-linking properties of SA solutions and gels is of great interest.

1.3.1. Alginate Solutions

The alginate solutions have been characterized by rheology tests extensively. The devices used for this purpose were mostly capillary viscometer and rotational rheometer to assess their shear behavior and investigate the factors affecting their viscosity. Alginate is mostly obtained in the powder form and the solutions are prepared by dissolving the alginate powder in the solvent until a homogeneous solution is obtained by stirring. [43][37][32][31][9][2][51][50].

The importance of M/G ratio was aforementioned in the previous chapters (See 1.1.2.1). Since G-blocks play an active role in Ca^{2+} binding, low M/G ratio leads to stiffer gels and rheological behavior of the solutions is highly affected by the intrinsic chemical composition (properties such as molecular weight and M/G ratio) of SA. Hence, in most of the studies, determination of M/G ratio of SA is the first step.

M/G ratio can be determined by FTIR spectroscopy [9] as these monomers have different absorption bands, or by NMR spectroscopy. [50][51]

Rheological tests on SA solutions

Steady state shear rheometry is one of the primary tools to investigate viscosity and the factors affecting the viscosity of the solutions. These tests also reveal the behaviors such as shear thinning. Results are reported as flow curves which display the viscosity as a function of shear rate. Figure 1-9 shows the flow curves for a shear thinning SA solution as the viscosity decreases with shear rate.

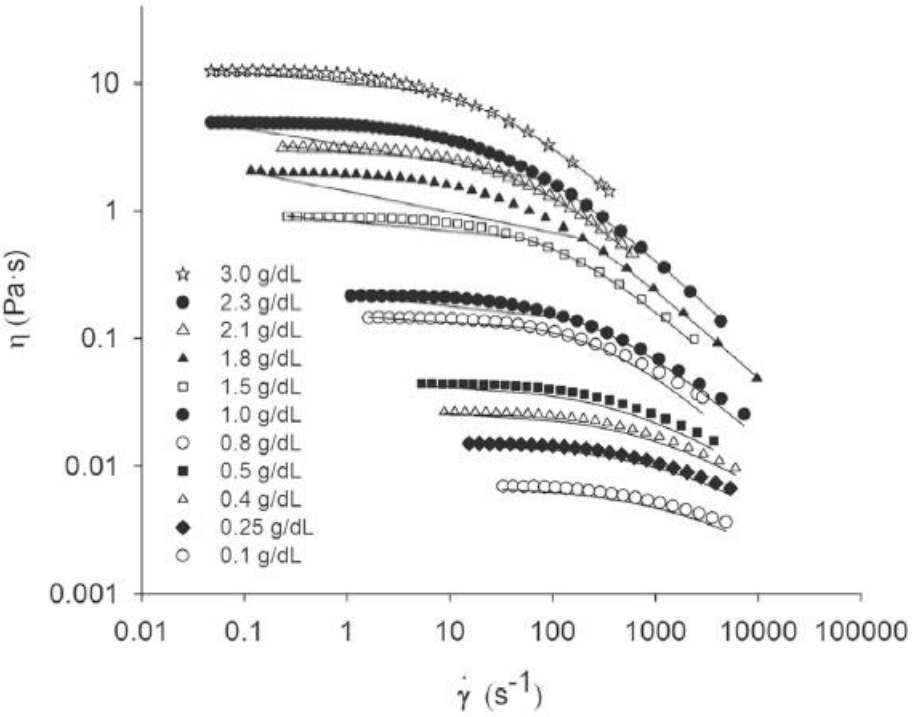

Figure 1-9: Flow curves for different SA concentrations-shear viscosity as a function of shear rate [37]

Using Cross equation to fit the data; the transition point from Newtonian to non-Newtonian behavior can be estimated. Parameters such as zero-shear viscosity, relaxation time, critical shear rate value for the transition and the power-law exponent for the solution can be found. [37]

Estimation of intrinsic viscosity

The intrinsic viscosity $[\eta]$ is determined by capillary viscometry [37][2] or rotational rheometry. [9][43] It provides insight about the solute-solvent interaction and can be found from the reduced viscosity (η_{sp}/c) by extrapolation to zero concentration [37] as in the equation : $[\eta] = \lim_{c \to 0} \frac{\eta_{sp}}{c}$.

Once the intrinsic viscosity is found, the molecular weight can be estimated via Mark-Houwink equation: $[\eta] = K(M)^a$ where K and a are empirical constants and M is the viscosity average molecular mass. For globular proteins a=0, while for θ-solvents a=0.5, for random coil conformation in good solvents 0.7< a <0.8 and at higher values for rod-like molecules in good solvent (up to 1.8). [2] The number average and weight average molecular

weights can be found from NMR tests, but Mark-Houwink equation provides the advantage of estimating them from simpler rheology tests. Empirical relation for number average molecular weight (M_n) is the following: $[\eta] = 0.095(M_n)^{0.963}$ and for the weight average molecular weight (M_w): $[\eta] = 0.023(M_w)^{0.984}$.

When these two properties are found, polydispersity index can be calculated from the ratio between M_w and M_n. [9] Since SA is of a natural origin, polydispersity index is usually very high.

$[\eta]$ can also be determined from Huggins and Kramer equations from the variation of apparent viscosity with polymer concentration. Huggins equation gives:

$$\frac{\eta-\eta_s}{\eta_s c} = [\eta] + k_H[\eta]^2 c + \cdots \qquad (1)$$

where k_H is a measure of polymer-solvent and polymer-polymer interactions [51].

Kramer equation is as follows:

$$\frac{\ln(\frac{\eta}{\eta_s})}{c} = [\eta] + (k_H - \frac{1}{2)[\eta]^2 c} + \cdots \qquad (2)$$

We obtain a reliable result for $[\eta]$ if both equations give the same result. [9][51]

There is also a truncated Taylor expansion of the Huggins equation (Eq. 1) which can be used to determine $[\eta]$, and this version can be applied to all concentration regimes with a better fitting, even to the concentrated regime [43].

$$\eta_{sp} = [\eta]c + k_H[\eta]^2c^2 + A[\eta]^n c^n \qquad (3)$$

One of the most significant differences between polyelectrolytes and neutral polymers is that the reduced viscosity decreases as polymer concentration increases, reaches a minimum value and then increases with the polymer concentration, differently than neutral polymers. This phenomenon results in a U shape reduced viscosity versus polymer concentration curve as Figure 1-10[37] &, Figure 1-11[32] displayed below. When truncated Taylor expansion of Huggins equation is applied to a polyelectrolyte solution, the region at which the reduced viscosity drop is neglected.

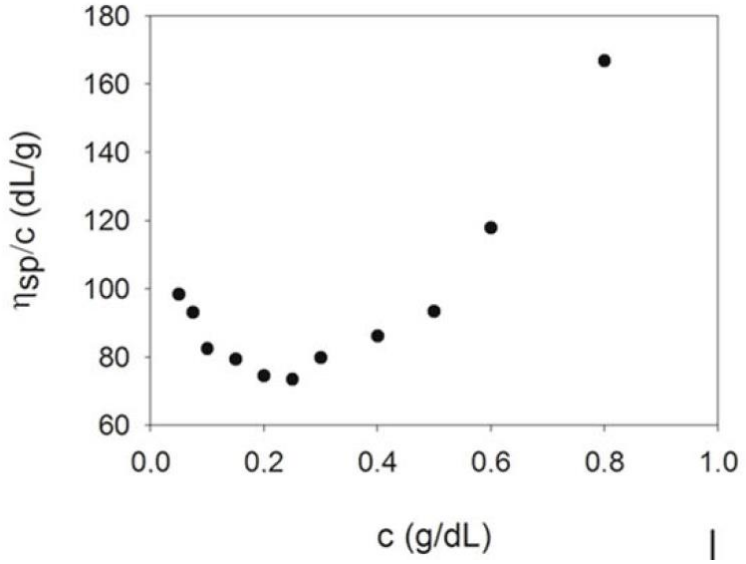

Figure 1-10: Effect of alginate concentration on the reduced viscosity(n_{sp}/c) of sodium alginate aqueous solutions [37]

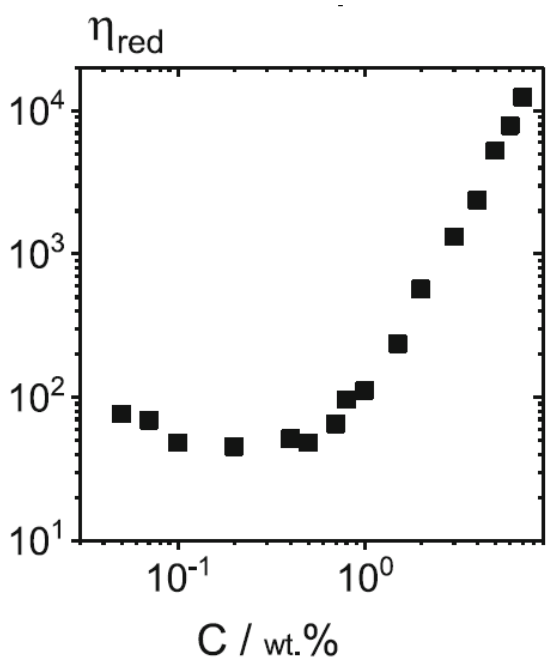

Figure 1-11: Reduced viscosity as a function of alginate concentration [32]

Another important investigation is to distinguish concentration regimes of the solutions. When specific viscosity is reported as a function of polymer concentration (c), we obtain a power-law relation such as $\eta_{sp} = b * c^a$ wherein a is the scaling factor. When this relation is plotted in a double logarithmic scale, the slope of the linear fit gives the scaling factor. Then the critical concentration corresponding to concentration regimes can be distinguished from the points at which the slope changes. If the material has high polydispersity, distinguishing the concentration regimes might be harder.[43] The differences between polyelectrolytes and neutral polymers can be deducted from the differences with the scaling factors especially in the semi-dilute regimes. [9] However, the concentrated regime comes with high entanglement density and the screening of electrostatic interactions due to the presence of many free ions in the solution. Since the screening of charges would change the rod-like conformation of polyelectrolytes to a globular-collapsed conformation, concentrated region of a polyelectrolyte has a similar scaling behavior as the neutral polymer in good solvent does. [32] Hence, they are hard to distinguish from each other in the concentrated regime.

While the semi-dilute regions can be determined without much struggle, the boundary of the dilute regime, overlap concentration c^* is hard to point out by experimental measurements.

Since the viscosity values in the dilute regime is very low, c^* is usually found from the point at which the η_{sp} is around 1(Figure 1-12) for both the polyelectrolytes and neutral polymers. [9]

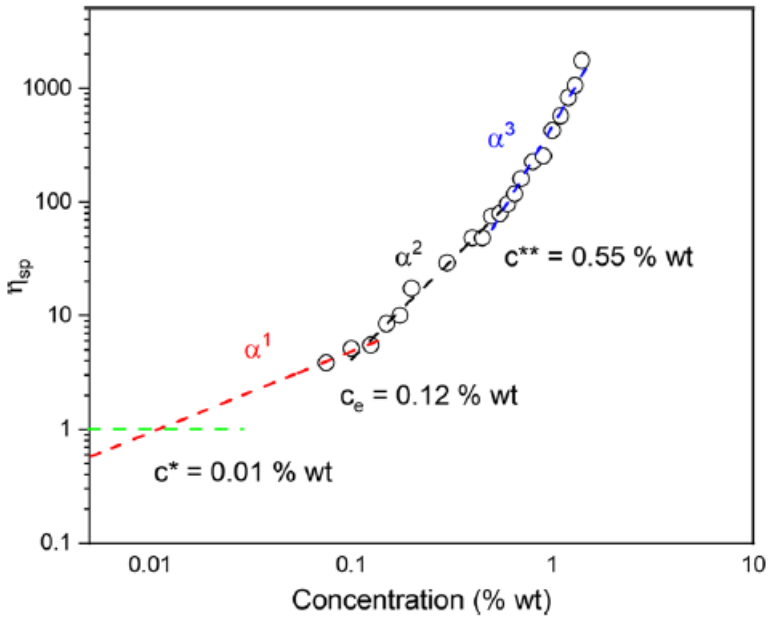

Figure 1-12: Concentration regimes and scaling factors for SA medium viscosity solution in water.[9]

When 2 samples differing in M/G ratio were studied (24b), the molecular weight has shown an important influence on the critical concentrations. High molecular weight (high viscosity) solutions display lower critical concentrations since the entanglement density is higher for longer chains.

Experimental results showed that the scaling factors deviate from the theoretical predictions. Table 1-5 shows the comparison of the theoretical predictions and experimental findings from [9][37][32] for the scaling factors in different concentration regimes. This variation might arise from the differences in the chemical properties of SA such as the chain size or M/G ratio. Figure 1-12, Figure 1-13 and Figure 1-14 shows the experimental results used to distinguish the scaling behavior and concentration regimes of SA solutions.

Scaling factors for polyelectrolyte in salt-free case	Semi-dilute unentangled	Semi-dilute entangled	Concentrated	References
Theoretical predictions	0.5	1.5	3.75	
Alginate solution	0.6 ± 0.1	1.6 ± 0.1	3.4 ± 0.1	[32]
Sodium alginate solution	0.8	1.48	2.88	[37]
SA mvM	0.71	1.73	2.97	[9]
SA mvG	0.55	1.52	3	[9]
SA LV	0.95	2.3	4.03	[9]

Table 1-5: Scaling factors in concentration regimes of SA solutions from [9][37][32] vs theoretical predictions (mvM: medium viscosity M-rich; mvG: medium viscosity G-rich; LV: low viscosity)

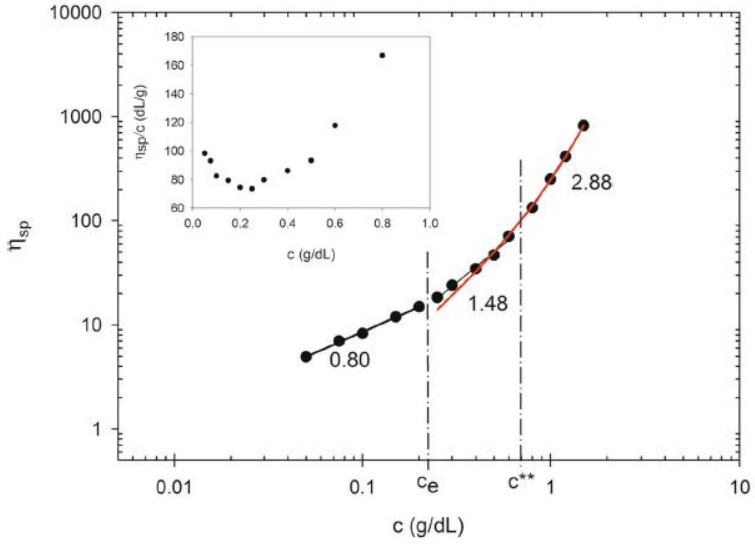

Figure 1-13: Effect of alginate concentration (c) on the specific viscosity (η_{sp}) of SA aqueous solutions: experimental data (symbols) and data fitting (red line) [37]

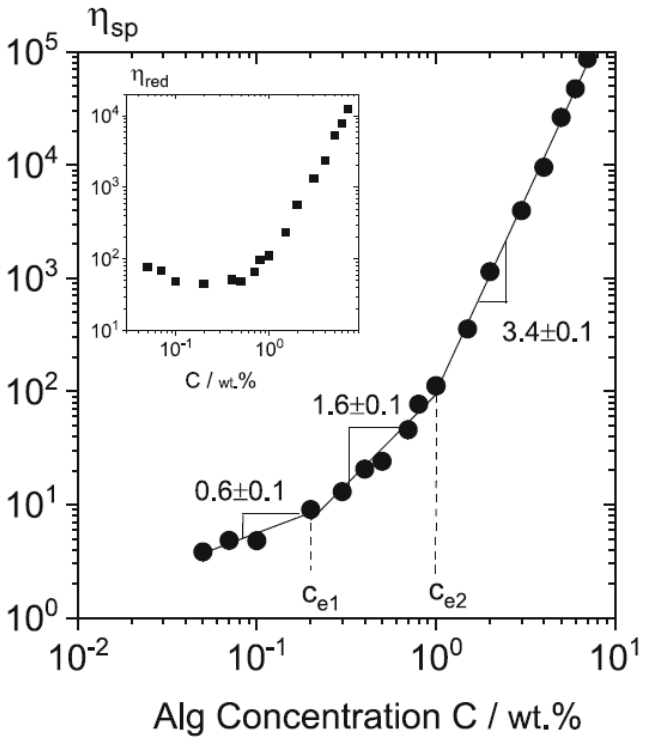

Figure 1-14: Specific viscosity as a function of alginate concentration in salt-free solutions at 20 °C. Inset shows the reduced viscosity as a function of alginate concentration [32].

Effect of Ionic Strength

Ionic strength of the solution is one of the most important parameters which affect the rheological and chemical properties of materials such as polyelectrolytes. Rheology tests have been used to investigate the effect of ionic strength on viscosity of the solutions [50][51]

According to Odijk-Skolnick-Fixman (OSF) theory, total electrostatic persistence length L_t has two contributions which are intrinsic (L_p) and electrostatic (L_e) persistence lengths such that $L_t = L_p + L_e$. Intrinsic one is due to the rigidity of the uncharged chain while the electrostatic one arises from the repulsion between adjacent ions. When the ionic strength increases, the electrostatic persistence length decreases due to the screening of the charges whereas the intrinsic one remains constant. Hence, the total persistence length decreases which explains the decrease in molecular stiffness with the increase of ionic strength.

[50][32] Electroviscous effects on polyelectrolytes have been the subject of several theoretical treatments as well as the experimental studies. [51]

The role of the salt concentration (C_s) to the intrinsic viscosity of the polyelectrolyte solution is shown by both experiments and the theoretical works. It is generally accepted in the following form:

$$[\eta] = [\eta]_\infty + SC_s^{-1/2} \quad (4)$$

Where $[\eta]_\infty$ is the intrinsic viscosity extrapolated to infinite ionic strength and S is the slope of the dependence of $[\eta]$ on Cs which is related to molecular stiffness. [51]

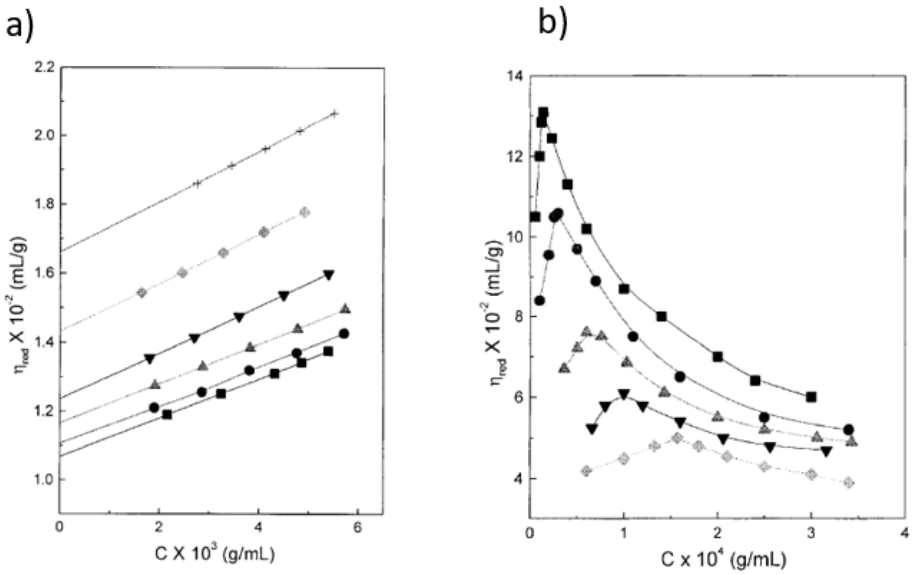

Figure 1-15: The reduced viscosity (ηred) vs. sodium alginate concentration (C) at NaCl concentrations: a) 0.5 M (square); 0.2 M (circle); 0.1 M (triangle); 0.05 M (inverted triangle); 0.02 M (diamond); 0.005 M (cross). & b) 1 E-5 M (square); 2 E-5 (circle); 5 E-5 (triangle); 1 E-4 (inverted triangle); 5 E-5 (diamond). [50]

When the reduced viscosity change is investigated at very high and very low C_s, it has been shown in Figure 1-15 (a) that reduced viscosity dependence on SA concentration is linear with a positive slope when the salt concentration is high enough to screen the electrostatic interactions. On the other hand, at low salt concentrations (Figure 1-15 (b)) addition of polyelectrolyte in pure water increases the viscosity at first, but then viscosity reaches a maximum value and starts to decrease beyond that SA concentration. The maximum value

of the viscosity decreases as the NaCl concentration increases which is the general effect of NaCl on the viscosity of polyelectrolytes.[50][51]

On the other hand, some interesting increase in viscosity with ionic strength have also been reported for polysaccharides such as xanthan and cationically modified cellulose solutions. [48][49][11] Figure 1-16 and 1-17 show the viscosity plots obtained from steady state shear rheometry. These figures display an interesting effect of ionic strength on the viscosity of the solutions in which the viscosity, by the addition of salt, decreases at low polymer concentration, whereas it increases at high polymer concentration.

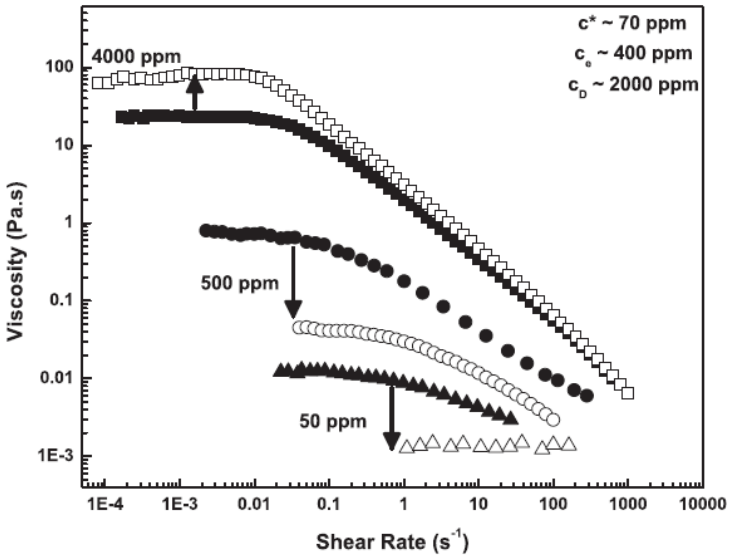

Figure 1-16: Viscosity as a function of shear rate for several xanthan concentrations in both salt-free solution (filled symbols) and 50 mM NaCl (open symbols). Figure from [49].

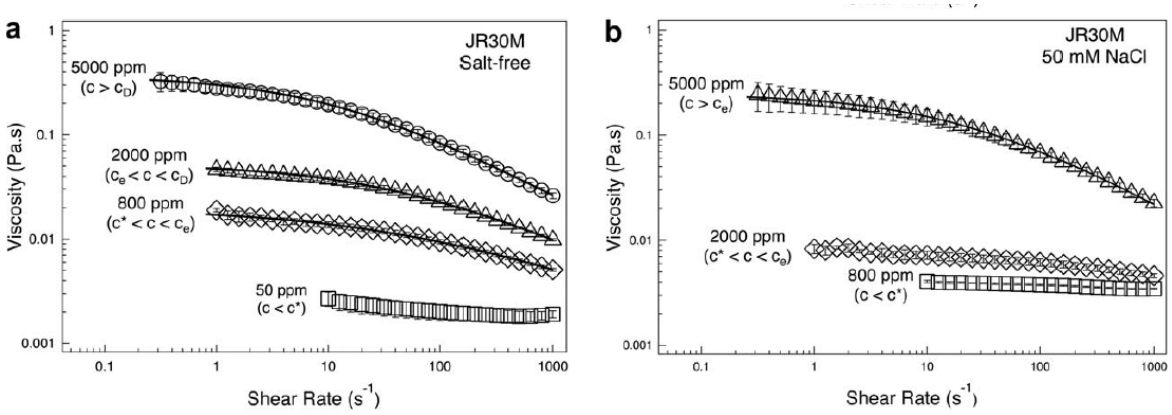

Figure 1-17: Viscosity as a function of shear rate for several JR30M(modified cellulose) concentrations in both a) salt-free and b) 50 mM NaCl solution. Solid lines represent the Cross model fits. [11]

Study on xanthan [49] has shown that dynamic measurements on SA solutions are affected by ionic strength, too. When the polymer concentration is low (Figure 1-18 (b)), the addition of NaCl decreases the dynamic moduli until a high frequency of oscillation, after which the situation is reversed. When the same test is applied to the xanthan solution with high polymer concentration (Figure 1-18 (b)), the decrease in dynamic moduli upon NaCl addition is limited with only a low frequency range.

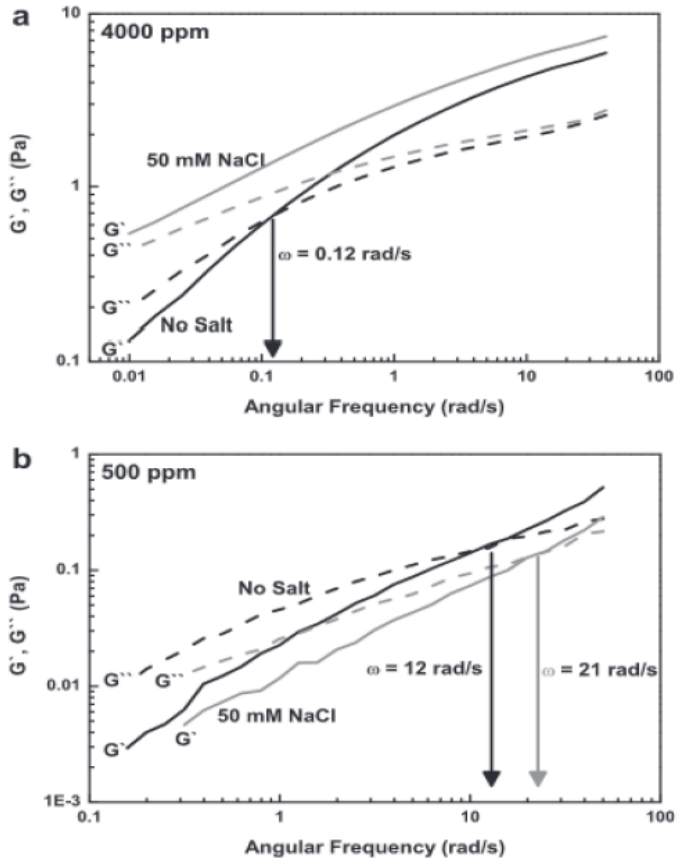

Figure 1-18: Dynamic oscillatory shear measurements show G' and G'' for 4000 ppm (top) and 500 ppm (bottom) xanthan in salt-free solution (black curves) and in 50 mM NaCl (grey curves) [49].

1.3.2. Alginate Hydrogels

The ionotropic gelation via divalent ions which leads to alginate gels has been under focus in many studies. [5][46][29][30][45][23][24] Findings of the experimental studies have shown that SA solutions undergo a sol-gel transition at a critical cross-linker concentration which leads to the formation of gel network. Determination of the critical cross-linker concentration is one of the priorities of the studies on the hydrogels. Also, the factors affecting the critical cross-linker concentration have been investigated. [29][30][45][23]

C-NMR studies have been carried out on alginate solutions going through sol-gel transition in the presence of cations. [46] C-NMR allows for the investigation of interactions between cross-linker ion and the polymer chain. In the Ca-alginate systems, a specific interaction caused by a strong autocooperative binding between G blocks and Ca^{2+} ions has been reported and the findings have shown that all the functional groups of G blocks involve in this interaction. The situation is different when divalent ions of transition metals such as Cu^{2+}, Co^{2+}, Mn^{2+} are used as cross-linkers. C-NMR results suggest that the coordination of the metals occur with the contribution of both G and M blocks.

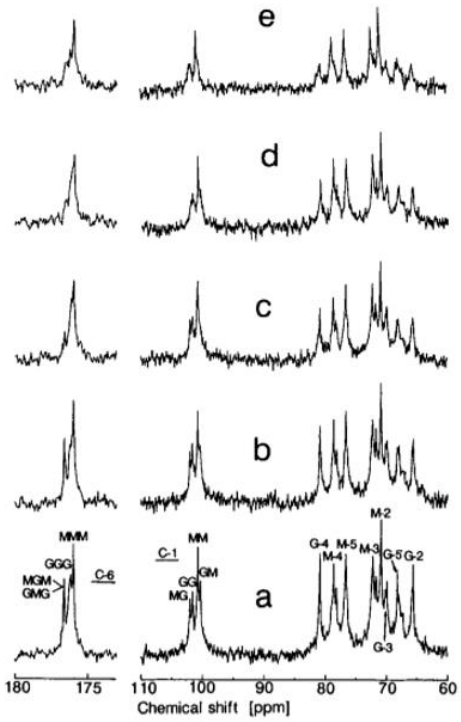

Figure 1-19: C-NMR spectra of 5wt% alginate solution at various Ca^{2+} concentrations measured at 100.6MHz and 30°C. (a) f = [Ca^{2+}/residues of alginate] = 0; (b) f = 0.04; (c) f = 0.083; (d) f = 0.11; (e) f = 0.18. (Figure from [46])

Molecular motion changes during sol-gel transition reflects as a variation in C-NMR spectra. Figure 1-19 shows the C-NMR spectra of an alginate solution at various $Ca2^{+}$ concentrations wherein the molar ratio of ions to alginate residues, f, varies over a range. Aforementioned autocooperative binding between G blocks and Ca^{2+} ions have been indicated by a remarkable line broadening for the signals of the G residue and the carbons with increasing Ca^{2+} concentration which supported the egg-box model [46][35].

The oscillatory rheology measurements can be used to determine the critical cross-linker concentration(c_g) at which the sol-gel transition initiates. [29][30][23] According to Winter-Chambon criterion, the loss tangents which can be found by a frequency sweep test, converge at the gelation point. Figure 1-20 and 1-21 display the tanδ plots against the molar ratio of Ca^{2+} ions to carboxyl groups in the alginate, f. The convergence point of tanδ values for different angular frequencies, reveals the critical f value for the gelation.

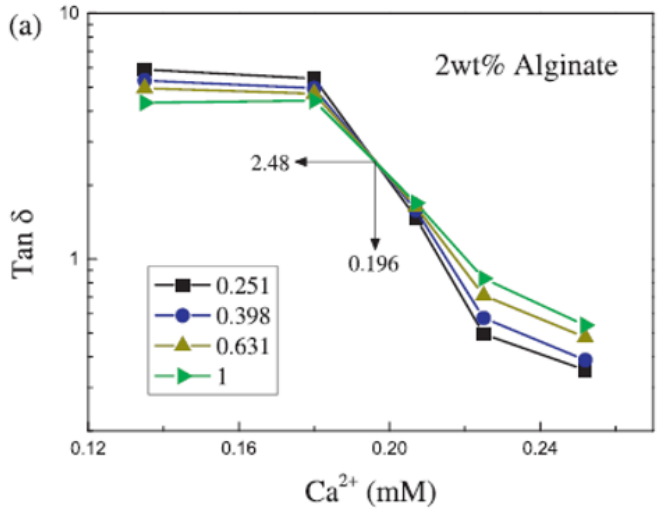

Figure 1-20: Dependence of loss tangent, tanδ, on calcium ion content for the 2wt% alginate solution at different angular frequencies [29]

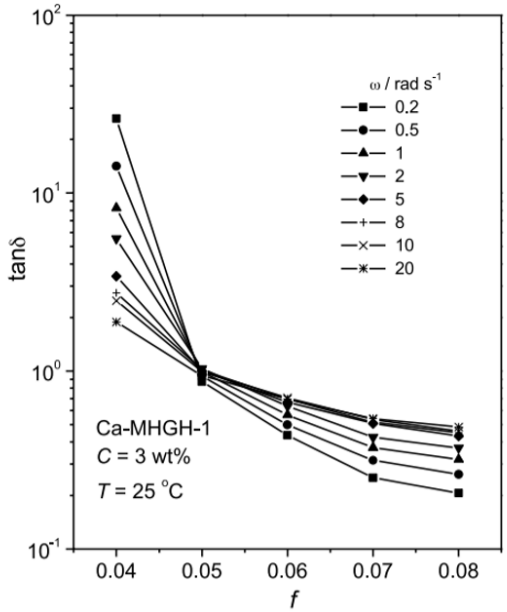

Figure 1-21: tanδ at indicated angular frequencies, ω, plotted against mole ratio of calcium ions, f. [30]

When the frequency sweep tests are repeated for SA solutions at different concentrations and for different angular frequencies, critical calcium crosslinker concentration, $c_{g,\,Ca^{2+}}$ has shown an increasing trend with alginate concentration (Figure 1-22). [29]

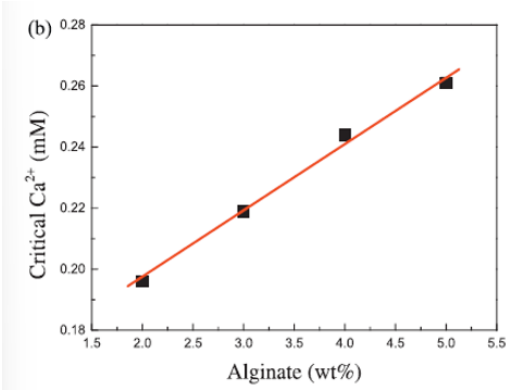

Figure 1-22: Change in $c_{g,\,Ca^{2+}}$ with alginate concentration [29]

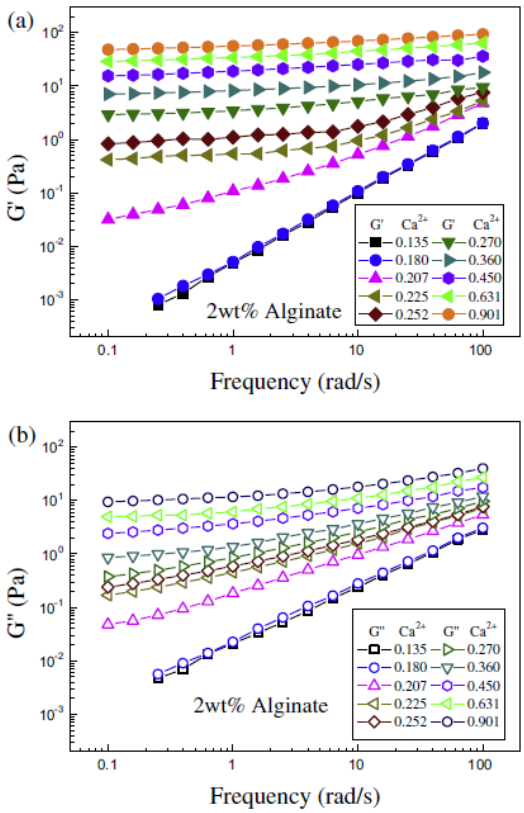

Figure 1-23: a) G' and b) G'' vs. angular frequency for 2wt% alginate solution at various Ca^{2+} concentrations [29]

Dynamic moduli show a high frequency dependence before the $c_{g,\,Ca^{2+}}$ and the G'' is higher than G' at low frequencies which correspond to the dynamic properties of a viscoelastic polymer solution. After the $c_{g,\,Ca^{2+}}$ is reached, a gel plateau appears, G' and G'' become independent of frequency with further increase of $^{Ca2+}$ ions, showing a solid-like material characteristic.(Figure 1-23, [29]) The plateau modulus G_e found in this stable gel state was dependent on Ca^{2+} concentration by a power-law scaling: $G_e = k\epsilon^{1.5}$ where ϵ is the relative distance of Ca^{2+} concentration from the gel point, $c_{g,\,Ca^{2+}}$ as shown in Figure 1-24 below.

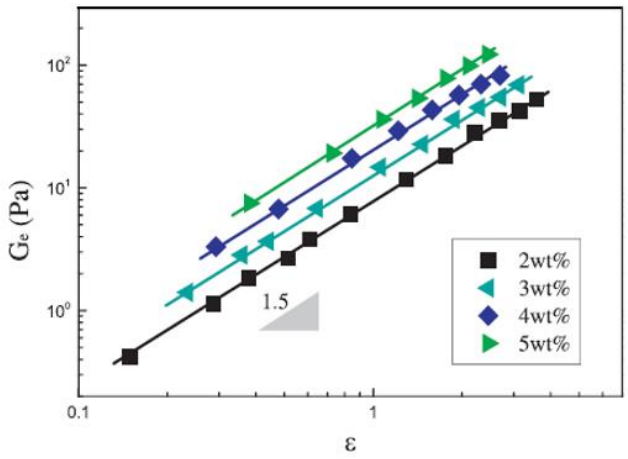

Figure 1-24: Dependence of the plateau modulus G_e on the relative distance Ɛ for alginate gels at various concentrations [29].

Critical gel concentration can also be determined from viscosity measurements. [45] When the relative viscosity η_{rel} is defined as a ratio between the viscosities of solution with and without divalent cation addition, the extent of the gel formation can be seen from the variation of relative viscosity with f (divalent ions fraction in the system). Figure 1-25 displays this variation at various alginate concentrations. The points at which the slope of the curves drastically changes give the critical f for gelation (f_{crit}) and it is shown that lower the alginate concentration, the greater the f_{crit}, indicating a strong dependence of polymer concentration on sol-gel transition and supported by the fact that there are more contact sites between polymer chains in concentrated solutions than in dilute solutions.

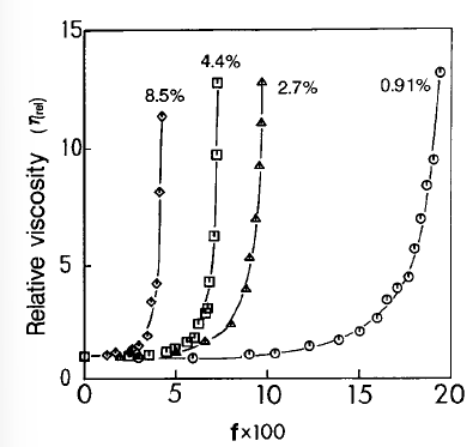

Figure 1-25: Relative viscosity vs. f, divalent ions fraction at various alginate concentrations. Figure from [45].

Aside from the ionotropic gelation, some examples of "cold gelation" have been reported [24]. Among various alginates solutions differing in M/G ratio, alginates with high M % have formed thermoreversible assemblies in the presence of potassium salts. Low solubility of M-blocks at low temperature and high ionic strength leads to this aggregation behavior and the proposed model for cold gelation of high M-alginates is represented in the Figure 1-26 below. [24]

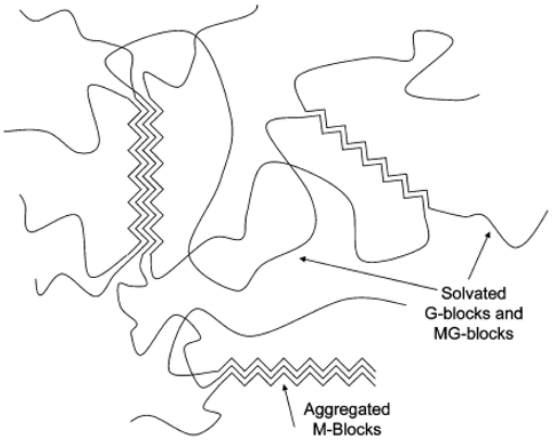

Figure 1-26: Proposed model for cold-gelation of high M-alginates in the presence of salt.[24]

As Figure 1-27 depicts, alginate sample with high M% (ALG-1) is easily distinguishable from the other samples, with the rapid decrease in complex viscosity during the temperature rise. It is able to form thermoreversible gels or at least thermoviscosifying solutions in the presence of potassium carbonate and, the hysteresis loop covers more than 20°C. [24]

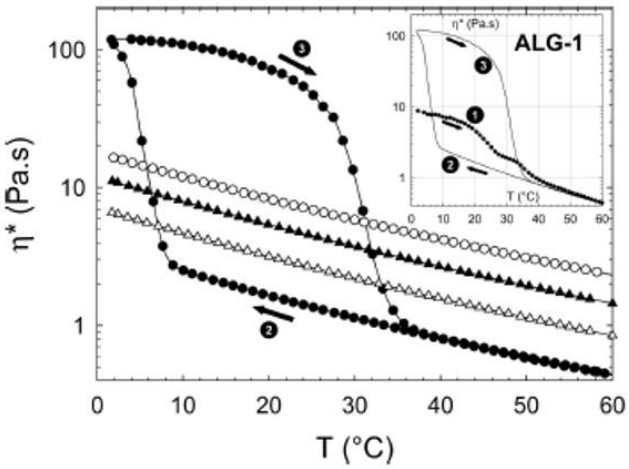

Figure 1-27: Temperature dependence of the complex viscosity for alginate solutions at 5 wt% in presence of potassium salts. ALG-1 (filled circles), ALG-2 (filled triangles), ALG-3 (empty circles), and ALG-4 (empty triangles). Inset shows the viscosity behavior during pretreatment For ALG-1.[24]

Factors affecting the alginate hydrogel properties

Viscoelastic properties of alginate gels show a strong dependence on thermal treatment parameters such as rate of cooling, time and temperature of storage and also on polymer and salt concentrations. The influence of molecular weight on the hydrogel strength is depicted in Figure 1-28. [13]

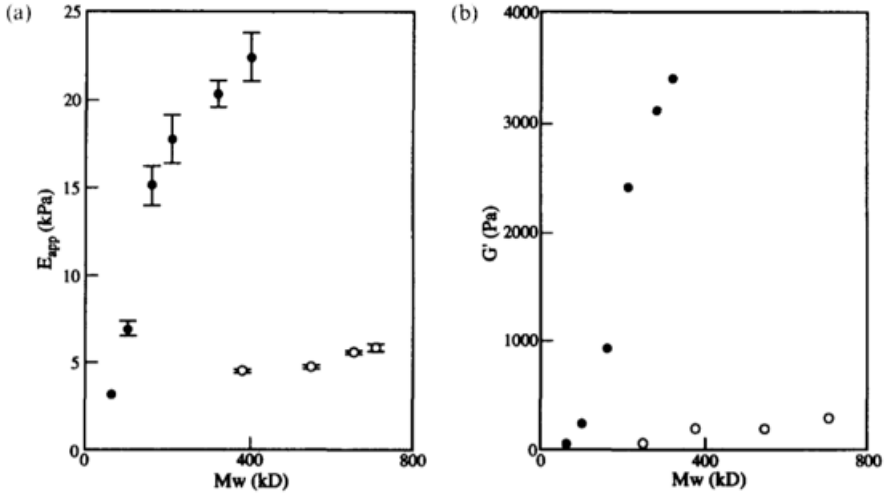

Figure 1-28: Gel strength of alginic acid gels of different molecular weights determined by a) apparent Young's Modulus and b) dynamic storage modulus. Solid and empty symbols represent different natural origin.[13]

Alginate hydrogels formed by the addition of Ca^{2+} ions to aqueous solutions of sodium alginate have strain dependent viscoelastic properties. [47] When their rheological and mechanical behaviors are studied by an axisymmetric probe tack apparatus, hydrogels behave elastically at small strains and become viscoelastic at large strains. Figure 1-29 below shows that load-displacement relationship is linear when applied strain is less than 1 but, it increases more rapidly as the strain increases further. The shaded region represents the nonlinear response which undergoes a stress relaxation. Limited nonrecoverable creep and dynamic moduli for these hydrogels are only weakly frequency dependent when strain is lower than 0.25.

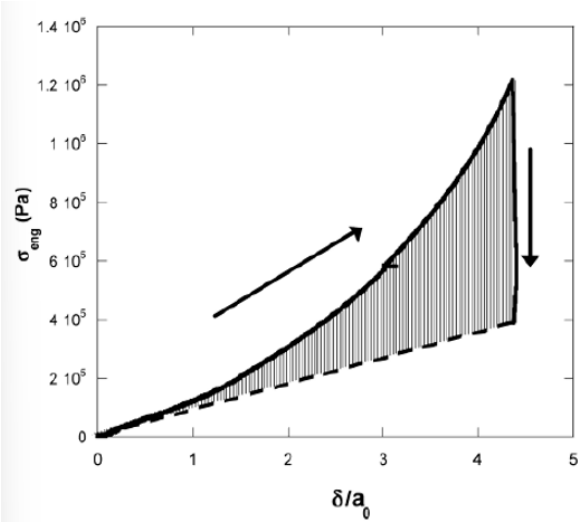

Figure 1-29: Plot of stress vs normalized displacement from a stress relaxation experiment. Dotted line represents the initial, linear load-displacement. [47]

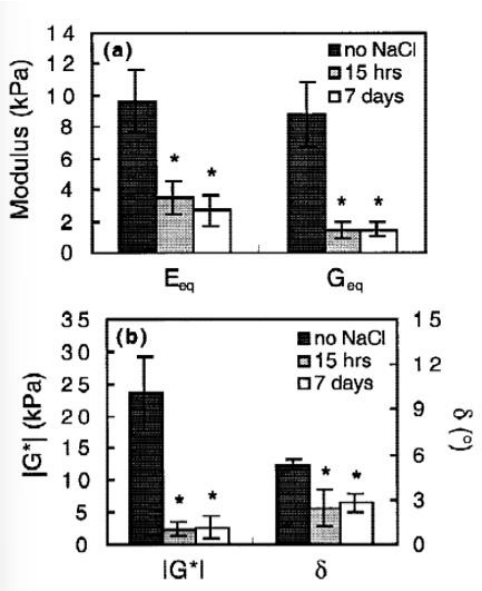

When the calcium alginate gels are exposed to physiological concentrations of NaCl, their viscoelastic properties change.[28] According to compressive and shear relaxation tests, and oscillatory shear tests, the compressive, equilibrium E_{eq}, shear G_{eq}, and dynamic shear moduli $|G^*|$, along with loss angle δ, decrease after hours of NaCl exposure. (Figure 1-30)

Figure 1-30: a) E_{eq} and G_{eq} moduli and b)$|G^*|$ and δ of

2 wt% alginate gel before and after exposure to NaCl.

Hydrogels from other polysaccharides also show mechanical properties which can alter by ionic effects. It has been reported that dynamic Young's modulus E', of gellan gels display an interesting trend at different salt and polymer concentrations. [34] The results obtained from rheology tests suggest that E' increases with polymer concentration in the salt-free case (Figure 1-31 left part); at a fixed concentration of polymer, E' first increases and then decreases as the salt concentration is increased (Fig. 1-31 middle and right part).

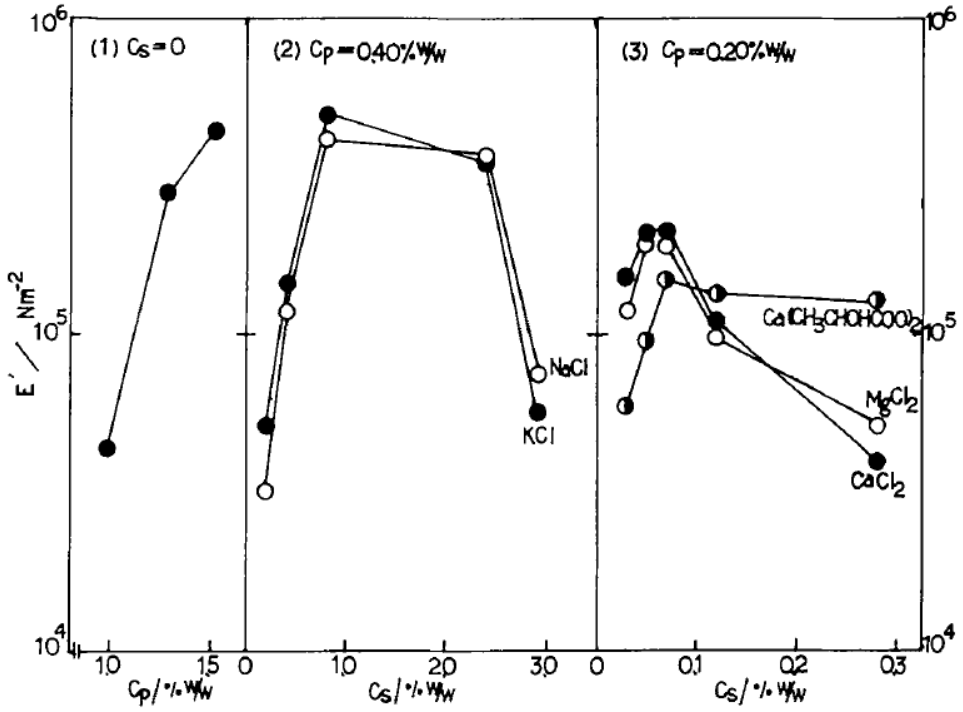

Figure 1-31: E' of gellan gels 1) vs polymer concentration (c_p) without salt, 2) at 0.4 %(w/w) c_p vs increasing NaCl(empty circles) and KCl(filled circles) concentration, 3) at 0.2 %(w/w) c_p vs increasing salt concentration. [34]

Although there has been attempts to find a meaningful correlation between the rheological properties of solution and the hydrogels, findings were merely satisfactory. A study by Fu et al. [19] on calcium alginate gels prepared from six different grades of sodium alginate has looked for a relation between deformation work (L_E) of gels which were subjected to compression to fracture, and apparent viscosity (η_{app}) of the solutions.

Deformation work at gel fracture (L_E), per unit volume, can be calculated as the area under the stress-strain curve as shown in the equation:

$$L_E = \int_{\epsilon_E=0}^{\epsilon_E \, at \, fracture} \sigma_E d\epsilon_E \quad (5)$$

Among the SA grades with similar G-block monomer concentration (G%), a significant correlation between L_E and η_{app} has been reported. However, when partial correlation tests for statistical analysis have been conducted, results have showed that L_E was significantly correlated with G%, but not with the rheological properties of sodium alginate solutions. These results suggest that there are other properties which might be influencing the mechanical properties of the gels, such as polydispersity or the randomness of guluronic acid sequencing. According to the tests among several batches of one specific grade of SA, inter-batch differences in the rheological behavior of SA were insufficient to predict the corresponding calcium alginate gel's mechanical properties, Figure 1-32 depicts below that the apparent viscosities of the SA solutions from multiple batches of the same grade were not indicative of the resultant calcium alginate gel strength.

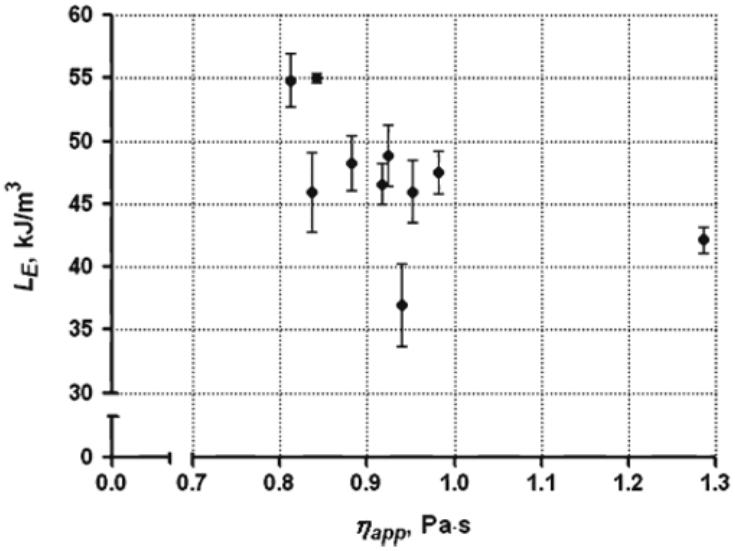

Figure 1-32: L_E of calcium alginate gel samples prepared from the multiple batches of same grade vs corresponding apparent viscosity (η_{app}) of sodium alginate solutions. [19]

2 Materials & Methods

2.1. Materials

Sodium alginate (SA, Batch number: MKCJ1280), calcium carbonate ($CaCO_3$), and glucono-delta-lactone (GDL) were purchased from Sigma Aldrich in the powder form. Powder form of sodium chloride (NaCl) was used to prepare aqueous solutions in distilled water. All these materials are non-toxic, edible and biodegradable. They were stored in closed containers in dry environment. The solutions and the hydrogels prepared from these materials were stored in refrigerator at 4° C to avoid any growth of microorganisms. Maximum storage time was 24 hours.

2.2. Sample Preparation

2.2.1. SA Solutions

SA was dissolved in aqueous solution of NaCl (in distilled water) upon magnetic stirring for 24 hours to obtain homogeneity. For the dissolution process, first a strong vortex of the solvent was formed by a rotation speed at over 1000 rpm (rotations per minute). Then, the SA powder was added in the vortex slowly and continuously to avoid any aggregation. After all the powder was introduced in the system without the formation of aggregates (duration is approximately 1 min), the rotation speed was decreased to ~250 rpm and the solution was left for stirring overnight to make sure that the solution was homogeneous.

The concentration range chosen for this work is given in the Table 2-1 below:

SA (%w/v) / NaCl (%w/v)	0.1	0.2	0.3	0.4	0.6	0.8	1	1.5	2	3
0	●	●	●	●	●	●	●	●	●	●
0.057	●	●	●	●	●	●	●	●	●	●
0.15	●	●	●	●	●	●	●	●	●	●
0.7	●	●	●	●	●	●	●	●	●	●
1	●	●	●	●	●	●	●	●	●	●

Table 2-1: SA & NaCl concentration range of solutions

This work is the continuation of the previous one which was investigating the effect of SA concentration and ionic strength on the rheological behavior of SA solutions only. Although the concentration range is the same as the previous one, the solutions were prepared one by one instead of starting from a mother solution and modifying it by a salting or a dilution procedure as done in the previous work. [53] This decision was made in order to minimize possible cumulative errors.

The chosen concentration range for SA is in accordance with the studies on SA based hydrogels for in vitro mucus modelling. Sardelli et al. has reported that 0.4 wt%* alginate hydrogels exhibited viscoelastic properties similar to the loose layer of human gastrointestinal mucus. [52] When it comes to the NaCl concentration, the chosen values are mostly the typical concentrations present in physiological mucus:

- 0.057 wt%: low-salt concentration present in intestinal mucus
- 0.7 wt%: NaCl concentration in the pathological pulmonary mucus of patients affected by cystic fibrosis
- 1 wt%: approximate typical physiological value (e.g., for cervix uteri ~0.93 wt%)

* all “wt%” within the text refers to the w/v, which corresponds to the grams of solute per 100 ml of solution.

2.2.2. SA- based hydrogels

Formation of crosslinks is necessary for the formation of a gel network. As described in the previous section, in the presence of divalent ions, G-blocks of the SA chains allow for a physical crosslinking which leads to a structure that is called an “egg-box”. In this work, Ca^{2+} ions were used as the crosslinker divalent ion and the source of Ca^{2+} was $CaCO_3$ to

obtain a slow, homogeneous internal crosslinking. GDL was used as the acidifier agent for the controlled release of Ca^{2+} ions to the system.

After the homogeneous SA solutions were obtained, SA hydrogels were prepared with the addition of crosslinker $CaCO_3$ and the acidifier GDL by double-syringes procedure as described below in steps:

1) 0.7 wt% $CaCO_3$ suspension was prepared in the same solvent that was used in the SA solution.

2) SA solution and $CaCO_3$ suspension were mixed by the double syringe procedure [36] which refers to repeated flow of the mixture from one syringe to another through a connector that links the two, as Figure 2-1 depicts. The volume ratio of SA solution to $CaCO_3$ suspension was 5:1, and this ratio was the same for all hydrogels independent on the SA and NaCl concentrations. In this step, the homogeneous dispersion of $CaCO_3$ in SA solution was aimed, and it was achieved without any visible precipitates of $CaCO_3$.

3) 7 wt% GDL solution was prepared in the same solvent as the $CaCO_3$ suspension, and mixed with the previously prepared mixture of SA solution and $CaCO_3$ suspension in a 1:6 volume ratio. The mixing process was carried out by the double syringe procedure also in this case. As already mentioned, the role of GDL is to allow the slow dissociation of $CaCO_3$ into ions.

4) Content of the syringe was transferred into 5 Petri dishes (~1.5 mL each) which were stored in the refrigerator (~4°C) for 24 hours for the crosslinking process to end.

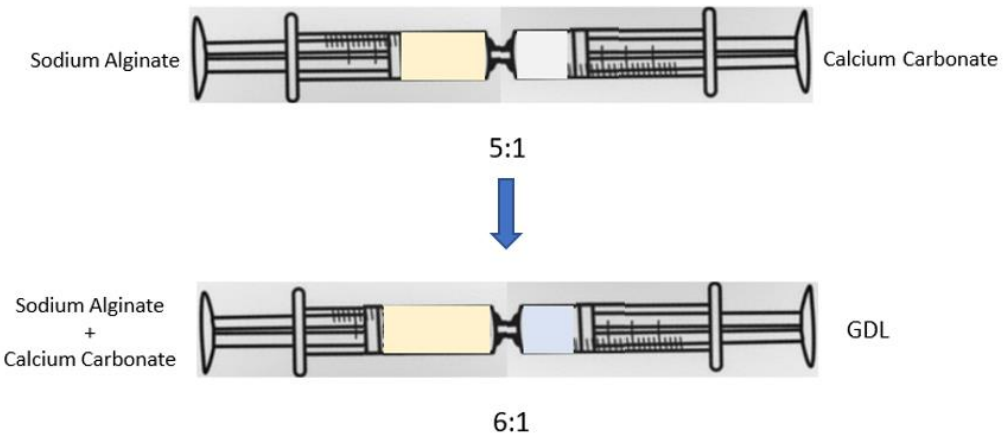

Figure 2-1: Double syringes procedure: Syringes are connected by a plastic support-connector. Syringe plungers are pressed by 2 hands from both sides consecutively 27 times to mix the contents of each syringe.

By the addition of $CaCO_3$ and GDL, the SA concentration of the hydrogel becomes different than that of the solution. e.g., Hydrogel prepared from 1wt% SA solution has 0.7 wt% SA. Figure 2-2 below shows the calculated SA concentration of hydrogels.

SA wt% in solution	0.1	0.2	0.3	0.4	0.6	0.8	1	1.5	2	3
SA wt% in hydrogel	0.07	0.14	0.21	0.28	0.42	0.57	0.7	1	1.4	2.1

Figure 2-2: SA concentration in hydrogels

2.3. Instruments & Methods

The rheometer used for the characterization of SA solutions and gels was an Anton Paar Modular Compact Rheometer (MCR) 502 (shown in Figure 2-3) which operates in stress control. Steady state shear rheometry was used to characterize the solutions whereas oscillatory rheometry was used to characterize the hydrogels.

Figure 2-3: Anton Paar MCR502

2.3.1. Measurements

2.3.1.1. Flow Test by Steady State Shear Rheometry for SA Solutions

The test mode that is used in this work is the rotational test with controlled shear rate. (CSR)

Rotation CSR	Test Preset	Results
Raw data	Rotational Speed, n (min^{-1})	Torque, M (mNm)
Rheological Parameters	Shear Rate, $\dot{\gamma}$ (s^{-1})	Shear Stress, τ (Pa)
Viscosity Calculation		$\eta = \tau/\dot{\gamma}$ (Pa.s)

Table 2-2: Raw data and rheological parameters for rotational tests with CSR [55]

Parallel plate (PP) configuration which has plates with a diameter of 50 mm was selected for the characterization of the SA solutions. Figure 2-4 shows a PP system that consists of 2 plates wherein R is the radius of plates. The distance between 2 plates, referred to as the gap, h was set to 1 mm, in agreement with standard prescriptions which require h << R.

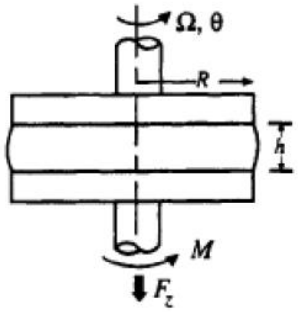

Figure 2-4: Parallel Plate geometry

PP systems can be used to evaluate the rheological behavior of gels, pastes, soft solids, and viscous fluids. To obtain the most accurate results, it is important to fill the gap correctly, thus avoiding overfilling and underfilling.

Shear rate in a PP gap can be calculated as: $\dot{\gamma}(R) = \frac{R\Omega}{h}$ where Ω is the angular velocity. We can also calculate the shear stress from the equation below with the Rabinowitsch correction for non-Newtonian fluids:

$$\tau_{\theta z} = \frac{M}{2\pi R^3}\left(3 + \frac{dln(M)}{dln(\dot{\gamma}(R))}\right) \quad (6)$$

where M is the torque. Then, the viscosity, η can be calculated by the equation: $\eta = \tau/\dot{\gamma}$

Viscosity curves are plotted with shear rate, $\dot{\gamma}$ on the x-axis and viscosity, η on the y-axis. A log-log scale is normally adopted. The test procedure chosen in this work is the following:

Interval #1: Pre-shear step at a constant shear rate value of 10 s^{-1} applied for a minute to homogenize the sample.

Interval #2: A set of shear rate steps at shear rates increasing from 0.1 s^{-1} to 100 s^{-1}

Interval #3: A set of shear rate steps at shear rates decreasing from 100 s^{-1} to 0.1 s^{-1}

All the tests were performed at 25°C.

2.3.1.2. Steady State Oscillatory Rheometry for SA hydrogels

Oscillatory tests are also referred to as dynamic mechanical analysis and they are used to examine the mechanical response of all kinds of viscoelastic materials when a periodic stimulus is applied.

Tests in this work were carried out imposing a sinusoidal shear strain: $\gamma(t) = \gamma_A * \sin(\omega t)$

where γ_A, ω and t are shear strain amplitude, angular frequency, and time, respectively.

The result is the τ- curve as a phase-shifted sine function: $\tau(t) = \tau_A * \sin(\omega t + \delta)$

where δ is the phase shift angle between input and output due to the viscoelasticity.

Then, the storage (G') and loss(G'') moduli can be found to assess the viscoelastic response of the hydrogels by the relations:

$$G'(\omega) = \frac{\tau_A * \cos(\delta)}{\gamma_A} \quad (7)$$

$$G''(\omega) = \frac{\tau_A * sin(\delta)}{\gamma_A} \quad (8)$$

G' is a measure of the material's ability to store the deformation energy that is applied externally, thus representing the elastic (or so-called the solid-like) behavior whereas G'' is a measure of the dissipation of the deformation energy, therefore representing the viscous (liquid-like) behavior.

Another important property is the loss factor, tanδ which is the ratio between G'' and G': $\tan\delta = \frac{G''}{G'}$. When the material is;

- in the liquid-state, tanδ > 1
- in the solid (gel)-state, tanδ < 1
- at the sol-gel transition point, tanδ=1.

A PP measuring system with 25 mm in diameter (PP25) was used for the tests of hydrogels. Since the sample thickness was not the same for all the hydrogels, selecting a constant gap height was problematic. When the sample thickness was much larger than the selected gap height, the sample was exposed to a large compressive stress leading to even breakage. Therefore, instead of fixing a constant gap height, we monitored the normal force (N) as we lowered the upper plate onto the sample. To avoid the risk of slippage, gap height was decreased until the point at which the normal force turned to positive (~ 0.2 N) from negative values. However, the variation in sample thickness was limited, so the gap height was around 1 mm for all the tests. Even when the gap height was different for the measurement of 5 samples of the same composition, the results were overlapping better when compared to the measurements with constant gap height.

Before running any frequency sweep tests to evaluate the G' or G'', the limits of the linear viscoelasticity regime (LVER) should be determined by an amplitude sweep test. LVER corresponds to the regime wherein the material structure is not affected by the applied strain

and in which it is possible to get insights on the real viscoelastic properties. An amplitude sweep test gives out the shear strain amplitude range corresponding to the limits of the LVER. In this work, 0.5% shear strain amplitude was chosen within that range, as the constant γ_A for the time and frequency sweep tests.

Time sweep tests were also carried out to make sure that the structure is not evolving with time, hence the crosslinking process is already complete before the tests. At a shear strain amplitude, γ_A=0.5% and constant oscillation frequency at 1Hz, the change in G' and G'' was monitored for 5 mins to make sure these moduli values remain constant.

After the time sweep test for 5 mins, the frequency sweep test at the same shear strain amplitude of 0.5% was done in an oscillation frequency range from 0.1 to 20 Hz.

The same procedure was applied to all 5 samples of the same batch of SA hydrogel and the average values of G' and G'' were taken for the evaluation. The average values of G' and G'' at 1 Hz were used to compare the results of all SA hydrogels.

3 Experimental Results & Discussion

3.1. Solutions

The effect of SA concentration and the ionic strength on the SA solutions were investigated in a previous work [53], however it was necessary to prepare the SA solutions and assess their rheological properties before taking the study further for the evaluation of the hydrogels. Hence, flow tests have been carried out on the SA solutions in the scope of this work as well, to make sure the results of both studies are in accordance and the SA batch has not changed over time, for instance due to degradation.

The results of the flow tests by steady state shear rheometry on the SA solutions are reported in Figure 3-2 as a function of shear rates, which ranged between 0.1 s^{-1} and 100 s^{-1}. As already explained in the materials and methods chapter, the flow curves were determined applying shear rates in the reported range first in increasing steps, and then in decreasing steps. Viscosity curves are plotted to show the dependence of viscosity on the shear rate in the log-log scale. SA solutions are known to display a shear-thinning behavior like most of the structured liquids. A typical flow curve of such behavior would consist of 3 main regions as shown in Figure 3-1 below:

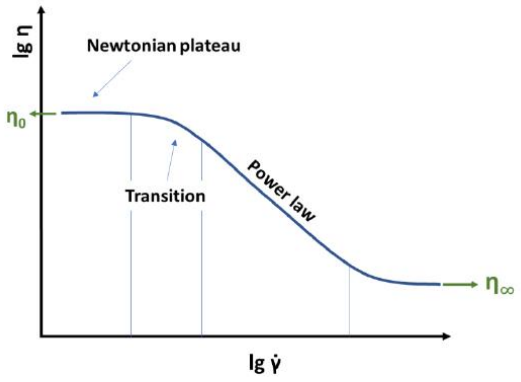

Figure 3-1: Typical flow curve for shear thinning liquids.

As the Figure 3-1 displays, the viscosity does not vary at low shear rate values, therefore a Newtonian plateau is observed at a constant viscosity value η_0 which is called the zero-shear rate viscosity. As the shear rate increases up to a certain value, a transition from

Newtonian to shear thinning behavior occurs, hence the viscosity starts to decrease obeying to a power law equation, $\eta = K\dot{\gamma}^{n-1}$ in which K is the consistency and n is the flow index with a value in between 0 and 1 for shear thinning liquids. The third region is characterized by another Newtonian plateau at very high shear rates however, this region is mostly beyond the range of the measurements.

3-A-1- Effect of SA Concentration

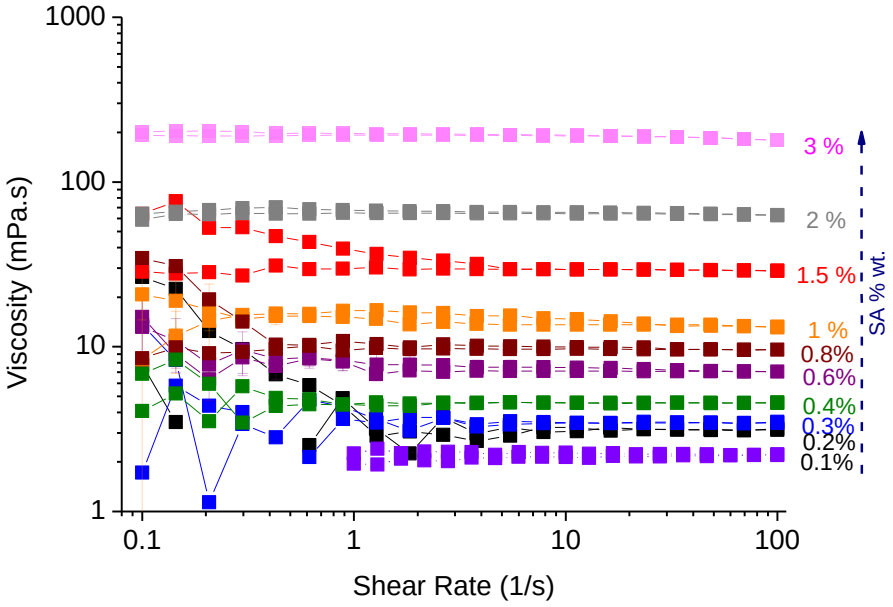

Figure 3-2: Flow Curve of SA solutions in distilled water.

According to Figure 3-2 which shows the flow curve of SA solutions in distilled water, SA solutions show a Newtonian behavior with a constant value of viscosity in the range of shear rates considered in this work. Shear thinning behavior seems to be apparent in the case of SA 3 wt% solution only at the highest shear rate values (around 100 s^{-1}). In some cases, a difference can be observed in viscosities measured by increasing or by decreasing the share rate. This should be considered as an artifact in the test, possibly due to some start-up phenomenon. In general, the rheological behavior is observed to be independent on both experimental time and history, so these variables can be excluded in the rest of the investigation. The data has perturbations at the low shear rate values for low SA concentration which is probably due to the low torque limit of the rheometer. The low torque

region is excluded from the flow curves of the SA solutions in NaCl 0.057, 0.15, 0.7 and 1 wt% reported below in Figure 3-3.

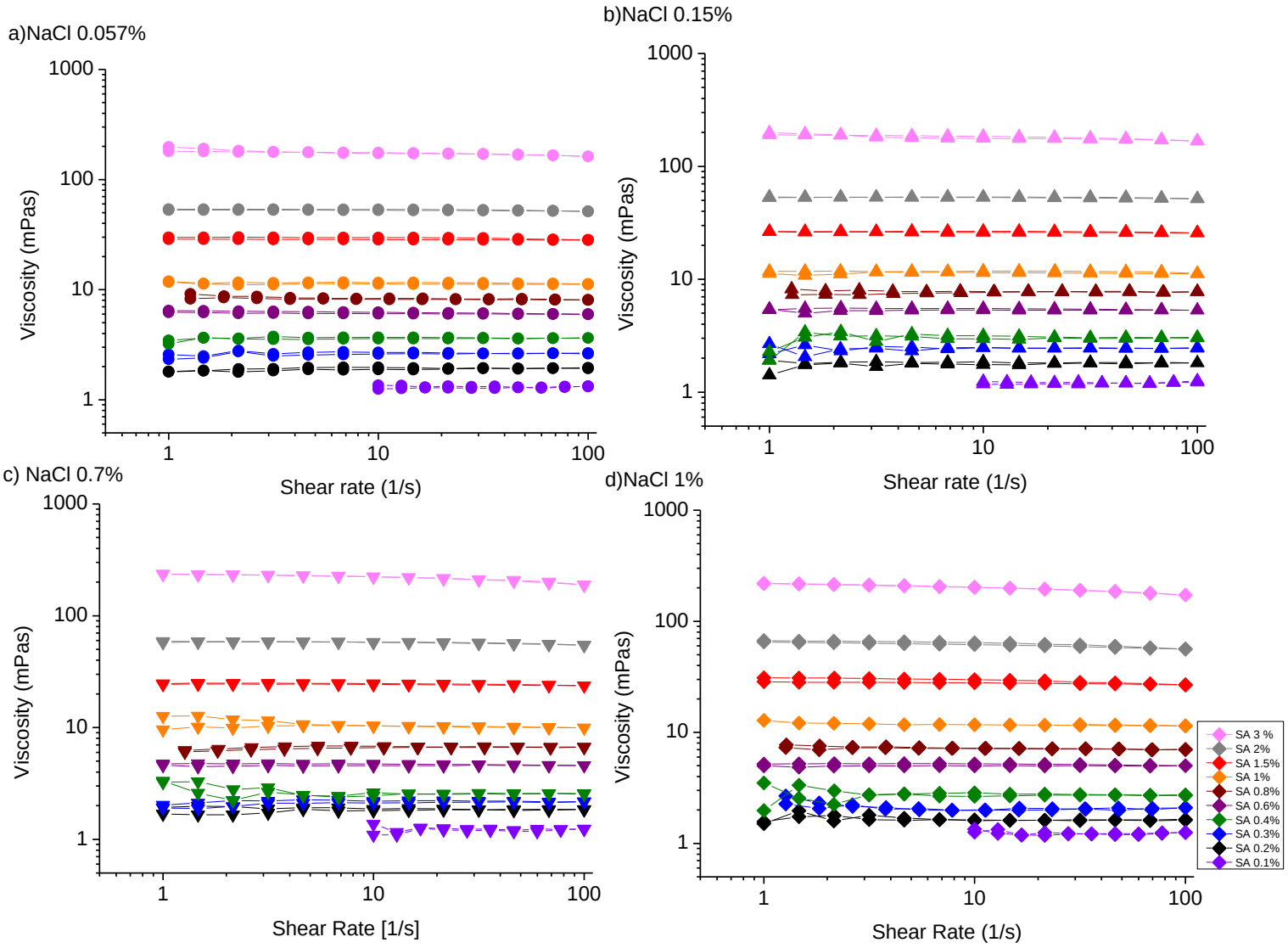

Figure 3-3: Flow curve of SA solutions in NaCl/dH$_2$O solvents with a)0.057 wt%, b)0.15 wt%, c)0.7 wt% and d)1 wt%. The legend shows the SA wt% of the solutions from 0.1-3 wt%.

Figure 3-2 and 3-3 show that the viscosity of the solutions increases in all cases with increasing SA concentration as expected since the number of polymer chains increases in the system. The polymer contribution to the viscosity can be described by specific viscosity, η_{sp}:

$$\eta_{sp} = \frac{\eta_0 - \eta_s}{\eta_s} \qquad (9)$$

where η_s is the solvent viscosity. $\eta_s \sim$ 0.9 mPa.s for distilled water, NaCl 0.057 wt% and NaCl 0.15 wt% solvents whereas η_s ~ 1 mPa.s for NaCl 0.7 wt% and NaCl 1 wt% solvents (at the test temperature of 25°C). [25]

η_0 was determined by taking the average value for viscosity from the Newtonian plateau of the flow curves. However, for the solutions which display shear thinning behavior around ~100s^{-1}, η_0 was determined from the Cross model for the non-Newtonian liquids (power-law region in Figure 3-1). According to Cross model;

$$\eta(\dot{\gamma}) = \eta_\infty + \frac{\eta_0 - \eta_\infty}{1+(\lambda_c \dot{\gamma})^m} \qquad (10)$$

where η_∞ is the infinite shear rate viscosity, λ_c is the relaxation time and, m is a power index which is higher than 1 for shear thinning fluids and 0 for Newtonian fluids. In most of the cases including this work, η_∞ is negligible, therefore another version of this equation which is called the "Cross 0" can be written as:

$$\eta(\dot{\gamma}) = \frac{\eta_0}{1+(\lambda_c \dot{\gamma})^m} \qquad (11)$$

	NaCl wt%									
	0		0.057		0.15		0.7		1	
SA wt%	Zero shear rate viscosity	Specific Viscosity	Zero shear rate viscosity	Specific Viscosity	Zero shear rate viscosity	Specific Viscosity	Zero shear rate viscosity	Specific Viscosity	Zero shear rate viscosity	Specific Viscosity
0.1	2.14	1.38	1.30	0.45	1.21	0.34	1.22	0.22	1.23	0.23
0.2	3.06	2.41	1.89	1.10	1.75	0.95	1.81	0.81	1.60	0.60
0.3	3.45	2.83	2.61	1.90	2.47	1.75	2.12	1.12	2.00	1.00
0.4	4.56	4.07	3.59	2.99	2.96	2.29	2.46	1.46	2.65	1.65
0.6	7.11	6.90	6.04	5.71	5.33	4.92	4.56	3.56	5.00	4.00
0.8	9.69	9.77	8.16	8.06	7.74	7.60	6.62	5.62	7.15	6.15
1	13.62	14.13	11.26	11.51	11.43	11.70	10.33	9.33	11.72	10.72
1.5	29.43	31.70	28.51	30.68	26.03	27.92	24.32	23.32	27.93	26.93
2	63.81	69.90	52.60	57.44	52.96	57.84	57.91	56.91	60.02	59.02
3	219.23	242.58	185.47	205.08	199.25	220.39	255.07	254.07	293.30	292.30

Table 3-1: Zero-shear rate viscosity η_0 and specific viscosity η_{sp} reported for all SA solutions.

The software OriginPro allowed for the data fitting with an equivalent equation of Cross 0 and, the determination of η_0 for the shear-thinning fluids. In the Table 3-1 below, η_0 and η_{sp} for all solutions are reported.

After determining the η_{sp} values, scaling behavior was found by plotting the η_{sp} as a function of SA wt%, for comparison with the theoretical predictions and the previous work. [53]

Figure 3-4 below shows the increase in η_{sp} as SA concentration increases, for all solvents. Scaling behavior for each salt concentration was found from the slopes of these curves after the concentration regimes were distinguished as can be seen from Figure 3-5 for distilled water and 3-6 for NaCl solutions.

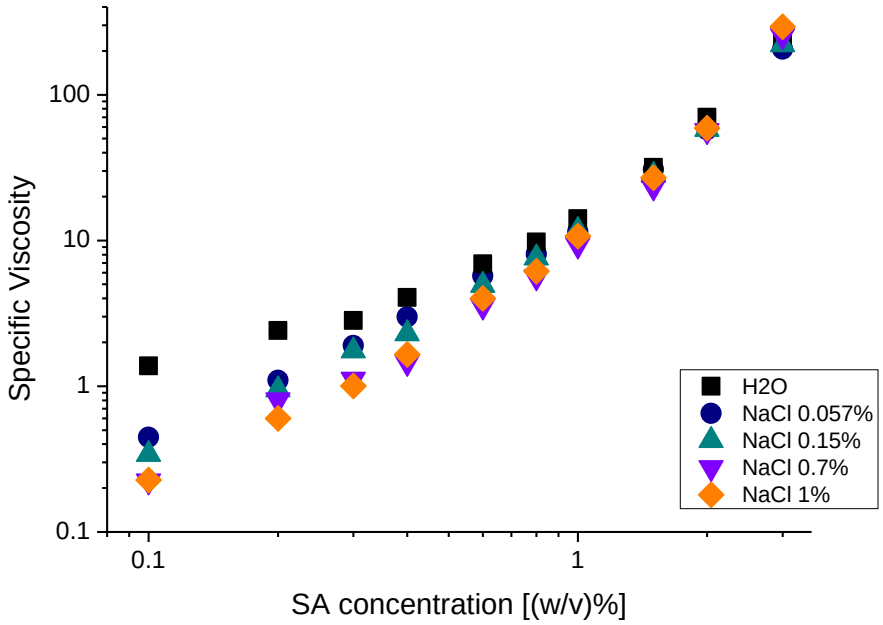

Figure 3-4: Scaling behavior of specific viscosity for all solvents.

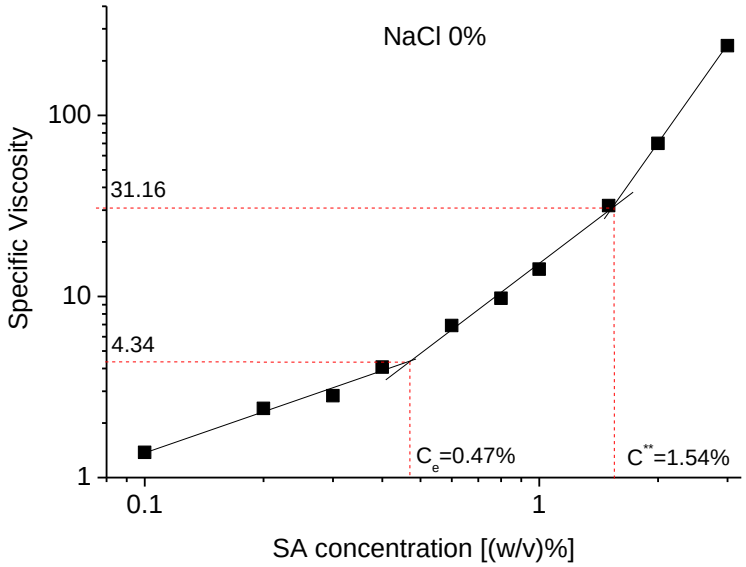

Figure 3-5: Scaling behavior of specific viscosity for SA solutions in distilled water, displaying 3 concentration regimes.

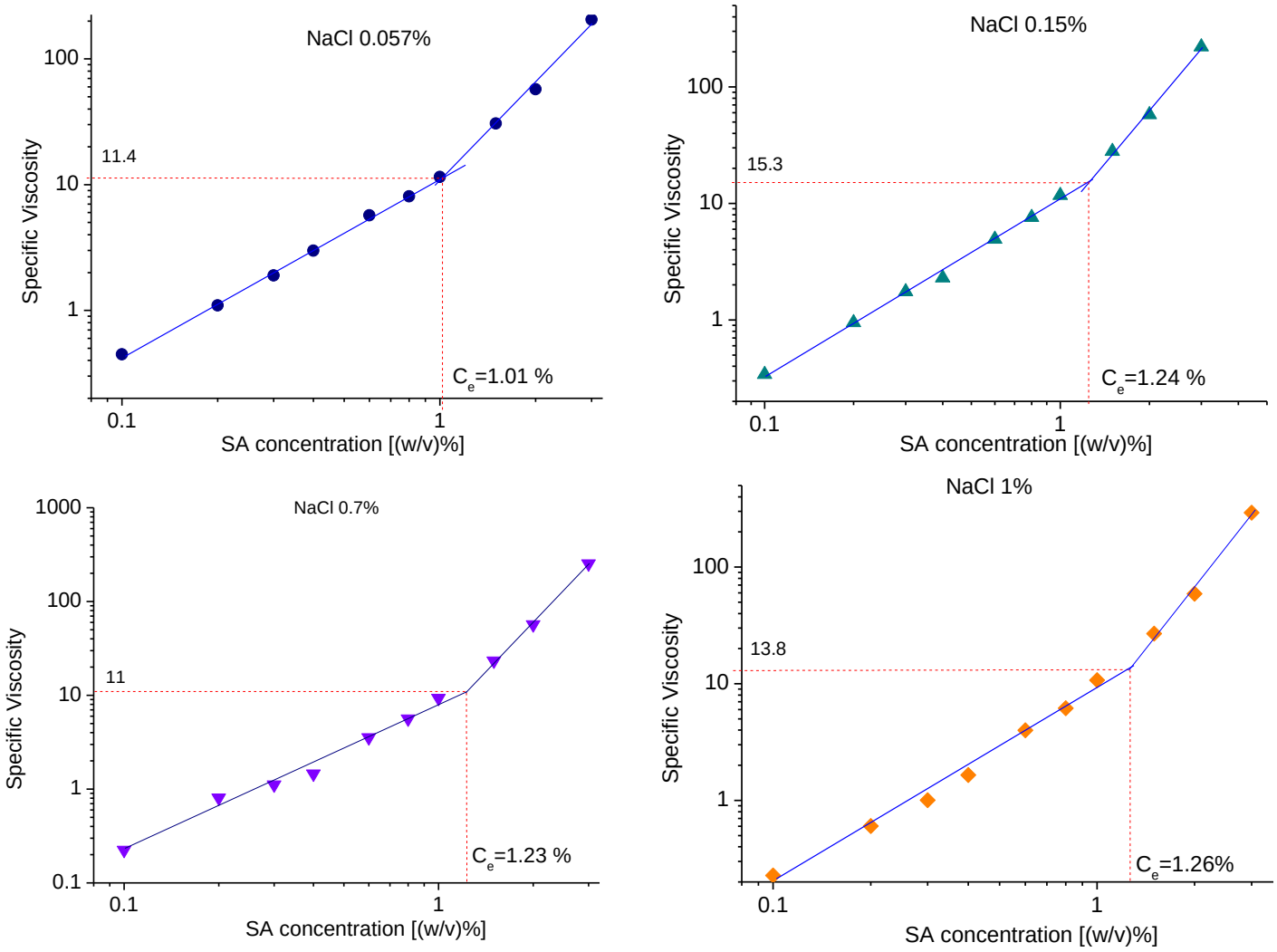

Figure 3-6: Scaling behavior of specific viscosity for SA solutions at different salt concentrations, displaying 2 concentration regimes.

As explained in the introduction part, neutral polymer solutions have 3 concentration regimes which are dilute, semi-dilute unentangled, and semi-dilute entangled whereas polyelectrolyte solutions in salt-free solvents have the same 3 regimes, plus a concentrated one after c**(or c_D) which make 4 regimes in total. Dilute regime appears at very low viscosities which are outside of the range of our measurements. Hence, the reported experimental findings display the semi-dilute unentangled, semi-dilute entangled and the concentrated region for polyelectrolytes in salt-free solutions (see Figure 3-5). Since Figure 3-6 displays only 2 concentration regimes (semi-dilute unentangled and entangled) for all

solutions in the presence of NaCl, we can claim that a transition from polyelectrolyte in salt-free case to the neutral polymer case occurred even with a small amount of NaCl addition into the solvent. Scaling factors were determined from the slope of the linear fits shown in Figure 3-5 and 3-6 and they are reported in Table 3-2 below.

	Slopes			Entanglement concentration Ce	Specific Viscosity at Ce
NaCl wt%	Semidilute unentangled	Semidilute entangled	Concentrated		
Theoretical for polyelectrolyte	0.5	1.5	3.75		
0	0.74	1.68	3.06	0.47	4.34
0.057	1.41	2.59		1.01	11.44
0.15	1.51	3		1.24	15.3
0.7	1.55	3.46		1.23	11
1	1.67	3.47		1.26	13.2196
Theoretical for neutral polymer	1.25	3.75			

Table 3-2: Scaling factors from experimental results and from theoretical predictions. Entanglement concentration, C_e and the η_{sp} at C_e are also reported from the experimental results.

As expected from theoretical predictions [1][3] and other studies in literature [50], scaling factor increases along with the increase in NaCl concentration. Although the scaling factor values found in our study do not coincide with the theoretical predictions, they are in accordance with previous studies [48][49][32][11]. The difference between experimental results and the theoretical predictions might be arising from SA polydispersity (typical of most of the biomaterials) considering that the theoretical predictions are made under the hypothesis of monodispersed materials.

3-A-2- Effect of Ionic Strength

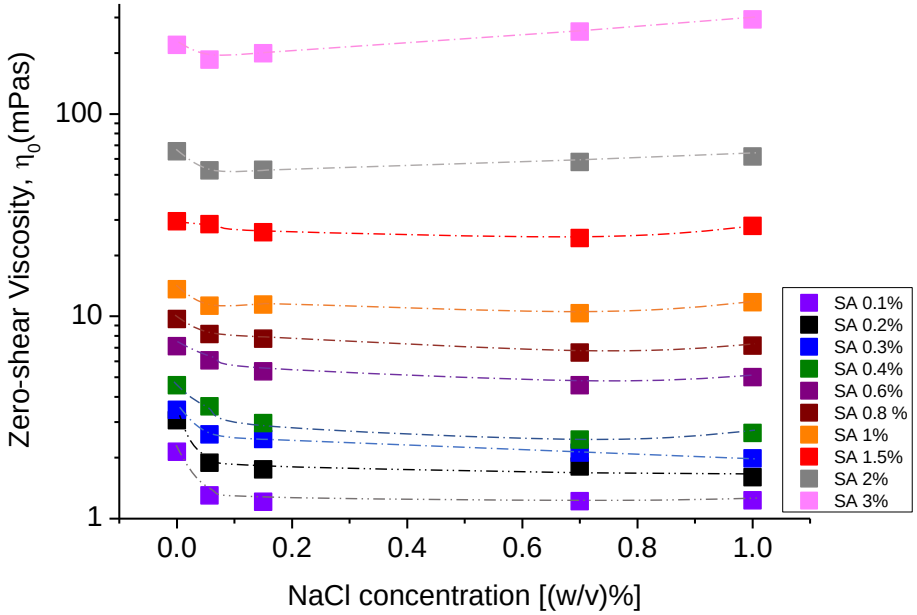

Figure 3-7: Zero-shear Viscosity change with the increase of ionic strength for all SA solutions.

Besides the effect of ionic strength on the scaling law describing the dependence of alginate concentration on solution viscosity, Figure 3-7 and 3-8 allow to assess the same effect in terms of the zero-shear viscosity of all solutions' dependence on the NaCl concentration. Figure 3-7 shows how the SA concentration effect is dominant with respect to that of NaCl concentration. However, if the effect of NaCl is observed with an appropriate magnification, as in Figure 3-8, two opposite effects can be observed:

i. there is a remarkable decrease in zero shear viscosity with the increase of NaCl concentration when the SA concentration is low (up to SA 0.8- 1 wt%).

ii. beyond SA 1 wt%, the viscosity starts to increase as NaCl concentration increases above 0.7 wt% NaCl. This increase in the viscosity becomes even more significant as SA concentration increases even further. For SA 2 wt% and 3 wt% solutions, the decrease in the zero shear viscosity is observable only at the transition from salt-free case to NaCl 0.057 wt% solvent, then it increases as the ionic strength increases.

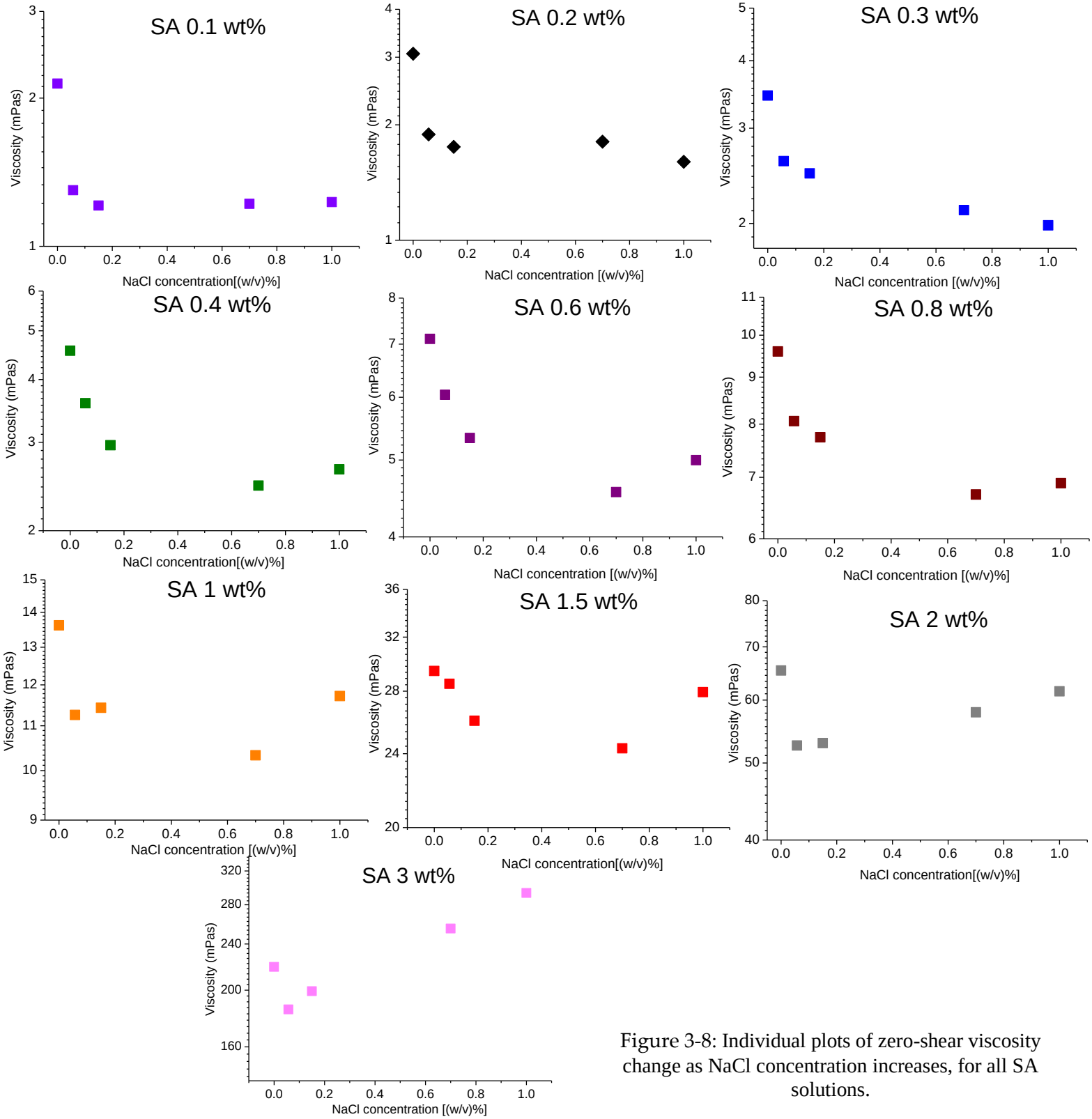

Figure 3-8: Individual plots of zero-shear viscosity change as NaCl concentration increases, for all SA solutions.

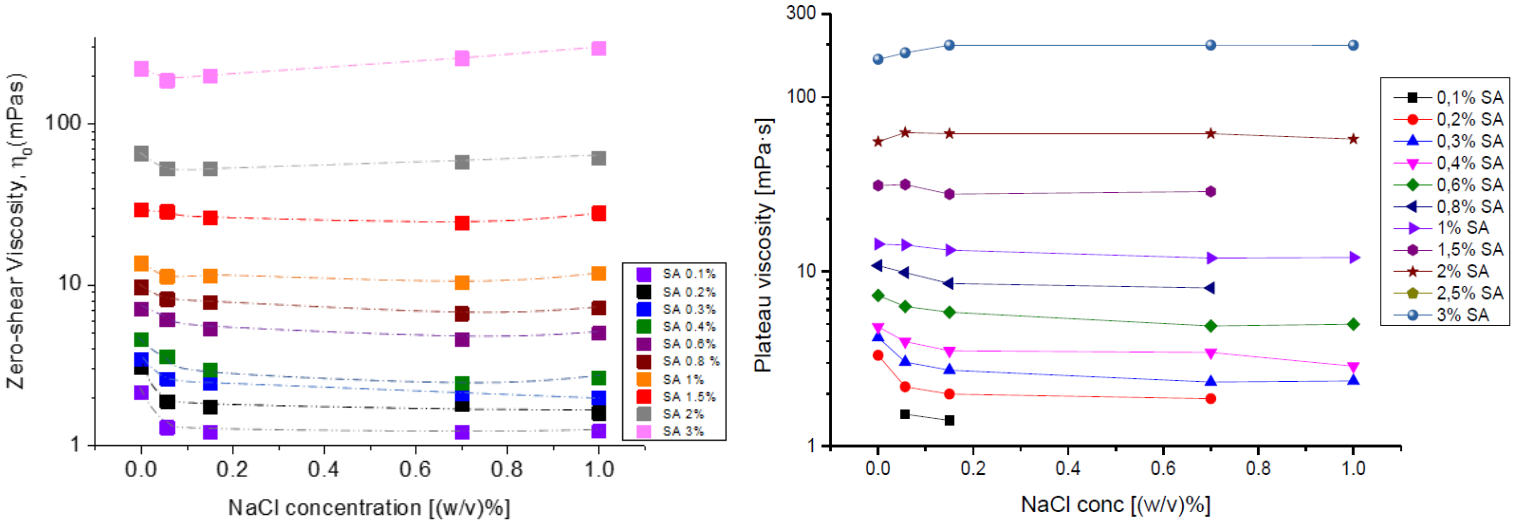

Figure 3-9: Zero-shear viscosity dependence on salt concentration for all SA solutions by the current work (left) and the previous thesis work (right) [53].

The results obtained in this work were compared to those obtained in the previous thesis, and the comparison in Figure 3A-9 confirm a nice data reproducibility. This confirmed that SA did not undergo any degradation process during the storage time.

In any case, for the sake of consistency, in the following parts; when comparing the results of rheological characterization of gels and solutions, the comparison will be carried out considering the solutions produced during this work (along with the relevant rheological behavior) which were the ingredient for the specific gel.

3.2. Hydrogels

3-B-1-Effect of SA Concentration and the Ionic Strength

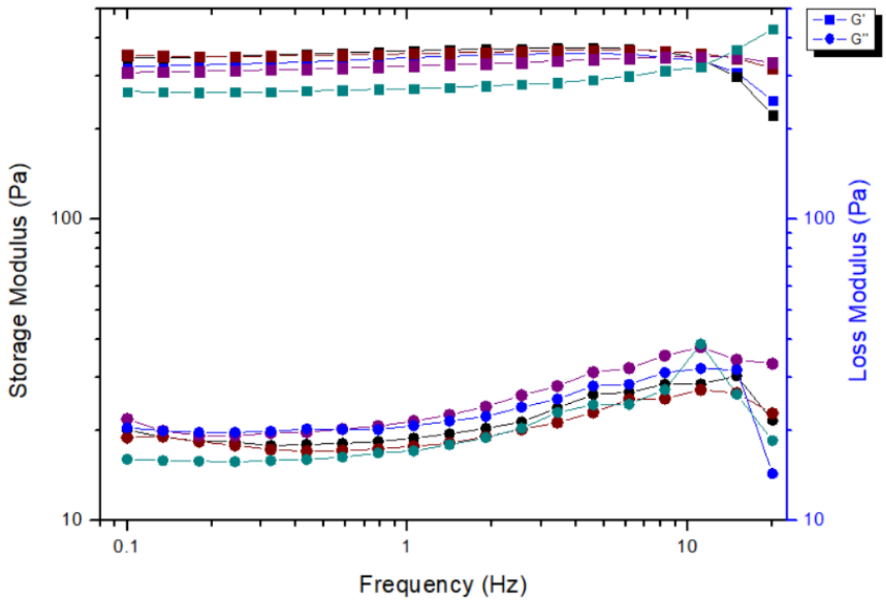

Figure 3-10: Storage and loss moduli dependence on frequency for the case of a SA 1 wt% in 0.7 wt% NaCl hydrogel.

Frequency sweep tests on SA hydrogels revealed the storage (G') and loss (G'') moduli; an example of the dependence of dynamic modulus components on frequency is given by for 5 samples of SA 1 wt% hydrogel in 0.7 wt% NaCl is given by Figure 3-10. The first thing we remark for all SA hydrogels we tested, is that G' is always higher than G'' which confirms the solid-like (gel) state of the material. Furthermore, G'' is about 10 times lower than G', and the latter is almost independent of frequency. Hence, the gelation took place via the introduction of $CaCO_3$ and GDL into the system even when the SA concentration is at the lowest.

Given the good reproducibility of data, the average values of G' and G'' and the relevant standard deviation were determined at each frequency, and the average curves for each SA concentration are reported in Figure 3-11 and Figure 3-12.

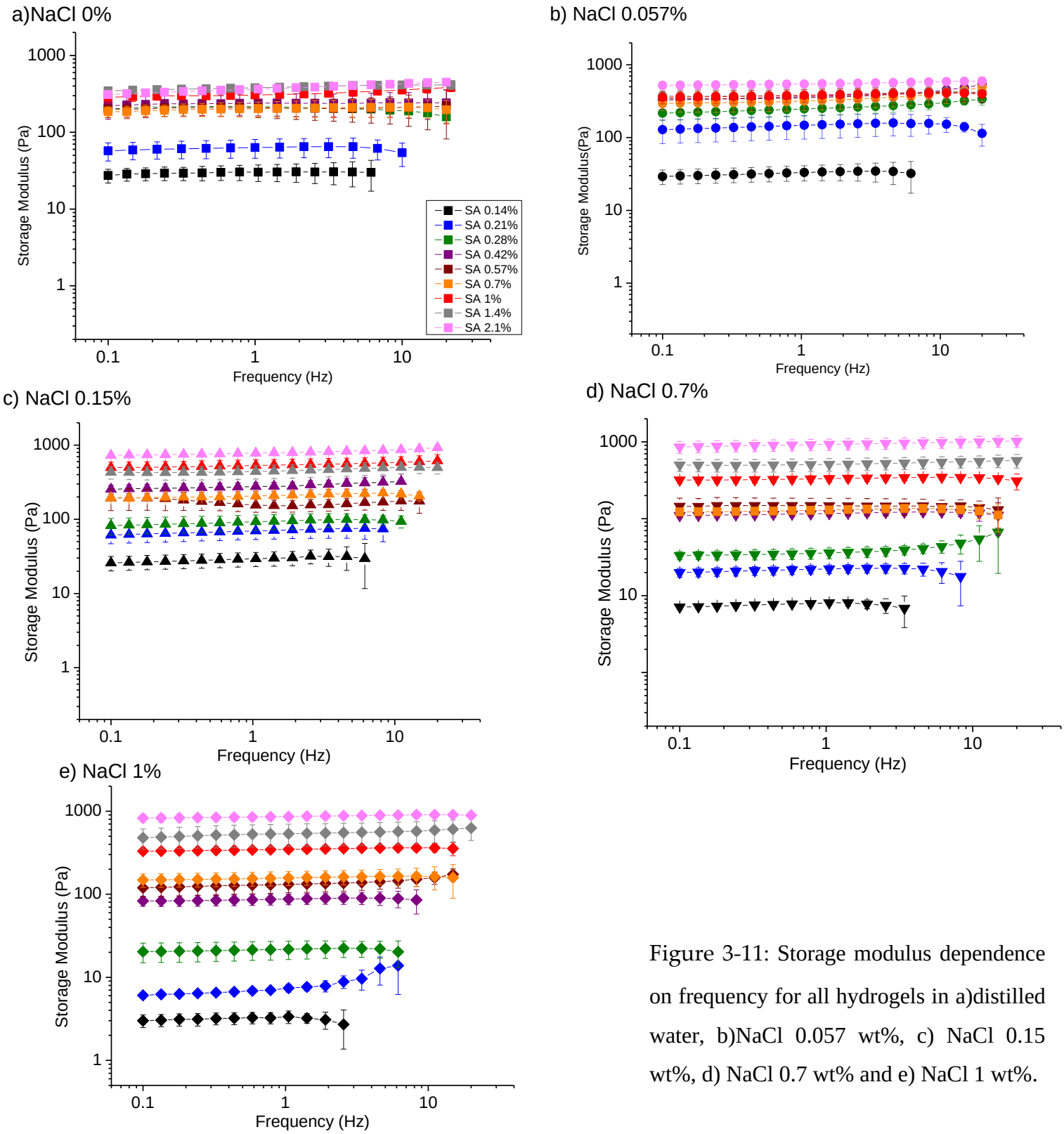

Figure 3-11: Storage modulus dependence on frequency for all hydrogels in a)distilled water, b)NaCl 0.057 wt%, c) NaCl 0.15 wt%, d) NaCl 0.7 wt% and e) NaCl 1 wt%.

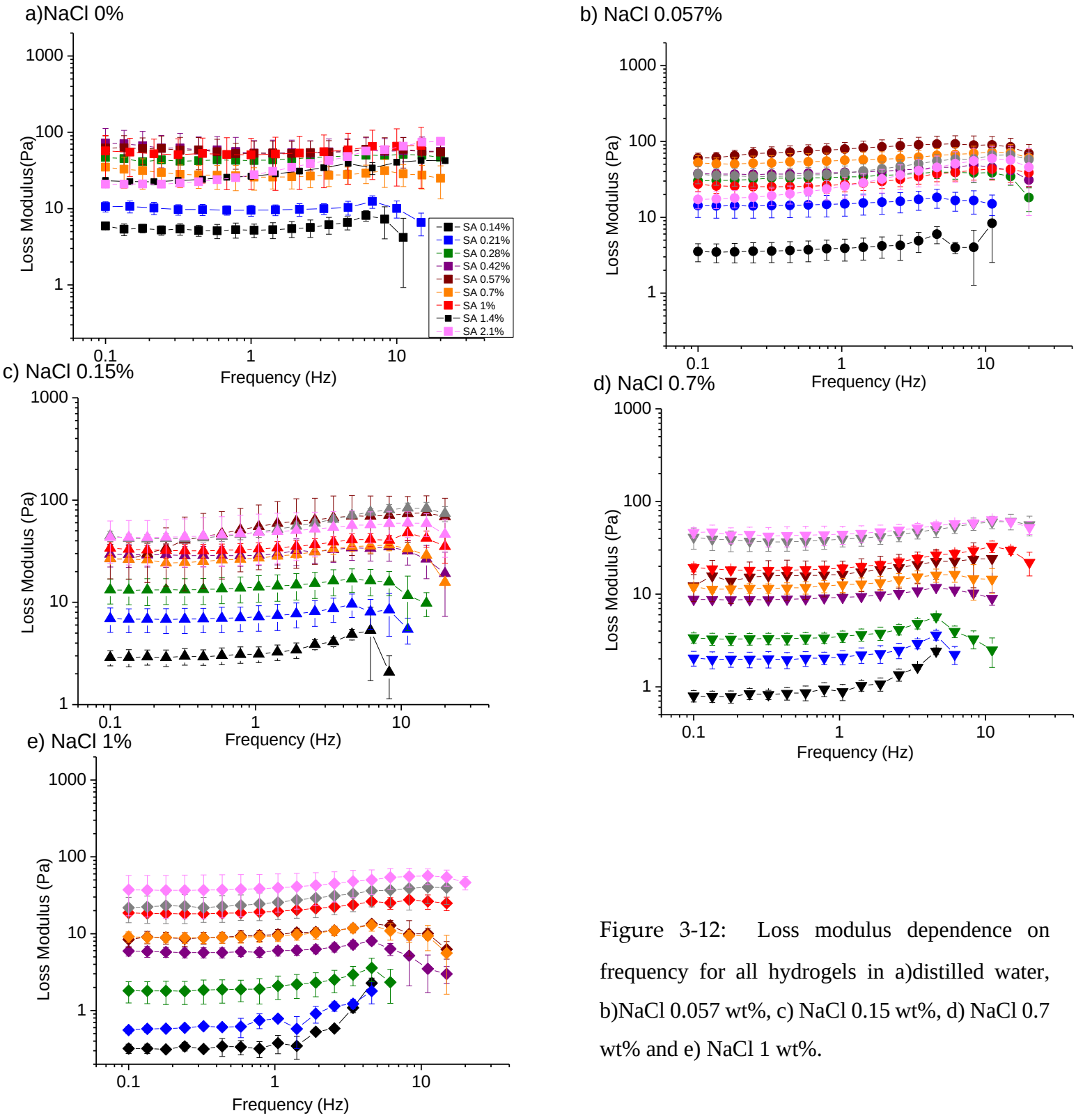

Figure 3-12: Loss modulus dependence on frequency for all hydrogels in a)distilled water, b)NaCl 0.057 wt%, c) NaCl 0.15 wt%, d) NaCl 0.7 wt% and e) NaCl 1 wt%.

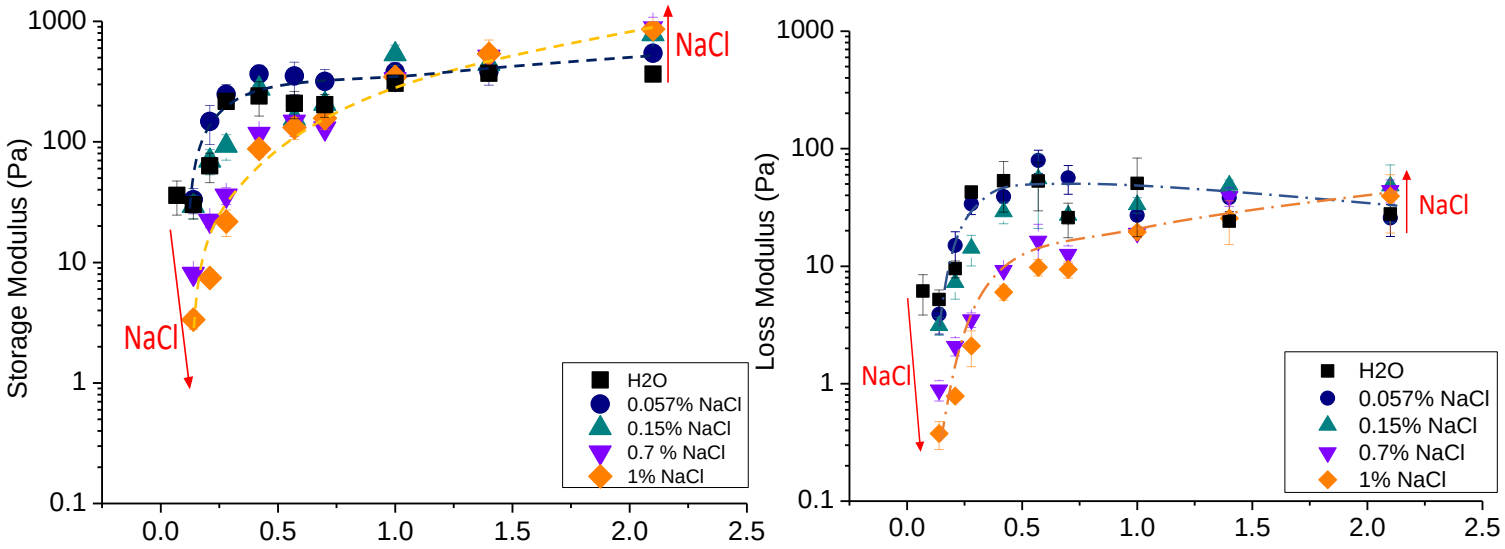

Figure 3-13: Storage (on the left) and loss (on the right) modulus variation with SA concentration at different NaCl concentrations. Red arrows indicate the increase in NaCl concentration. Blue dashed line represents the increasing trend of storage modulus in the case of distilled water, NaCl 0.057 and 0.15 wt% solvents while orange one indicates the same for NaCl 0.7 and 1 wt% solvents.

Given the limited effect of frequency (especially in the case of G'), from the experimental curves, the effect of polymer and NaCl concentrations were investigated considering the response at a fixed frequency, which was arbitrarily set to 1 Hz. The results are reported in Figure 3-13 for G' (on the left) and G'' (on the right).

As Figure 3-13 shows, G' increases as SA concentration increases for all hydrogels, with a variation of about three orders of magnitude going from 0.1 wt% to 2 wt%. The increase is more significant at low SA concentrations, and levels when moving towards higher concentrations. An effect of NaCl concentration reflects as two separate regimes which can be distinguished, one for NaCl concentration lower than 0.7 wt%, and one for higher concentration.

The different increasing trends are represented by the blue and orange dashed lines in Figure 3-13. SA hydrogels in distilled water, NaCl 0.057 and 0.15 wt% seem to have storage moduli higher than those of SA hydrogels in NaCl 0.7 and 1 wt%, when the SA concentration is lower than ~1 wt%. When we go beyond SA 1 wt%, the situation seems to be reversed and SA hydrogels in NaCl 0.7 and 1 wt% have higher storage moduli than the others. Further in this second case, G' has not reached to a plateau vale. Similar observation can also be made

for G''. The effect of NaCl on gels' dynamic mechanical response is therefore qualitatively similar to that observed in the case of SA solutions.

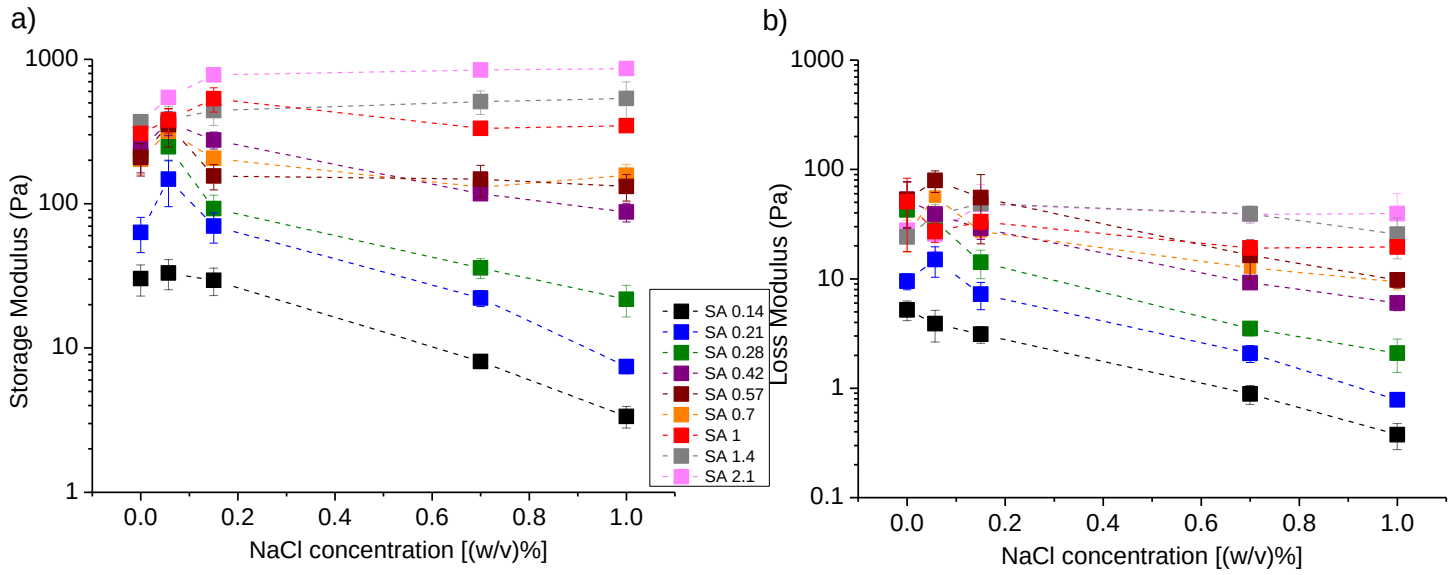

Figure 3-14: a) Storage Moduli change with NaCl concentration for all SA hydrogels. b) Loss Moduli change with NaCl concentration for all SA hydrogels.

Figure 3-14 represents the same data as Figure 3-13, highlighting the effect of NaCl concentration at fixed SA concentration. This data representation shows the unexpected increase in storage modulus when the NaCl concentration is increased from 0 wt% to 0.057 wt%. As this effect is, to some extent, hidden by the (most significant) effect of SA concentration, data are replotted in Figure 3-15: storage modulus values were divided by those of SA hydrogels in distilled water and plotted against NaCl concentration. Only a few hydrogels at different SA concentration are reported not to overcrowd the plot, however it is possible to see that G' even doubles its value in the case of SA 0.21 wt%. Then, a Student's t-test was conducted to determine whether these 2 sets of data (hydrogels in NaCl 0 wt% and NaCl 0.057 wt%) are significantly different than each other or not. One expects to obtain 90-95% confidence level to claim a significant difference however, according to our findings, the confidence level was only 80%. Although 80% confidence level is not very high, it is too high to neglect: we, then, speculate that increase we observed is real even if partly hidden by some experimental errors. We might speculate that the increase in G' may

arise from the increase in swelling degree in the case of ionic networks which was described by Donnan membrane equilibria. [18]

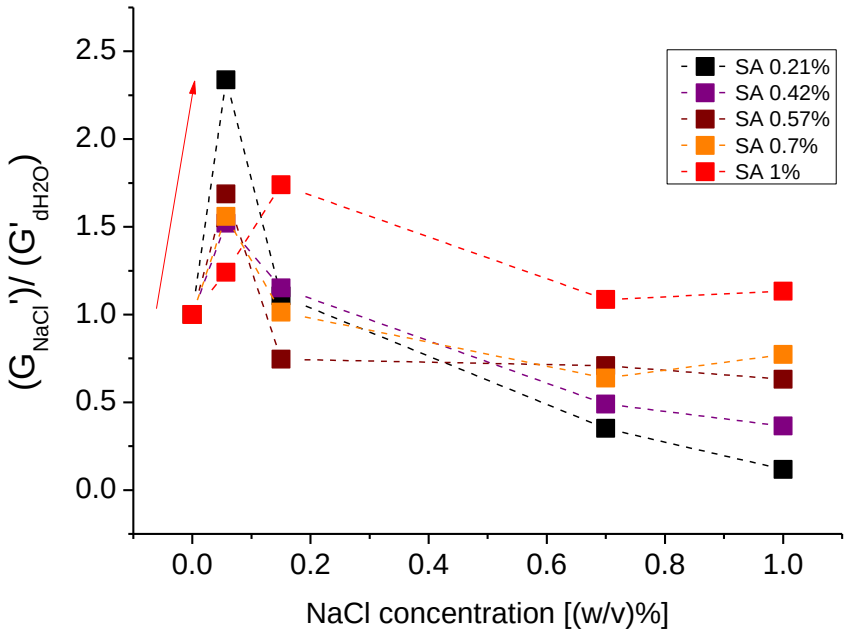

Figure 3-15: G' for hydrogels prepared from solutions at different NaCl concentrations, divided by G' of hydrogels prepared from distilled water solution as a function of NaCl concentration. Different curves represent results for SA concentrations equal to 0.21, 0.42, 0.57, 0.7 and 1 wt%. The increase in G' with respect to that in distilled water when passing to 0.057 wt% NaCl concentration is highlighted with the red arrow.

Considering the physical gelation mechanism of SA in the presence of divalent cations, introduction of Na^+ ions into the hydrogel leads to the partial replacement of Ca^{2+} ions (which are the crosslinkers between G blocks of adjacent SA chains) with Na^+ ions as represented in Figure 3-16. Hence, the addition of NaCl is expected to disrupt the

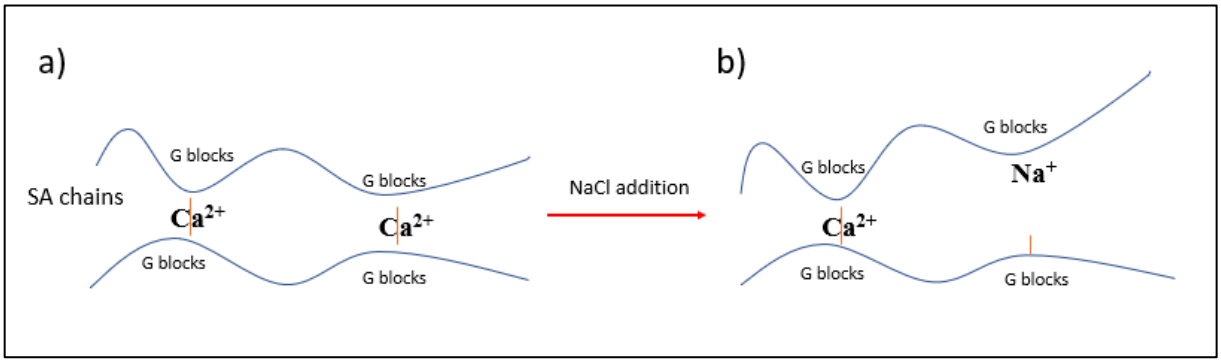

Figure 3-16: a) Ca^{2+} ions facilitate physical crosslinking between the G blocks of adjacent SA chains. b) Addition of Na^{+} ions to the system leads to the partial substitution of Ca^{2+} with Na^{+} and the consequent disruption of crosslinking.

crosslinking, therefore, to decrease the elasticity of the network which can explain the decrease in G' as the ionic strength increases.

On the other hand, we observed an opposite situation in which the G' increases with increasing ionic strength above a certain SA concentration, indicating the different effect of ionic strength also reported in the case of the solutions' viscosity. Although it requires more investigation to explain the mechanism behind it, studies report a similar effect of ionic strength on the viscosity and, also on the G' and G'' of xanthan solutions measured by the dynamic mechanical analysis as Figure 3-17 shows. [49]

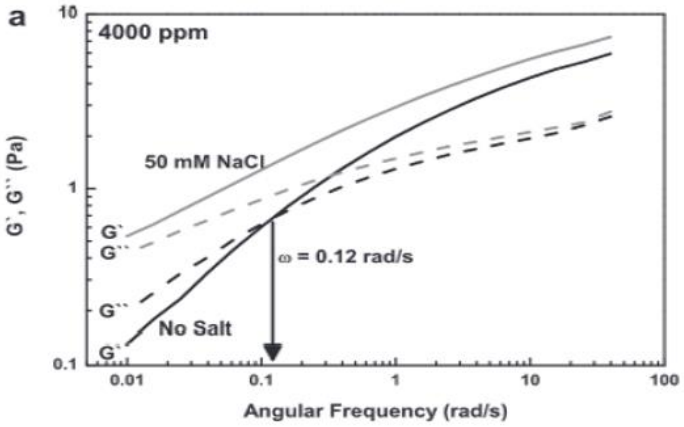

Figure 3-17: Dynamic moduli for 4000 ppm (top) and 500 (bottom) xanthan in salt free solution (black curves) and in 50 mM NaCl (grey curves) [49].

3.3. Relationship Between SA Solutions' Viscosity & Corresponding Hydrogels' Dynamic Mechanical Behavior

When designing hydrogels with tailored mechanical properties, a widespread approach consists in changing the starting solution composition up to the attainment of the desired performance. Even if driven by expertise driven qualitative indication, this operation is at least partly carried out in a trial-and-error approach. The present work aims at defining a correlation between the results of the rheological characterization of solutions and gels deriving from the solutions, and to investigate if some link can be made with the structure of the solutions themselves, for example in terms of critical concentrations.

Figure 3-18 represents the G' and G'' values of SA hydrogels reported with the corresponding zero-shear viscosity values of the SA solutions from which SA hydrogels were prepared, to look for a correlation between solution and hydrogel properties. Each curve refers to a different NaCl concentration. Despite the curve-to-curve difference, a general trend can be observed, with a steep increase in G' and G'' at increasing zero shear viscosity (of solutions) in a low zero-shear viscosity range (up to about 10 mPa s), and then a further increase, which is however less steep. Given this trend, and in order to give an analytical description of the observation, the curves were fitted by a bilinear trend (in the log-log scale, Figure 3-19). The results of this fitting are reported in Figure 3-20 for each NaCl concentration. The intercept and slope of the fitting lines are reported in Table 3-3 and compared in Figure 3-19.

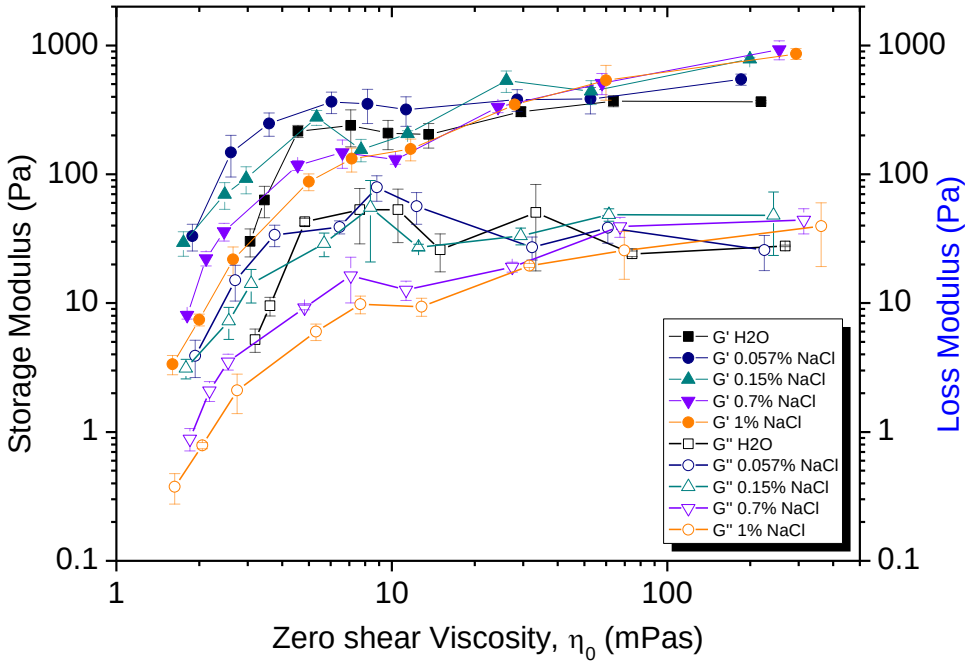

Figure 3-18: G'(solid symbols) and G''(open symbols) values of SA hydrogels reported with the corresponding zero-shear viscosity values of the SA solutions from which SA hydrogels were prepared.

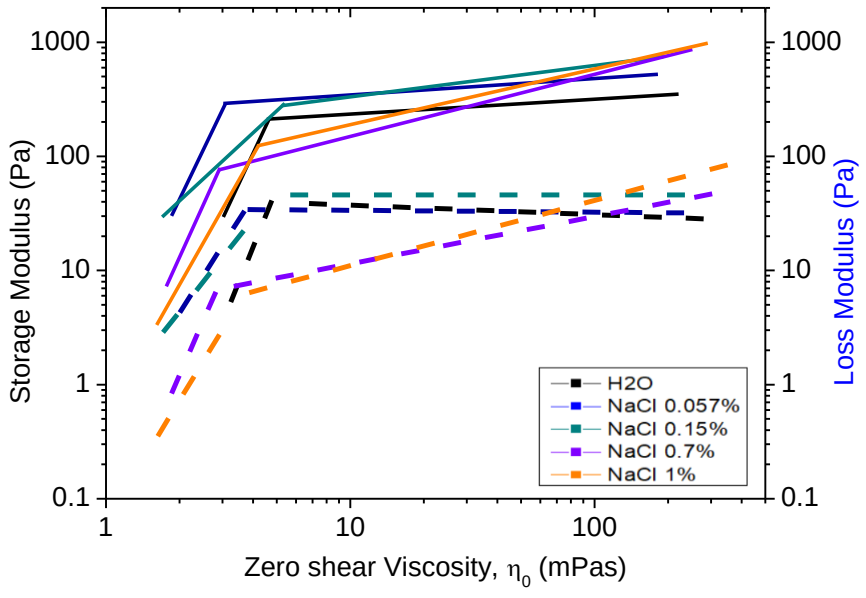

Figure 3-19: Trendlines of curves in Figure 3A-18. Solid lines belong to the G' curves while dashed lines belong to the G'' curves.

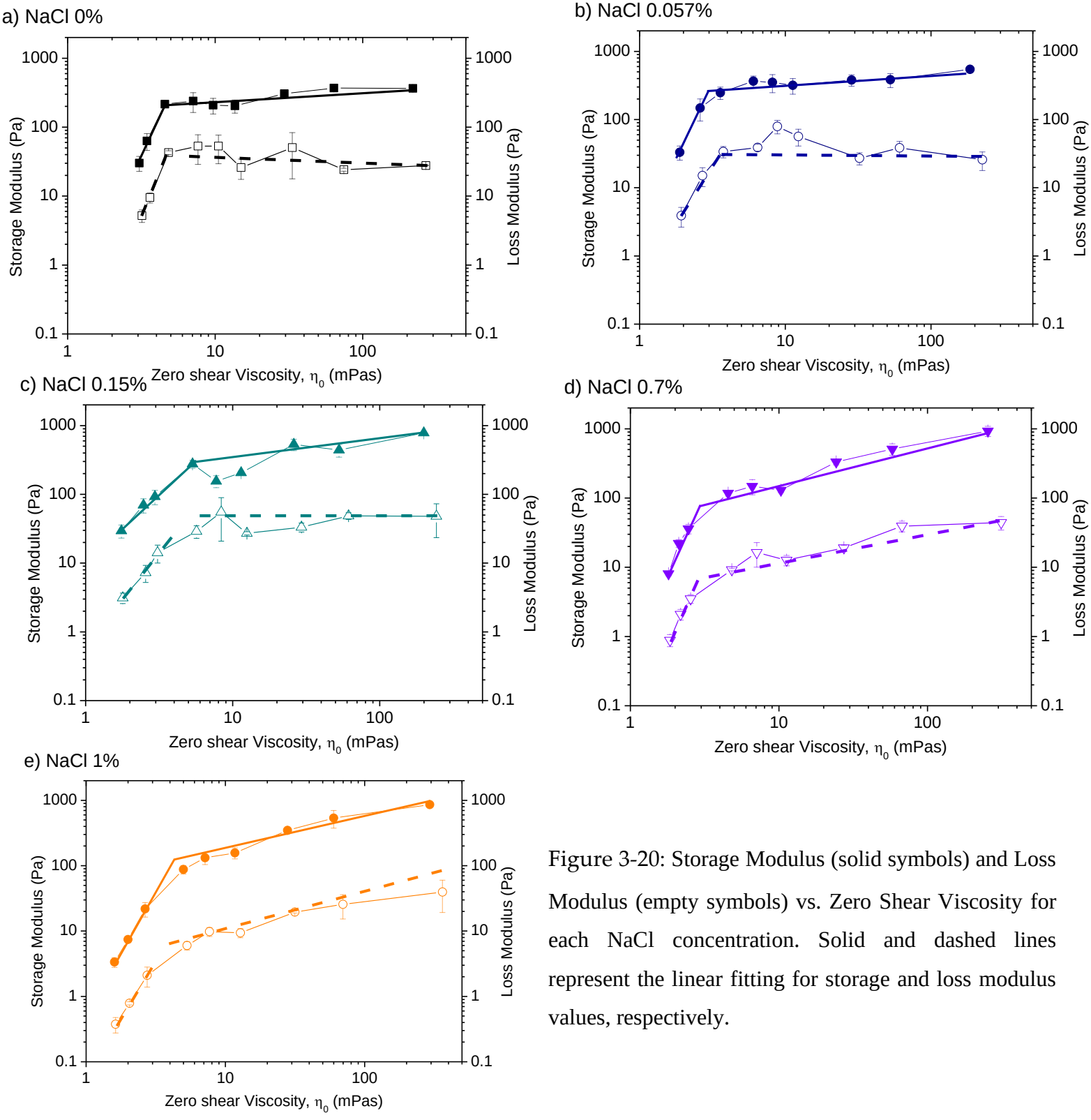

Figure 3-20: Storage Modulus (solid symbols) and Loss Modulus (empty symbols) vs. Zero Shear Viscosity for each NaCl concentration. Solid and dashed lines represent the linear fitting for storage and loss modulus values, respectively.

NaCl (wt%)	Upper slope	Intercept (upper)	Lower slope	Intercept (lower)
0	**0.06**	2.44	**3.65**	2.4
0.057	**0.13**	2.46	**2.72**	2.46
0.15	**0.24**	2.49	**1.35**	2.46
0.7	**0.43**	2.06	**2.68**	2
1	**0.38**	2.2	**1.76**	1.85

Table 3-3: Intercept and slope of the linear fitting lines for storage modulus (G') represented in Figure 3-19.

The viscosity values at the intersection between the two lines were determined and the relevant specific viscosity values, which will be referred to as "critical", $\eta_{crit,sp}$ were compared with the specific viscosities at critical concentration for entanglement found for the SA solutions ($\eta_{sp,ent}$). Results are reported in Table 3-4 and Figure 3-21.

NaCl (wt%)	$\eta_{sp,\,ent}$	$\eta_{crit,sp}$
0	4.34	4.24
0.057	11.44	2.44
0.15	15.3	5.18
0.7	11	2.06
1	13.22	3.53

Table 3-4: Table of $\eta_{crit,sp}$ and $\eta_{sp,ent}$ values for each NaCl concentration.

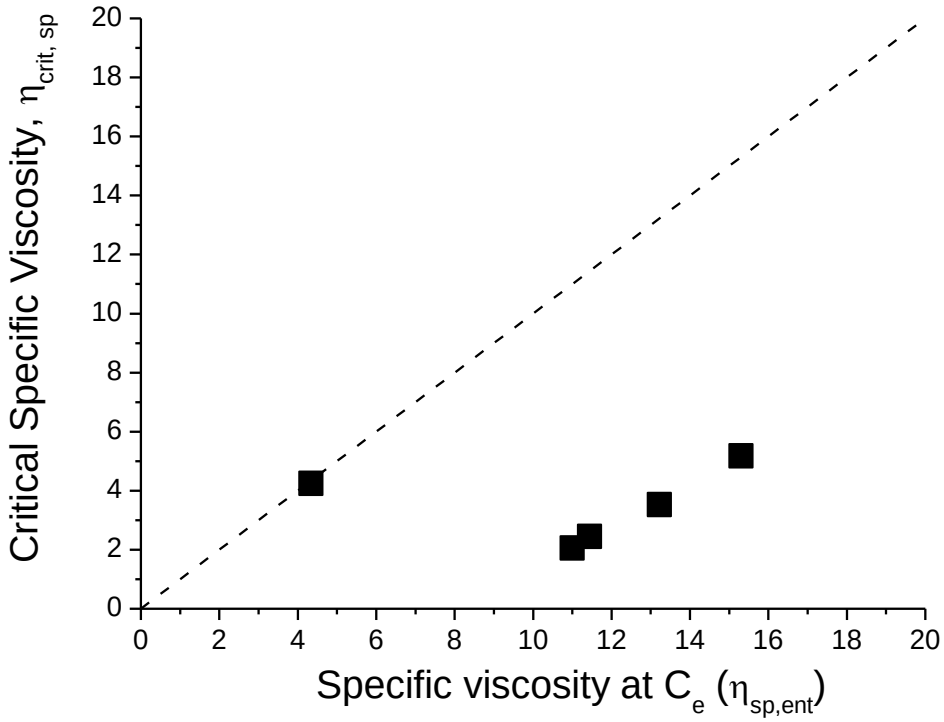

Figure 3-21: 3A-21: "Critical specific viscosity" $\eta_{crit,sp}$ plotted with respect to Specific viscosity at C_e, $\eta_{sp,ent}$. Dashed line is a linear 1:1 curve.

Interestingly, $\eta_{crit,sp}$ and $\eta_{sp,ent}$ coincide in the case of solution in distilled water, suggesting a structural cause for the change in G' and G'' dependence on solution viscosity; the dependence itself, requires further investigation. On the other hand, when NaCl is added to the solution, the matching of $\eta_{crit,sp}$ and $\eta_{sp,ent}$ values is lost, suggesting a complex combined effect of SA and NaCl concentration, which is still to be interpreted.

It is worth-mentioning that there is a local minimum in G' and G'' curves of Figure 3-22 which correspond to a solution concentration of SA 0.8-1 wt% in all cases. The critical concentration of the solutions for the entanglement regime C_e, and the polymer concentrations corresponding to that minimum value ($C_{SA, crit, min}$) are reported in Table 3-5 and plotted with respect to each other in Figure 3-23. From Table 3-5 and Figure 3-23, we may point out that the entanglement concentrations are close to those $C_{SA, crit,min}$ values especially for the cases in presence of salt.

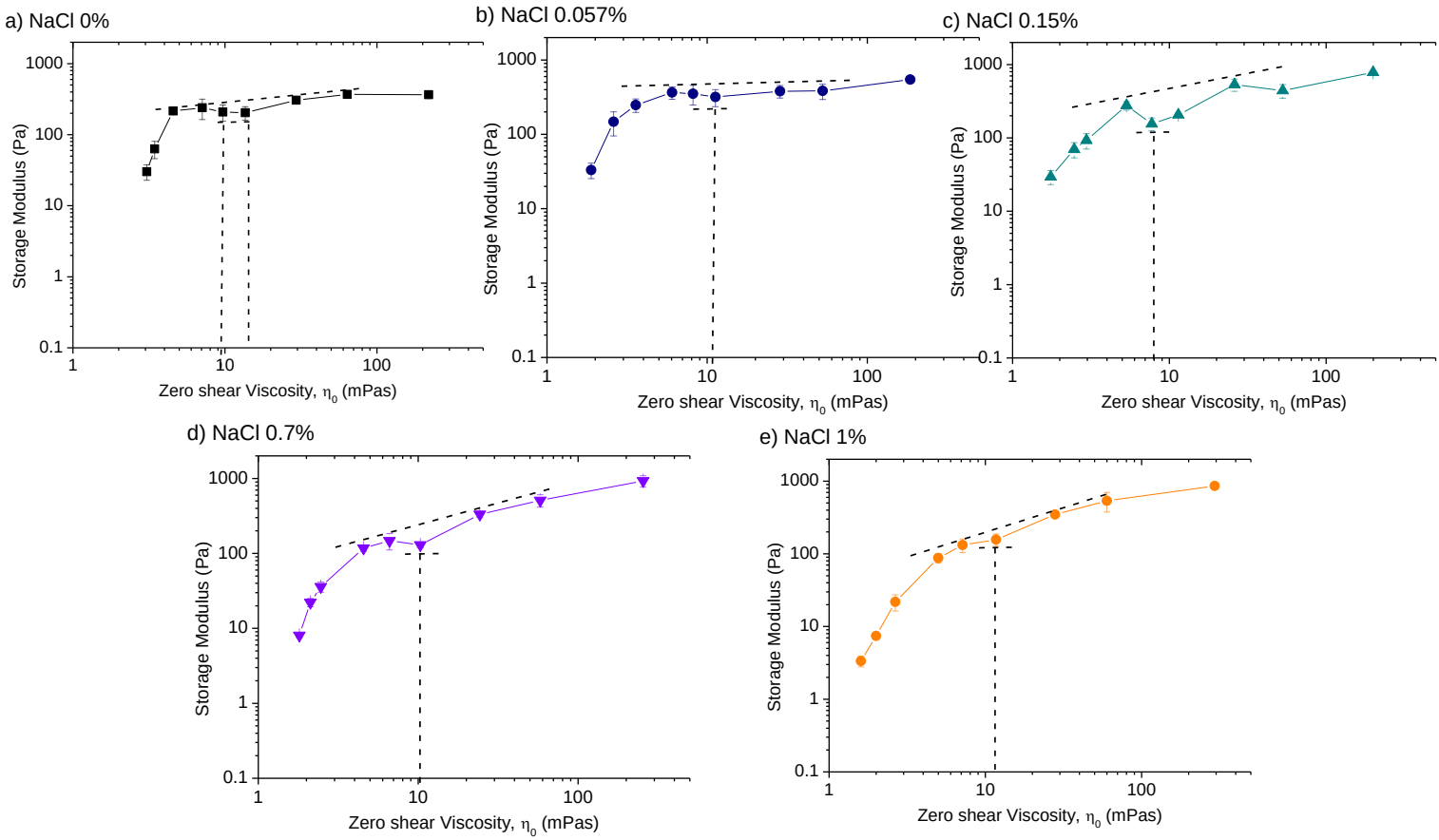

Figure 3-22: Individuated G' curves of Figure 3A-18 to display the drop in G' value in the intermediate range (represented by black dashed lines) corresponding to a solution concentration of SA 0.8-1 wt% in all cases of a)NaCl 0wt%, b) NaCl 0.057 wt%, c)NaCl 0.15 wt%, d) NaCl 0.7 wt% and e) NaCl 1 wt%.

NaCl (wt%)	$C_{SA,\ crit,min}$	C_e
0	0.8-1	0.47
0.057	1	1.01
0.15	0.8	1.24
0.7	1	1.23
1	1	1.26

Table 3-5: SA concentration which correspond to a minimum value in Figure 3-20 ($C_{SA,crit,min}$) and entanglement concentration C_e values are reported in all NaCl concentrations.

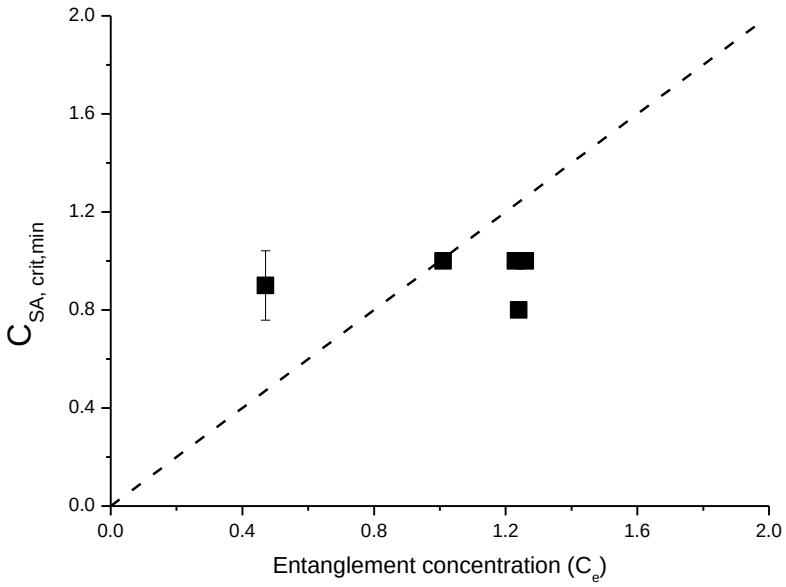

Figure 3-23: $C_{SA,\ crit,min}$ plotted with respect to C_e. Dashed line is a linear 1:1 curve.

To sum up, the link between the rheological properties of SA solutions and SA hydrogels seems to be complex and more research and investigation are required to reveal it. Nevertheless, it is possible to present a map that connects the solution viscosity and the storage and loss moduli of the hydrogels and that might be useful in future studies. In addition, the trend observed could be described, at least in a first approximation, as bilinear in the double logarithmic scale, with an inflection point at a viscosity which, in the case of

neutral solvent, is similar to that observed at the transition between the semi-dilute unentangled and the entangled regime. The addition of NaCl to the solution causes a change of both the slopes of the bilinear trend and the viscosity at inflection point, that cannot be correlated with rheological transitions.

4 Conclusions

This thesis aimed at investigating the effect of Sodium Alginate concentration and NaCl concentration on the dynamic mechanical behavior of Sodium Alginate-based hydrogels and the precursor aqueous solutions. The investigation is motivated by the interest for the use of hydrogels as in vitro mucus models, and the consequent requirements on their mechanical properties also in environments representative of the physiological conditions. Given the hydrogel preparation method involving the dissolution of the Sodium Alginate and a long (at least 24hr) crosslinking time, being able to control the final properties of the hydrogel by adjusting the viscosity of the solution is of great interest.

Steady state shear rheometry tests on sodium alginate (SA) aqueous solutions have shown that the viscosity of solutions strongly depends on the polymer concentration, and NaCl concentration in the solvent. Furthermore, a dependence on shear rate could be observed only at the highest Sodium Alginate and NaCl concentrations: in this condition solutions displayed a shear thinning behavior at high shear rate values.

The dependence of specific viscosity of Alginate concentration could be described by scaling laws reported for a polyelectrolyte, and the effect of NaCl was the expected neutralization of ionic sites on the macromolecule, so that even with the smallest amount of NaCl (0.057 wt%), rheological behavior of SA solution has turned to neutral polymer-like, showing only two inflection points in the concentration range investigated. Although the expected increase in scaling factor was observable as the ionic strength increases, the values of the scaling exponents were not in complete accordance with the theoretical predictions, which might be due to the high polydispersity of SA deriving from its natural origin.

Besides the effect on scaling law exponents, electrostatic screening effect of salt concentration on the viscosity of polyelectrolyte solutions have been reported: viscosity of the solutions at semi-dilute regime decreased with increasing ionic strength. In the concentrated regime, however, an opposite effect has been observed: an increase in viscosity was observable with ionic strength at alginate concentrations beyond about 1 wt%.

SA- based hydrogels were prepared via crosslinking in the presence of calcium ions successfully, as verified by frequency sweep tests revealing the solid-like behavior: even when the hydrogels were prepared at the lowest SA concentration, storage modulus (G') was greater than loss modulus (G''). Both properties increased with polymer concentration as expected. An interesting effect of ionic strength was observed: dynamic moduli of low Sodium Alginate concentration-hydrogels decreased in the presence of NaCl, which was probably due to the partial substitution of calcium crosslinkers with free sodium ions in the solvent. However, an opposite effect of ionic strength has been observed at high values of SA concentration (beyond 1 wt%), similar to what we observed in solution viscosity: dynamic modulus of the hydrogels increased with ionic strength. The inversion occurred at higher SA concentration for G'' as compared to G'.

Finally, a correlation between precursor solution viscosity and hydrogel dynamic modulus has been observed. G' and G'' increase with viscosity in a bilinear fashion in a log log plot, with higher slope in the low viscosity (and low Alginate concentration) range and lower slope at higher viscosities. Slope values depend on NaCl concentration.

In the case of solutions without salt, the viscosity at the inflection point is very similar to that at the transition between the semi-dilute unentangled and the semi-dilute entangled regimes. Absence of this coincidence in the presence of salt suggests a complex combined effect which requires further interpretation.

A further feature common to all the considered hydrogel is the presence of a negative deviation (a local minimum) from the linear trend in the lower slope branch of the bilinear behavior. This feature occurs in a very limited range of SA concentrations – between 0.8-1 wt% independent of the NaCl concentrations. Interestingly, this concentration range is close to the concentration range of the transition from semi-dilute unentangled to semi-dilute entangled regime for solutions containing salt.

In conclusion, this work allowed to build a map for the formulation of precursor solutions of Sodium Alginate in a physiological-like environment, which will, through crosslinking, lead to hydrogels with customized dynamic mechanical properties. Further, the effect of Na^+ ions on both solutions and hydrogels has been assessed, and tentatively explained in terms of screening of anionic sites present on the Sodium Alginate macromolecules.

A point which remains open is the structural interpretation of the correlation between solution viscosity and hydrogel mechanical behavior.

Finally, in view of the use of the hydrogels as a substrate for bacteria or cells growth, it would be interesting to check if the presented map can be applied also when complex systems, such as supplements for microorganisms growth, are added to the alginate solution so that they are included in the gel network even from the start of the crosslinking.

Bibliography

1.Carabotti, M., Scirocco, A., Maselli, M. A., & Severi, C. (2005). The gut-brain axis: Interactions between enteric microbiota, central and enteric nervous systems. *Annals of Gastroenterology.*

2.Clementi, F., Mancini, M., & Moresi, M. (1998). Rheology of Alginate From Azotobacter vinelandii in Aqueous Dispersions. *Journal of Food Engineering*.

3.Colby, R. (2009). Structure and linear viscoelasticity of flexible polymer solutions: comparison of polyelectrolyte and neutral polymer solutions. *Rheologica Acta.*

4.Crowther, R., Marriott, C., & James, S. (1984). Cation Induced Changes in the Rheological Properties of Purified Mucus Glycoprotein Gels. *Biorheology* (s. 253-263). Pergamon Press.

5.Dai, H., Ou, S., Huang, Y., Liu, Z., & Huang, H. (2018). Enhanced swelling and multiple-responsive properties of gelatin/sodium alginate hydrogels by the addition of carboxymethyl cellulose isolated from pineapple peel. *Cellulose.*

6.de Gennes, P.-G. (1979). Scaling Concepts in polymer Physics. Cornell University Press.

7.Demouveaux, B., Gouyer, V., Gottrand, F., Narita, T., & Dessyn, J.-L. (2017). Gel-forming mucin interactome drives mucus viscoelasticity. *Advances in Colloid and Interface Science.*

8.Dobrynin, A., Colby, R., & Rubinstein, M. (1995). Scaling Theory of Polyelectrolyte Solutions. *Macromolecules.*

9.Dodero, A., Vicini, S., Alloisio, M., & Castellano, M. (2019). Sodium alginate solutions: correlation between rheological properties and spinnability. *Journal of Materials Science.*

10.Doi, M., & Edwards, S. (1994). The Thory of Polymer Dynamics. Oxford University Press.

11.Donnelly, M., Hailemichael, M., & Liberatore, M. (2014). Altering the viscosity of cationically modified cellulose polymers by the addition of salt. *Journal of Applied Polymer Science.*

12.dos Santos, L. (2017). Natural Polymeric Biomaterials: Processing and Properties. S. Hashmi içinde, *Reference module in materials science and materials engineering.*

13.Draget, K., Skjak Braek, G., & Smidsrod, O. (1994). Alginic acid gels: the effect of alginate chemical composition and molecular weight. *Carbohydrate Polymers.*

14.Edwards, S. (1966). The theory of polymer solutions at intermediate concentration. *Proceedings of the Physical Society.*

15.El Aferni, A., Guettari, M., Kamli, M., Tajouri, T., & Ponton, A. (2020). A structural study of a polymer-surfactant system in dilute and entangled regime: Effect of high concentrations of surfactant and polymer molecular weight. *Journal of Molecular Structure.*

16.Ewoldt, R., Clasen, C., Hosoi, A., & McKinley, G. (2007). Rheological fingerprinting of gastropod pedal mucus and synthetic complex. *Soft Matter.*

17.Fang, Y., Al-Assaf, S., Phillips, G., Nishinari, K., Funami, T., Williams, P., & Li, L. (2007). Multiple Steps and Critical Behaviors of the Binding of Calcium to Alginate. *Journal of Physical Chemistry.*

18.Flory, P. (1953). Principles of Polymer Chemistry. New York: Cornell University Press.

19.Fu, S., Thacker, A., Sperger, D., Boni, R., Buckner, I., Velankar, S., . . . Block, L. (2011). Relevance of Rheological Properties of Sodium Alginate in Solution to Calcium Alginate Gel Properties. *American Association of Pharmaceutical Scientists.*

20.Fu, S., Thacker, A., Sperger, D., Boni, R., Velankar, S., Munson, E., & Block, L. (2010). Rheological Evaluation of Inter-grade and Inter-batch Variability of Sodium Alginate. *American Association of Pharmaceutical Scientists.*

21.Graessly, W. (1980). Polymer chain dimensions and the dependence of viscoelastic properties on concentrtaion, molecular weight and solvent power. *Polymer.*

22.Graulus, G., Mignon, A., Van Vlierberghe, S., Declercq, H., Feher, K., Cornelissen, M., Dubruel, P. (2015). Cross-linkable alginate-graft-gelatin copolymers for tissue engineering applications. *European Polymer Journal.*

23.Hernandez, R., Sacristan, J., & Mijangos, C. (2010). Sol/Gel Transition of Aqueous Alginate Solutions Induced by Fe2+ Cations. *Macromolecular Chemistry and Physics.*

24.Karakasyan, C., Legros, M., Lack, S., Brunel, F., Maingault, P., Ducouret, G., & Hourdet, D. (2010). Cold Gelation of Alginates Induced by Monovalent Cations. *Biomacromolecules.*

25.Korosi, A., & Fabuss, B. (1968). Viscosities of Binary Aqueous Solutions of NaCl, KCl, Na2SO4, and MgSO4 at Concentrations and Temperatures of Interest in Desalination Process. *Journal of Chemical Engineering.*

26.Lai, S., Wang, Y.-Y., Wirtz, D., & Hanes, J. (2009). Micro- and macrorheology of mucus. *Advanced Drug Delivery Reviews.*

27.Leal, J., Smyth, H., & Ghosh, D. (2017). Physicochemical properties of mucus and their impact on transmucosal drug. *International Journal of Pharmaceutics.*

28.LeRoux, M., Guilak, F., & Setton, L. (1999). Compressive and shear properties of alginate gel: Effects of sodium ions and alginate concentration. *Journal of Biomedicals Material Research.*

29.Liu, S., Liu, H., Thang, B., Bi, S., & Li, L. (2016). Scaling law and microstructure of alginate hydrogel. *Carbohydrate Polymers.*

30.Liu, X., Qian, L., Shu, T., & Tong, Z. (2003). Rheology characterization of sol–gel transition in aqueous alginate solutions induced by calcium cations through in situ release. *Polymer.*

31.Ma, J., Lin, Y., Chen, X., Zhao, B., & Zhang, J. (2014). Flow behavior, thixotropy and dynamical viscoelasticity of sodium alginate aqueous solutions. *Food Hydrocolloids.*

32.Maciel, B., Oelschlaeger, C., & Willenbacher, N. (2019). Chain flexibility and dynamics of alginate solutions in different solvents. *Colloid and Polymer Science.*

33.Mancini, M., Moresi, M., & Sappino, F. (1996). Rheological Behaviour of Aqueous Dispersions of Algal Sodium Alginates. *Journal of Food Engineering.*

34.Moritaka, H., Fukuba, H., Kumeno, K., Nakahama, N., & Nishinari, K. (1991). Effect of monovalent and divalent cations on the rheological properties of gellan gels. *Food Hydrocolloids.*

35.Morris, E., Rees, D., & Thom, D. (1973). Characterization of Polysaccharide Structure and Interactions by Circular Dichroism: Order-Disorder Transition in the calcium Alginate System. *Journal of the Chemical Society.*

36.Pacheco, D., Butnarasu, C., Briatico, F., Pastorino, L., Visai, L., Visentin, S., & Petrini, P. (2019). Disassembling the complexity of mucus barriers to develop a fast screening tool for early drug discovery. *Journals of Materials Chemistry.*

37.Rodriguez-Rivero, C., Hilliou, L., Martin del Valle, E., & Galan, M. (2014). Rheological characterization of commercial highly viscous alginate solutions in shear and extensional flows. *Rheologica Acta.*

38.Rubinstein, M., & Colby, R. (2003). Polymer Physics. Oxfor University Press.

39.Rubinstein, M., Colby, R., & Dobrynin, A. (1994). Dynamics of Semidilute Polyelectrolyte Solutions. *Physical Review Letters.*

40.Sachan, N., Pushkar, S., Jha, A., & Bhattcharya, A. (2009). Sodium alginate: the wonder polymer for controlled drug delivery. *Journal of Pharmacy Research.*

41.Sardelli, L., Pacheco, D., Ziccarelli, A., tunesi, M., Caspani, O., Fusari, A., . . . Petrini, P. (2019). Towards bioinspired in vitro models of intestinal mucus. *Royal Society of Chemistry.*

42.Sardelli, L., Tunesi, M., Briatico, F., & Petrini, P. (2021). 3D-Reactive printing of engineered alginate inks. *Soft Matter.*

43.Storz, H., Zimmermann, U., Zimmermann, H., & Kulicke, W.-M. (2010). Viscoelastic properties of ultra-high viscosity alginates. *Rheologica Acta.*

44.Teraoka, I. (2002). Polymer Solutions: An Introduction to Physical Properties. John Wiley & Sons.

45.Wang, Z.-Y., Zhang, Q.-Z., & Saito, S. (1994). Sol-Gel Transition of Alginate Solution by the Addition of Various Divalent Cations: A Rheological Study. *Biopolymers.*

46.Wang, Z.-Y., Zhang, Q.-Z., Konno, M., & Saito, S. (1993). Sol-Gel Transition of Alginate Solution by the Addition of Various Divalent Cations:C-NMR Spectroscopic Study. *Biopolymers.*

47.Webber, R., & Shull, K. (2014). Strain Dependence of the Viscoelastic Properties of Alginate Hydrogels. *Macromolecules.*

48.Wyatt, N., & Liberatore, M. (2009). Rheology and Viscosity Scaling of the Polyelectrolyte Xanthan Gum. *Journal of Applied Polymer Science.*

49.Wyatt, N., Gunther, C., & Liberatore, M. (2011). Increasing viscosity in entangled polyelectrolyte solutions by the addition of salt. *Polymer.*

50.Zhang, H., Wang, H., Wang, J., Guo, R., & Zhang, Q. (2001). The effect of Ionic Strength on the Viscosity of Sodium Alginate Solution. *Polymers for Advanced technologies.*

51.Zhang, H., Zheng, H., Zhang, Q., Wang, J., & Konno, M. (1998). The Interaction of Sodium Alginate with Univalent Cations. *Biopolymers.*

52. Sardelli, L. 2018, Engineering bioinspired graded in vitro intestinal mucus models, Master Thesis, Politecnico di Milano, Italy.

53. Bignami, A., 2019, Effects of NaCl and Alginate Concentrations On The Rheological Properties of Aqueous Solutions And Hydrogels, Master Thesis, Politecnico di Milano, Italy.

54. Boegh, M., Baldursdottir, S., Müllertz, A., & Nielsen, H. (2014). Property profiling of biosimilar mucus in a novel mucus-containing in vitro model for assessment of intestinal drug absorption. *European Journal of Pharmaceutics and Biopharmaceutics*.

55. Mezger, T. (2006). *The Rheology Handbook.* Vincentz Network.

56. Rubinstein, M., Colby, R., Dobrynin, A., Joany, J.F. (1996). Elastic Modulus and Equilibrium Swelling of Polyelectrolyte Gels. *Macromolecules.*

57. Schosseler, F., Ilmain, F., Candau, S.J. (1991) Structure and Properties of Partially Neutralized Poly(acrylic acid) Gels. *Macromolecules.*

58. Skouri, R., Schosseler, F., Munch, J.P., Candau, S.J. (1995) Swelling and Elastic Properties of Polyelectrolyte Gels. *Macromolecules.*

List of Figures

List of Tables

List of symbols

n = number of monomers on a real chain
l = size of monomers on a real chain
N = number of Kuhn monomers, or degree of polymerization
b = size of Kuhn monomer
L = extended size for plyelectrolyte chain
M = chain molar mass
R_n = end-to-end distance
$\langle R^2 \rangle$ = mean square end-to-end distance
R_{max} = max end-to-end distance
C_N = characteristic Flory's ratio
R = general coil size
SA = sodium alginate
c = polymer concentration
C*= overlap concentration
Ce = entanglement concentration
C** or CD = critical concentration for polyelectrolytes to enter the concentrated regime
Cs = salt concentration
ρ = polymer density
V = pervaded volume
v_{mon} = monomer volume
v = excluded volume
ξe = size electrostatic blob
ξ = correlation length
A = average number of monomers between charges
ζ = friction coefficient (Rouse model)
ω = frequency (rad/s)
D = self-diffusion coefficient
DR = Rouse diffusion coefficient
DZ = Zimm diffusion coefficient
τ = generic relaxation time
τ_{rep} = reptation time
η_{sp} = specific viscosity
[η] = intrinsic viscosity
η_{red} = reduced viscosity
η_{rel} = relative viscosity
η_0 = zero-shear viscosity
η_s = solvent viscosity
k_H= Huggins coefficient
K = coefficient in Mark-Houwink eq

λ_c=relaxation time in Cross equation
$\dot{\gamma}$ = generic shear rate
m = power index in Cross eq.
n (ambiguous) = flow index in power law eq. or power index in the extended Huggins eq.
k = consistency (power-law eq.)
G'=storage modulus
G''=loss modulus
G*=complex modulus
τ= shear stress